



---

A H2020 Research and Innovation Action project, Grant Agreement number 814985

## D5.1 - Report on Best Available Technologies (BAT) for central receiver systems



This deliverable report D5.1 is part of a project that has received funding from the European Union's Horizon 2020 research and innovation programme under Grant Agreement No. 814985

WP 5: Techno-economic, social and environmental assessments

Task 5.1: Techno-economic, social and environmental assessments

Version: 01 version, Thursday, 5<sup>th</sup> December 2019

## Technical References

Deliverable No.	5.1
Dissemination level <sup>1</sup>	PU
Work Package	WP5
Task	T5.1
Lead beneficiary	Abengoa Energia
Contributing beneficiary(ies)	University of Seville
Due date of deliverable	30 November 2019
Actual submission date	5 December 2019

## History of Changes

Version	Date	Changes
0.a	30/11/2019	Original version created by Abengoa Energia and USE
0.b	04/12/2019	Comments by Prof. Giampaolo Manzolini (Coordinator)
01	05/12/2019	Approved by Dr. Cristina Prieto (Abengoa Energia)

## Table of Contents

<b>Technical References</b>	<b>2</b>
<b>History of Changes</b>	<b>3</b>
<b>Table of Contents</b>	<b>4</b>
<b>1 Executive Summary</b>	<b>6</b>
<b>2 Fundamentals of CSP for STE</b>	<b>7</b>
2.1 Introduction to CSP-STE Technologies . . . . .	7
<b>3 Review of Solar Subsystems</b>	<b>10</b>
3.1 Solar Field . . . . .	10
3.2 Receiver . . . . .	14
3.2.1 Gas Receiver . . . . .	15
3.2.2 Liquid Receiver . . . . .	16
3.2.3 Solid Particle Receiver . . . . .	16
3.3 Thermal Energy Storage System . . . . .	17
3.3.1 Storage based on steam accumulation . . . . .	18
3.3.2 Storage based on molten salts . . . . .	20
3.3.3 Steam Generator . . . . .	21
<b>4 Review of Power Block</b>	<b>22</b>
4.1 Fundamentals of Rankine Cycles for Steam Turbines . . . . .	22
4.2 Power Block in a CSP-STE power plant . . . . .	25
4.3 Auxiliary systems of the power block . . . . .	27
4.4 Design and performance of the steam cycle . . . . .	28
4.5 Transient operation mode and control strategies of the steam cycle . . . . .	28
4.6 Current development trends of steam cycles in CSP plants . . . . .	29
<b>5 Techno-Economic Status of Solar Tower Plants</b>	<b>30</b>
<b>6 Hybridization</b>	<b>35</b>
<b>7 Power Block based on supercritical CO<sub>2</sub> cycles</b>	<b>38</b>
7.1 Origins of the supercritical CO <sub>2</sub> cycles . . . . .	38
7.2 Fundamentals of the supercritical CO <sub>2</sub> cycle and comparison against gas and steam cycles . . . . .	39
7.3 Candidate sCO <sub>2</sub> cycles for CSP-STE applications . . . . .	41
7.4 Expected thermal performance of CSP-STE power plants based on sCO <sub>2</sub> cycles . . . . .	45
7.4.1 Results . . . . .	45
7.4.2 Compared Analysis . . . . .	47
7.5 Expected economic performance of CSP-STE power plants based on sCO <sub>2</sub> cycles . . . . .	49

7.5.1	Capital costs . . . . .	49
7.5.2	Capital cost breakdown . . . . .	51
7.5.3	Levelized Cost of Electricity . . . . .	53
7.6	Projects under development worldwide . . . . .	55
7.6.1	North America . . . . .	55
7.6.2	Europe . . . . .	57
7.6.3	Rest of the world . . . . .	57
<b>8</b>	<b>Conclusions</b>	<b>60</b>
<b>9</b>	<b>References</b>	<b>61</b>

## 1 Executive Summary

The purpose of this document is to analyze the state-of-the-art of the CSP technology, focused on the solar tower configuration, and the possibility of integrating a supercritical CO<sub>2</sub> (sCO<sub>2</sub>) cycle to substitute the traditional steam cycle. To that end, the document is divided in six sections. The first section presents a description of the fundamentals of Concentrating Solar Power (CSP) technology for the production of solar thermal electricity (STE). In the second section, a review of the solar subsystems is provided, describing the solar field, receiver and Thermal Energy Storage (TES) system. This second section incorporates a detailed description of all the key components present in a CSP facility, familiarizing the reader with the current state of the art of the technology. In the next section, the power block of the CSP plants is reviewed and the usual steam cycles used in contemporary CSP facilities are discussed. After this analysis, a description of the economics of state-of-the-art solar tower plants is carried out, including a discussion about the expected cost reductions and market deployment in the mid and long terms. A study of possible hybridization solutions is performed in the fifth section, under a decarbonization scenario. The last section scrutinizes the supercritical CO<sub>2</sub> technology, both its fundamentals and a the potential application to CSP plants. This section approaches the technology from the technical and economic standpoints, akin to the preceding sections about state-of-the-art CSP plants based on steam turbines.

Overall, this document provides an insightful review of the Best Available Technologies for CSP applicatons that are either currently available or foreseen in the near future, along with the pathways to be followed in the short term to improve the performance of this power generation technology.

## 2 Fundamentals of CSP for STE

### 2.1 Introduction to CSP-STE Technologies

The global energy demand will increase by more than a quarter by 2040, owing to the higher standards of living overall and to the foreseen population growth, estimated at 1.7 billion, both of which effects will be more visible in developing countries [1]. The current energy sources are carbon intensive, hence contributing to increasing the concentration of carbon dioxide which represents over 70% of the greenhouse gas emissions worldwide [1, 2, 3, 4] and is the largest contributor to climate change. To compensate for the latter effect, several renewable technologies, such as photovoltaic panels or wind technology, have experienced a noteworthy development in recent years. Both technologies constitute a major source of affordable, environmentally-friendly electricity into the power generation landscape, but also bring about additional requirements for the reliable operation of power systems, thus stressing the grid [1].

Concentrating solar power (CSP) technology, on the other hand, has the potential to provide cheap, CO<sub>2</sub>-free electricity in locations with appropriate environmental conditions. Also, this technology allows for an easy integration of thermal storage systems (TES) able to store the energy required to operate the power plant at full capacity for up to 17 hours, hence enabling 24 hours of uninterrupted electric power generation. This capacity allows the system to tailor the production of electricity production to the instantaneous energy demand [5, 6, 7, 8]. Power dispatchability is therefore a unique feature of CSP-STE, setting it apart from other renewable energy sources like wind or solar-photovoltaic.

CSP-STE technologies are usually divided in four main categories, according to the configuration of the elements collecting and concentrating solar energy: linear Fresnel, parabolic dish, parabolic trough and solar tower. This is shown in Figure 1(a). In parabolic trough and linear Fresnel systems, the mirrors track the sun along one axis (line focus) whereas tracking has two degrees of freedom in solar towers and parabolic dish systems (point focus). Also, the receiver remains fixed in linear Fresnel and solar tower systems, while it changes position in parabolic trough and parabolic dish systems [9]. Among these technologies, only parabolic trough and solar tower are deployed commercially at a relevant scale.

In parabolic trough technology, the energy of the sun is concentrated by a linear trough resulting from a parabola extruded normal to its plane, and reflected onto a receiver tube running along the inner side of the collector [10]. The energy concentrated on the outer wall of the receiver is transferred to a heat transfer fluid (HTF), commonly synthetic oil, flowing inside and this HTF eventually transfers this energy to the power block where electricity is produced in a conventional steam turbine. Parabolic trough technology can also be integrated with existing coal-fired plants or combined cycles [11]. Solar power towers convert solar power into electricity using a large number of sun-tracking mirrors, also called heliostats (Figure 2), which focus sunlight on a receiver located atop a very high tower [12]. The HTF that flows inside the receiver (commonly molten salts or water/steam), or the water/steam flow in a direct steam generation embodiment, is heated by this sunlight and then used directly or through a conventional steam generator in a steam cycle to produce electricity. Linear Fresnel technologies [13] use flat or slightly curved mirrors mounted on trackers at ground level and configured to reflect sunlight onto one or more receiver tubes located above the mirrors. A small parabolic mirror is sometimes added atop the receiver to further concentrate the sunlight. Parabolic dish systems consist of a parabolic-shaped point focus concentrator in the form of a dish that reflects solar radiation onto a receiver located at the focal point [12]. These concentrators are mounted on a structure with two degrees of freedom which enable perfect tracking of the sun. The energy collected is typically used by a heat engine directly, mounted on the receiver and moving with the dish structure. Stirling and Brayton cycle engines are the usual prime-movers of choice for this applications [9].

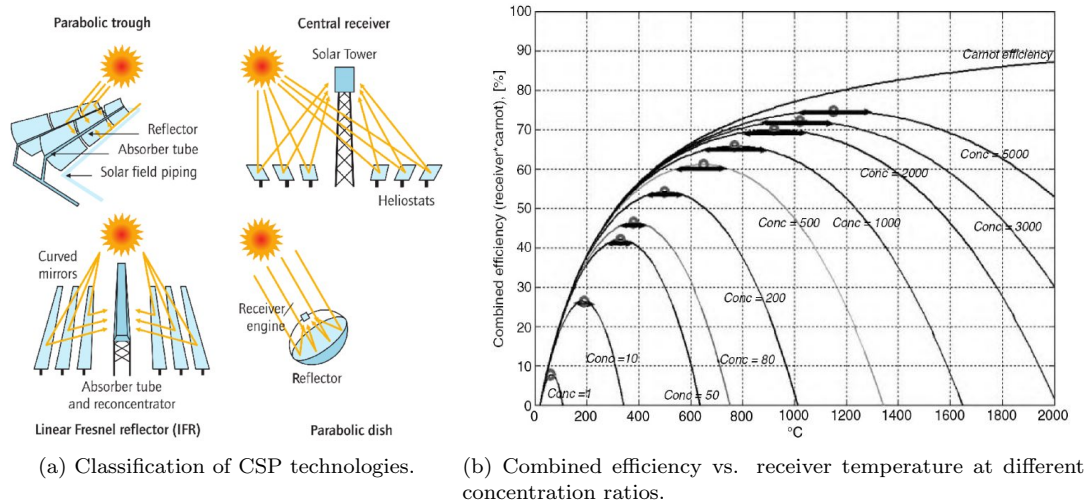


Figure 1: Solar technologies classification and limits.

The concentration ratio of each collector type is tightly linked to the maximum temperature that can be achieved at the receiver and, therefore, the maximum solar-to-electric conversion efficiency of the system. This is shown in Figure 1(b) where the dependence of the combined efficiency of receiver and power block on receiver temperature and concentration ratio becomes evident. For very high temperatures, the efficiency of the power block increases but the heat losses from the receiver more than compensate this effect, and the opposite is true for very low receiver temperature. The only means of achieving high receiver and power block efficiencies at higher temperature is increasing concentration ratio.

Linear technologies such as linear Fresnel and parabolic trough have concentration ratios lower than 100, which limits their performance according to the foregoing statement. Linear Fresnel has even lower efficiency than parabolic trough due to the losses inherent to the approximation of the true parabola by an array of flat mirrors. On the other hand, the concentration ratio of the parabolic dish is highest amongst the existing technologies, reaching values close to ten thousand. The disadvantages of the parabolic dish technology is the limited scale (due to the strong wind loads on the dish) and difficulty to enable Thermal Energy Storage. Accordingly, the parabolic dish technology ends up being a direct competitor of PV in the marketplace, but with higher costs and no visible advantages [14].

Parabolic trough technology has low concentration ratios, but it is still deployed commercially worldwide thanks to moderate capital costs and high technological maturity. The peak operating temperature is currently limited to 400°C as this is the maximum temperature achieved by the heat transfer fluids available. The integration of TES in parabolic trough technologies is easy, and it is commercially available using molten salts. Yet, as said, the maximum temperature of the TES system is limited by the maximum operating temperatures of the parabolic trough.

The concentration ratio of solar tower technologies lies between those of parabolic troughs and parabolic dish, in the order of several thousands. The upper limit for this concentration is nonetheless not set by optics but by receiver materials and HTF stability. Typical operating temperatures in the receiver of a solar tower plant are 565°C, set by the HTF (molten salts when indirect steam generation is used) or the steam turbine (if direct steam generation is used), with concentration ratios close to 1000. The solar tower technology is already proven, with different operational plants around the World. Moreover, the technology is still at the first part of the learning curve and thus strong cost reductions must be expected.

	Technology type			
	Linear Fresnel	Parabolic trough	Solar tower	Parabolic dish
Concentration ratio	60	80	1000	5000
Maximum Temperature	200	400	600	1200
R&D status	demonstration	commercial	early stage commercial	commercial
Global plant efficiency	15	16	19	24 [15]

Table 1: Comparison of CSP technologies.

In order to accommodate (i.e., to provide the necessary operating conditions for a meaningful integration of) Supercritical CO<sub>2</sub> power cycles, the receiver temperature of a CSP-STE plant must reach ca. 700°C. Such a high temperature can only be reached by point focusing technologies, in particular solar towers at the large scale, as explained before and presented in Figure 1(b). This is the reason why SCARABEUS is focused on solar tower technology whilst the other collector types are disregarded.

## 3 Review of Solar Subsystems

### 3.1 Solar Field

The solar field is responsible for collecting and concentrating the solar resource and for delivering it to the receiver. Solar energy is a sparsely distributed resource which needs to be concentrated to enable the high temperatures that are needed in a thermal power plant. Due to its scattering and low energy density, large collection (aperture) areas are necessary to collect the energy that is needed by a commercial-scale power cycle. In solar tower technology, there are two main factors under consideration for the solar field: the elements that reflect the sunlight onto the receiver, namely heliostats, and their distribution on the field.

Heliostats are comprised of a supporting structure, a mirror surface and a tracking system, Figure 2. The tracking system enables the relative movement whereby the mirrors follow the sun and ensures that the reflected beam aims at the receiver correctly. The aiming point is defined by a central system and each heliostat has an internal computer to calculate the correct, instantaneous relative positioning based on the position of the sun and the aiming point. For tracking purposes, the heliostats have two degrees of freedom which, in practice, are implemented as rotation around two axes. These axes might or might not be perpendicular. The most common configuration is the azimuth-elevation tracking system but there are other proposals like the target-aligned [16] or the slope-drive [17] tracking. Nowadays, tracking algorithms are not able to compensate dynamically for the sunspot position during operation. Also, the algorithms assume a rigid supporting frame not affected by external influences such as wind or weight deformation, and need to be calibrated periodically to correct any miss-tracking. Several self-calibration systems have been proposed, but there is not a commercial solution yet.



Figure 2: Abengoa heliostat with 8x4 facets.

The mirrors are the critical part of the heliostats. They are responsible for reflecting the sun rays onto the receiver. The highly reflective surface is typically a silver layer encapsulated between two protective layers. The upper layer is a glass or glass-like surface that protects the reflective layer from harmful environmental agents such as moisture, corrosion or abrasion. The back surface is normally a copper layer with protective paint. This surface is glued to the supporting structure by different techniques. For the glass surface, low weight

requirements are desirable but not critical, given that the main contributor to the mechanical design of the frame is wind loads and not weight. The critical property for the glass surface is optical performance, such as high transmittance (low iron composition), long lifetime with reduced O&M costs, easy cleaning and, in some cases, high flexibility. Aluminium and various metals are other possibilities for the reflective layer but they are less common in commercial applications.

State-of-the-art heliostats can achieve aperture areas of more than  $100 \text{ m}^2$ , such as Abengoa ASUP  $140 \text{ m}^2$  or Sener HE54  $178.5 \text{ m}^2$  [18]. The reflective surface is composed of an array of smaller mirrors called facets, as seen in Figure 2. To reduce the size of the reflected spot on the receiver surface, these facets are not contained on the same plane. On the contrary, the supporting frame provides an inclination to each individual facet so that all of them aim to the same point. This inclination is called canting and its effects can be seen in Figure 3. Sometimes, the facet is also curved to achieve a further reduction of the size of the solar spot on the receiver. Canting and curvature of facets can be used independently.

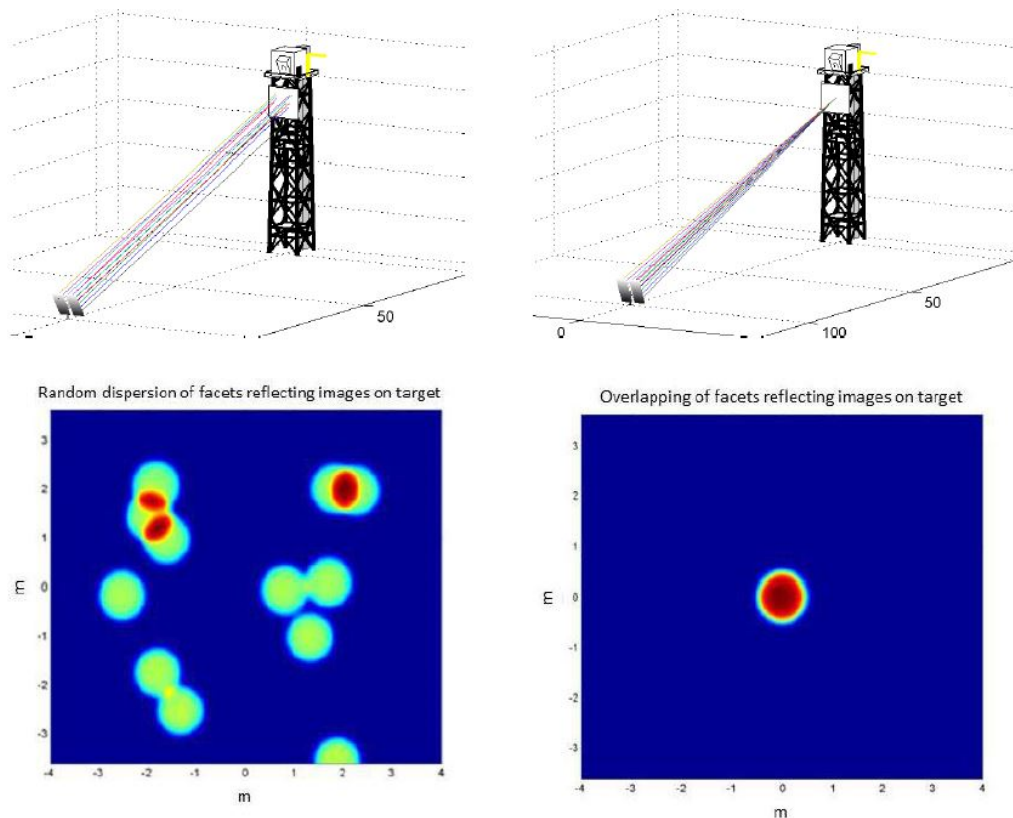


Figure 3: Effect of canting on the receiver [16].

The supporting structure keeps the mirrors in position and avoids deformations that could compromise the precision of the heliostat, which is tightly linked to the rigidity of the supporting structure. In order to apprehend how important this is, it is worth noting that the distance from the heliostat to the tower can be as long as 1 km, hence turning small variations of the heliostat geometry into several meters of aiming error at the receiver. The supporting structure has an important share of the total cost of the heliostat, and different designs have been proposed to reduce the associated weight (hence costs) and, if possible, reduce deformations. The foundations of the structure are usually made of concrete, specially for the larger heliostats. Smaller heliostats

make use of pedestals (poles) drilled into the ground directly, ground anchors or gravity-supported structures [16]. The type of foundation is selected based on the type and size of the heliostat to be installed, since a large number of small heliostats (with less costly foundations and shorter installation times) could make concrete foundations or even drilled-pedestals prohibitive. On the other hand, increasing the size of the heliostat is actually an opportunity to reduce costs due to the reduced number of actions in spite of the deeper installation of each foundation. The opposite happens for the drives. The smaller heliostats can use simpler and cheaper drives, while the larger ones need more robust and expensive drives to move the supporting frame and mirrors whilst avoiding unwanted movements as a consequence of wind or gravity loads.

In line with the foregoing discussion, heliostats of different size have been proposed, with a general trend towards larger sizes to reduce individual costs such as wiring, control boxes and other components. This scale-up of the heliostats increases the requirements of the supporting frame and reduces its accuracy. Therefore, a medium-size heliostat has recently been proposed as a compromise solution; nevertheless, there are no operational and economic data available yet to assess the economic gains relative to the +100 m<sup>2</sup> state-of-the-art heliostats.

There are five effects influencing the efficiency of a solar field layout: cosine  $\eta_{cos}$ , atmospheric attenuation  $\eta_{aa}$ , spillage  $\eta_{sp}$  (also called intercept factor), shadowing (both by the tower  $\eta_{st}$  and by neighbouring heliostats  $\eta_{sh}$ ) and blocking  $\eta_{bl}$ . These parameters vary for each heliostat and time instant, and they are normally evaluated for a certain time of the year. Globally, the efficiency of a particular layout is determined by a combination of the previous effects.

The different patterns used to distribute the heliostats on the field aim to maximize global efficiency, focusing on a reduced number of parameters or on a combination of them, due to the complexity of analyzing the whole problem. A lot of research has been devoted to this topic, and discussions are still ongoing. No optimal field or pattern has been found, and each project develops its own layout specifically for the site.

$$\eta = \eta_{cos} \eta_{aa} \eta_{sp} \eta_{st} \eta_{sh} \eta_{bl} \quad (1)$$

Due to the fixed position of the receiver on the tower, solar beams do not strike normal to the surface of the mirrors. Therefore, the effective area of the heliostat is smaller than the geometrical (aperture) area. The associated *cosine* losses are defined by the angle between the solar beam and the normal to the heliostat surface defines, Figure 4, which means that the cosine factor depends on the position of the heliostat relative to the tower, this effect being stronger for heliostats in the south field (considering that the plant is located in the Northern hemisphere). The cosine effect is purely geometrical and its impact is specific to each sun position.

The characteristic lengths involved in a typical solar tower field are very long and hence it is mandatory to account for the scattering of solar radiation across the air between heliostat and receiver. In general, atmospheric attenuation is caused by three main compounds: gases, aerosols and clouds. Gases have approximately constant concentration except for water vapour, whilst the concentration of clouds and aerosols fluctuates in space and time. This effect is usually modelled with the Lambert-Beer-Bouquet transmittance model which depends on local visibility through the extinction coefficient (Equation 2):

$$Attenuation = e^{-\sigma \Delta m} \quad (2)$$

Spillage represents the amount of reflected solar beams that miss the receiver surface. There are several reasons for this, such as a bad aiming strategy, tracking errors, undesirable movement of the heliostats due to wind loads or overflow of the sunspot on the receiver surface. This last effect occurs when the heliostat is far enough from the receiver and the reflected image size is larger than the receiver surface.

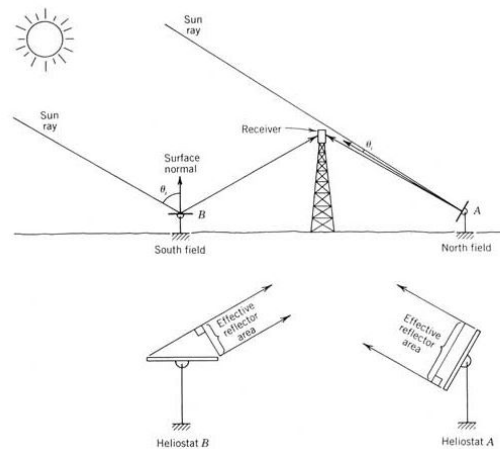


Figure 4: Cosine effect [19].

When the sun is low in the sky (morning and evening), some of the heliostats project their shadow on a neighbouring heliostat which, as a result, is partially covered as shown in Figure 5. At the same time, the shadow of the tower over the solar field covers a number of heliostats, an important effect that is sometimes ignored in order to simplify the optimisation problem. Blocking is similar to shadowing but, in this case, the interception of beams takes place after these have been reflected, as shown in Figure 5 also.

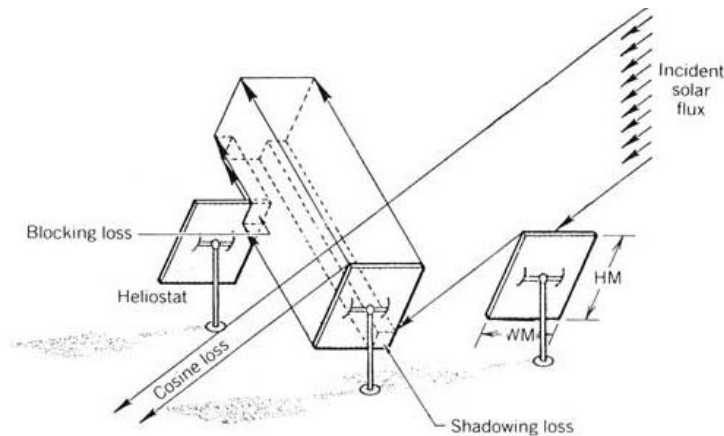


Figure 5: Combined effect of blocking, shadowing and cosine [19]

All these parameters depend largely on the height of the tower and the size of the receiver through the relative position of each heliostat, adding complexity to the heliostat-distribution problem. It is due to the complexity of this problem that different patterns are proposed for the positioning of heliostat positioning, the most studied of which are cornfield, radial stagger and spiral [20, 21, 14, 22]. Some authors propose the combination of these patterns to increase the efficiency of the solar field [23, 24] whilst other propose a free-pattern system to maximise the global efficiency [25, 26, 27, 28]. This pattern-free system is very promising, but the computational requirements are too high to be considered aside the academic field. A different approach to this problem is performed by Carrizosa et al. [29], where the utilisation of heliostats of different size in the same field is proposed.

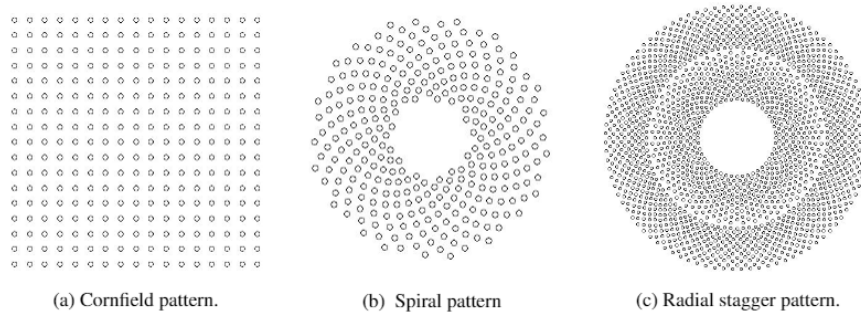


Figure 6: Heliostat distribution patterns.

At the moment, there are important limitations regarding materials of the receiver and stability of the HTF at high temperature. These constraints limit the amount of heat flux that can be delivered onto the receiver. It is then mandatory to develop an aiming strategy that yields an homogeneous flux over the receiver, avoiding hot or cold spots. Aside from the loss of efficiency, those spots can be dangerous for the equipment inasmuch as hot spots can trigger the degradation of the salts and receiver materials while cold spots can lead to solidification of the molten salts. The aiming strategy has been studied by different authors [30, 31, 32, 33], and is a well kept secret for each solar company. One of the main difficulties on this field is to get knowledge of the real aiming point of each heliostat. There is no reliable way of determining the exact pointing of each heliostat, nor the exact amount of flux over the surface of the receiver.

### 3.2 Receiver

A solar receiver is nothing but a heat exchanger. It absorbs the concentrated solar flux coming from the field of heliostats and transfers it to a working fluid (molten salt or water/steam) in the form of either temperature rise, phase change or both. Several classifications are possible according to criteria such as:

- Heat transfer fluid: air, CO<sub>2</sub>, particle suspensions, water/steam, molten salts, thermal oil, liquid metals, solid particles, helium, hydrogen [34].
- Geometry and/or arrangement of the absorption plane (surface impinged by the concentrated solar flux): external or cavity receivers.
- Internal layout of the heat exchanger: tubular, volumetric, suspension of particles, falling film receivers.

The evolution of commercial solar tower plants for electricity generation can be tracked through the geometry of the absorption plane. The first generation used cavity receivers in order to reduce losses while external receivers gained relevance later, in order to increase the aperture area of the receiver and, with it, the power output. In cavity receivers, concentrated sunlight enters the receiver across the aperture plane (window) and is trapped inside, hence bringing about fewer heat losses than an external receiver where the absorber is exposed to intense heat exchange with the environment. This apparently high absorption capacity makes cavity receivers especially favourable when a high operating temperature is sought, for instance when pursuing higher solar shares (i.e. the fraction of heat input to the cycle coming from concentrated solar energy in hybrid CSP-STE plants) [35]. Cavity receivers may also incorporate a secondary concentrator mounted in front of the aperture area [35].

In external arrangements, the incident solar irradiation strikes the outer surface of the receiver. Losses due to heat exchange with the environment are higher, but this configuration allows a larger solar field which increases the maximum power output and reduces the strict requirements on aiming strategies and tracking errors. Different configurations are known for this technology, such as the cylindrical plane or crescent receiver,

the truncated receiver, billboard receiver or flat-plate tubular panel [36].

The heat transfer fluid in contemporary solar towers is molten salts or water/steam, thus state-of-the-art receivers are based on these fluids. Nevertheless, other options to increase the efficiency of CSP technology using gaseous, liquid or solid HTFs are under development.

### 3.2.1 Gas Receiver

Gas receivers can be divided into (i) volumetric, (ii) tubular and (iii) particle suspension types depending on the configuration. It is nevertheless noted that even though suspension receivers are also included in this section, they should lie in a different category. Volumetric receivers (i) may be classified into atmospheric and pressurised systems, none of which enable storage, making it necessary to include an intermediate medium for that purpose. This type of receiver is usually integrated into an open loop configuration in combination with a steam Rankine cycle. A blower forces a stream of air through the absorber material and, in turn, air achieves a higher temperature. A waste heat recovery boiler downstream of the receiver takes advantage of the energy carried by the air flow to generate steam and eventually drive a turbine. It is interesting to note that the PS10 power plant in Spain, which is currently using a cavity receiver for direct steam generation, was originally conceived as an atmospheric air receiver [37].

Pressurised receivers have mostly been considered for gas turbine applications where they are installed downstream of the compressor to increase the temperature of compressed air. A closed loop configuration consists of a volumetric receiver receiving pressurised air at low or moderate temperature (this depends on the pressure ratio of the engine) and delivering it at a higher temperature either to a supplementary combustor in series or to the turbine directly. It is easily deduced that the lower the temperature gap between receiver outlet and turbine inlet, the higher the solar share and hence the lower the carbon footprint of the electricity produced. Pressurised air receivers are widely regarded as an alternative to fossil fuels, addressing issues such as increased efficiency, reduced water consumption and higher flexibility and dispatchability through hybridisation [38]. High pressure operation makes it necessary to install transparent windows to effectively separate the receiver cavity from the environment. The reliable operation of this window turns out to be critical to achieve the aforementioned goals both in terms of performance and reliability.

Tubular air receivers (ii) can conceptually be integrated into open loop or closed loop configurations depending on the design pressure of the air flow although, historically, the integration into a Brayton Cycle is the usual approach. The SOLUGAS plant was the first megawatt scale hybrid gas turbine system operating on concentrated solar energy and natural gas simultaneously [39]. It was designed, constructed and operated by Abengoa Solar at the Solúcar Platform in Seville, Spain. The receiver was a tubular cylinder comprised of 6 metre long pipes with a total diameter of 5 metres. Neither secondary concentrator nor glass window were considered. The design specifications were an outlet temperature of 800°C and 80% efficiency. The demonstration phase was successful and confirmed the operability/feasibility of the system [40].

A dense suspension of particles (DPS) is a combination of the classical solid particle heat transfer medium and an air/gas stream (iii). It takes advantage of the high temperature properties of solid particles and the easy handling of gases. The DPS consists of very small particles which can be fluidised at low gas speeds, thus being easily transported similarly to a gas. The operating principle of a DPS receiver relies on creating the upward circulation of a DPS (solid fraction in the range 30-40%) in vertical absorbing tubes subjected to concentrated solar energy irradiation. The higher the particle velocity, the higher the heat transfer coefficient, due to the increase in particle agitation. In addition, the higher the particle volume fraction, the higher the heat transfer coefficient, since particles occupy a larger volume and hence the contact area with the tube walls is larger as well [41]. The main advantages of this technology are the capability to reach high temperatures of up to 1000°C [42] and the possibility to be used directly as a storage solution. Also, from the point of view of reliability and safety, the lack of freezing issues and risk of explosion are very positive features of particles.

### 3.2.2 Liquid Receiver

There are different configurations of liquid receivers under study, but the only promising and already commercial type are the tubular receivers. Tubular receivers have been developed and used in various projects since the 1980's (demonstration plants Solar One [43], Solar Two [44], RAS [45] and CESA-1 [46] are some remarkable examples). Fluids typically used have been water/steam and molten salts. Alternative fluids mentioned in literature but not implemented commercially are carbonates, chlorides and metals [46]. Using water as a basic fluid has important environmental advantages but there are also several shortcomings. Amongst the former, it is worth noting the almost null environmental impact of any water/steam leakage and the direct use of this fluid as working fluid in the Rankine power block. Amongst the disadvantages, the maximum heat flux that the receiver is able to withstand, in the range from 200-500 kW/m<sup>2</sup>, and the lower thermal capacity when compared to molten salts or sodium. The first commercial projects implementing these receivers used saturated steam at intermediate pressure and temperature (PS10 and PS20), due to design (all the receiver as evaporator), safety (lower risk of hot spots due to absence of superheater) and operability (just wet steam production) concerns. Later commercial projects though, like Khi Solar One or Ivanpah, used superheated steam as working fluid with temperatures over 500°C [47]. Even if a superheated steam receiver increases the complexity in terms of design and operation, it enables higher efficiencies in the Rankine cycle.

Molten salt receivers (typically a mixture of NaNO<sub>3</sub> and KNO<sub>3</sub>) are, on the other hand, getting more and more usual in the commercial projects that are currently under development and construction. The main reason for this popularity is the implementation of thermal energy storage systems, which are currently considered a mandatory feature of this technology (for dispatchability considerations). Indeed, in tubular receivers using molten salts, a fraction of these are sent to the steam generator (heat exchanger) whilst the remaining flow is sent to a hot insulated tank for storage. Another clear advantage of using molten salts is the higher heat flux admissible on the solar receiver surface (due to a higher heat capacity of the fluid flowing on the inside), which enables higher concentration factors than for steam technology, hence higher efficiencies. Accordingly, the utilisation of molten salts brings about a generalised increase in performance both at component and system levels. Amongst the shortcomings, the decomposition of salts limits the operational temperature to less than 600°C [48], a very large inventory of salts is needed (in particular when large storage capacities are incorporated), and the freezing point increases to over 220°C, which requests auxiliary equipment to prevent solidification. Nonetheless, in spite of these operational and constructive difficulties, the number of molten salts based power plants in the pipeline is not declining. A more detailed explanation below can be found in Section 3.3.

### 3.2.3 Solid Particle Receiver

The concept of falling solid particles receiver consists of sand-like ceramic particles falling across a directly illuminated cavity receiver whilst absorbing heat by radiation. This concept enables easier implementation of storage capability and scale-up of the technology, hence exploiting the thermal properties of solid particles. Ceramic materials such as alumina, silica and zircon are good candidates, and other materials like iron-doped Al<sub>2</sub>O<sub>3</sub> spheroid have also been proposed for the particles [49]. Receivers with windows and aerowindows have been considered with expected efficiencies in the range of 80%, even if the prototypes have not exceed 50% [50]. In this regard, there are some parameters of influence that have to be taken into consideration in the design phase, such as type of particle [51, 52] and the aerowindow air jet flow [53, 54]. Other innovative solutions like the use of magnetic fields to increase the residence time and thermal absorptance of particles, as well as to reduce the particle flow destabilisation, have been assessed with computational models [55]. From an experimental standpoint, a centrifugal particle prototype has been designed by DLR with a thermal power of 500 kW and target particle temperature of 900°C; this prototype is expected to be tested in the near term at the Jülich tower facility [56]. On the negative side, technical solutions for other aspects like heat exchanger design and particle conveyance technologies are noted as important concerns for this technology. In this regard, remarkable

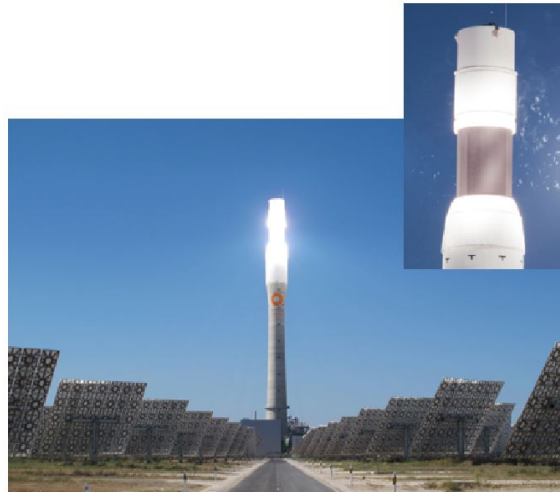


Figure 7: Liquid, external tubular receiver developed by Torresol ©.

research is going on at Sandia National Labs, where various solutions are being developed and tested, with the aim to demonstrate a complete unit at the small scale [57, 58]. Finally, regarding the practical implementation of solid particles receivers into the power plant, this category of receivers can be integrated into the power cycle through a fluidised bed heat exchanger. Steam or gases are possible heat transfer fluids, depending on heat exchanger design, thus both Rankine and Brayton cycles are feasible power block technologies.

### 3.3 Thermal Energy Storage System

Thermal energy storage solves the mismatch between solar energy supply and electricity demand, providing a distinctive advantage of STE plants over other renewable technologies like wind or photovoltaic [10]. To date, electrical energy storage using batteries at the large scale is not technically or economically feasible [59, 60, 61, 62, 63, 64] in comparison with other energy storage technologies like Thermal Energy Storage. No problems of shortage of storage media like water or nitrate mixtures are foreseen in the future, contrary to the uncertainty regarding lithium batteries, where large a much larger demand is foreseen within the next years [65]. Solar power plants with thermal energy storage systems can have different operational strategies, depending on the daily variations of supply/demand profiles. TES systems can be integrated to perform the following functions [66, 67]:

- Mitigation of short fluctuations during transient weather conditions, e.g. cloudy periods. Those periods of inclement weather can force the turbine to be operated in transient conditions, thus reducing the turbine efficiency due to start-up losses. Even if heat transfer fluids have some thermal inertia that could help the plant continue operating during short cloudy periods [68], the experience with large-scale facilities shows that it may not be enough to prevent turbine shut-down [69]. Small capacity storage systems could help to mitigate these short fluctuations of solar radiation.
- Shifting the generation period from peak hours of solar insolation to peak hours of power demand. Thermal energy storage systems can improve dispatchability by storing energy during off-peak hours and then discharging it during hour of peak demand [10].
- Extending operation beyond sunset, hence acting as baseload electricity generation and improving the annual capacity factor (this requires much larger solar fields than in plants without storage). This annual capacity factor is defined as a performance parameter that compares the net electricity delivered by the solar facility to the energy that could have been produced should the plant have been operated at full capacity throughout the year. Given that the solar resource is only available during some hours of the

day, thermal energy storage systems can improve the capacity factor enabling power generation when the sun is not available.

Two different thermal energy storage technologies are currently implemented in commercial solar thermal electricity plants: (i) steam accumulation in direct steam generation plants, and (ii) two-tank molten salt systems in either parabolic trough with thermal oil or solar tower with molten salt indirect steam generation plants.

### 3.3.1 Storage based on steam accumulation

Water can be used as heat transfer fluid and storage medium in so-called Direct Steam Generation (DSG) plants. DSG is commercially available today and it eliminates the need for intermediate heat transfer fluids while increasing overall plant efficiency and reducing the environmental impact. The steam produced in the receiver is supplied directly to the turbine without any intermediate heat exchanger. In addition, the limitations on peak operating cycle (live steam) temperature set by the degradation of the thermal oil (above 400°C) or nitrate molten salts (above 565°C) are released which enables more efficient power cycles [70]. Furthermore, investment costs are reduced due to the elimination of intermediate equipment.

Actually, steam accumulators are the only commercial TES solution for DSG plants. A steam accumulator is an active direct storage system based on the Ruth accumulator system, where steam is stored at high pressure in accumulator tanks directly. As of September 2019, there are only three commercial tower plants in operation using steam accumulators to store thermal energy: PS10, PS20 and Khi Solar One, all of them developed by Abengoa. PS10 and PS20 started commercial operation in 2007 and 2009, respectively, and they became not only the first two commercial solar towers in the world but also the starting point for the operation of direct steam generation technology. These first generation CSP towers use saturated steam as shown in Figure 8.

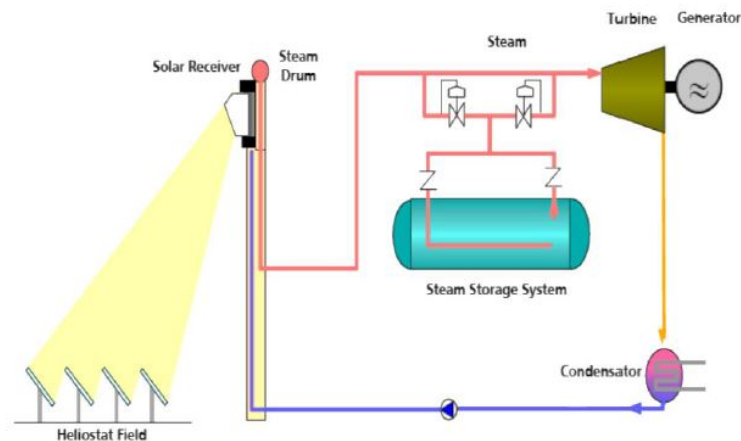


Figure 8: Schematic flow diagram of a direct steam generation tower plant with thermal energy storage system based on steam accumulation.

The second generation of CSP-DSG plants make use of superheated steam (Khi Solar One, 2016). In these superheated steam solar towers, a second receiver with the main function to re-heat the steam produced by the first receiver (evaporator) is needed, enabling higher temperatures than in first generation plants. Live steam, which feeds the turbine, can thus reach temperatures and pressures in excess of 540°C and 130 bar, thereby enhancing the efficiency of the power cycle by 30% relative to its forerunner PS20. Khi Solar One, a 50 MWe superheated steam tower, has a storage capacity of around 2 hours thanks to nineteen steam accumulation tanks which store saturated steam produced in the evaporators. This steam feeds the turbine when needed, enabling

power generation even when there is no sun. This is shown in Figures 9 and 10.

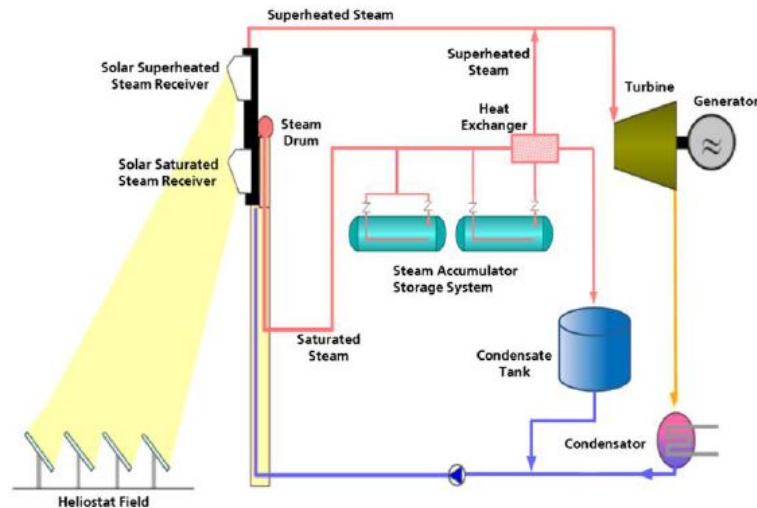


Figure 9: Schematic flow diagram of a direct superheated steam generation tower plant with thermal energy storage based on steam accumulation.



Figure 10: Steam accumulators in Khi Solar One.

Steam accumulators use sensible heat storage in the form of pressurised saturated liquid water [71], where the liquid and gaseous phases are in thermodynamic equilibrium. They profit from the high volumetric storage capacity of liquid water for sensible heat due to its high specific heat capacity [72]. Water is used as both storage medium and working fluid, so high discharge rates are possible, while the storage capacity is limited by the volume of the pressure vessel. The specific energy storage capacity depends strongly on the variation of saturation temperature resulting from the pressure drop during the discharge phase, with characteristic values in the range of 20-30 kWh/m<sup>3</sup> [72].

A steam accumulator is a steel pressure tank designed to withstand high pressure and temperature water/steam. Figure 11 shows a schematic representation of a steam accumulator, including its internal components. Steam accumulators usually have cylindrical bodies and elliptical bonnets, as this is the most effective shape from a mechanical standpoint, and they are made of carbon steel. For the design of such equipment, it is important to take thermal cycling into account to ensure that the material is able to withstand the continuous operation under variable conditions. To avoid problems related to thermo-mechanical stress in the accumulators,

temperature gradients in the vessel walls must be limited. Furthermore, even if the materials commonly used in these equipment are well-known, corrosion phenomena due to water impurities should not be overlooked. Finally, there are limitations regarding the maximum size of each steam accumulator, mostly due to peak pressure and to transportation concerns. However, several units can work in parallel to meet the total thermal energy storage requirements of the plant.

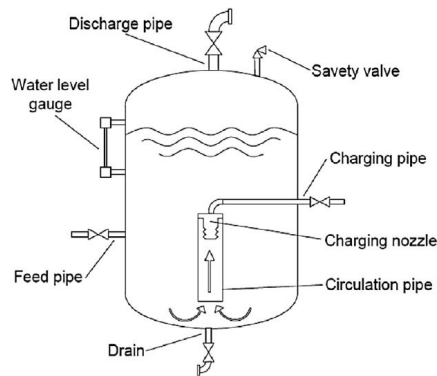


Figure 11: Variable-pressure steam accumulator [71].

During operation, steam accumulators are partially filled with water, commonly ranging from 50% to 90% of the total volume. The accumulator system is charged with the surplus saturated steam produced in the evaporator receiver (not used to produce superheated steam for the turbine). This surplus steam is injected into the pressurised storage vessel by means of a distribution manifold, which is fitted with steam injectors or nozzles. The nozzles are a crucial component in a steam accumulator due to their variable performance (injection rate) as the pressure in the vessel increases. The steam injected by the nozzles forms bubbles that increase the pressure of water/steam, leading to a higher saturation temperature. When correctly designed and operated, steam from a steam accumulator is clean, with steam quality approaching unity. During the discharge phase, steam is produced by lowering the pressure of the saturated liquid. When the pressure inside the tank drops, flashed steam is generated at the rate demanded by the power block and the water level inside the tank falls.

If superheated steam is desired, a separated higher-pressure steam accumulator is needed along with a steam/steam heat exchanger to reach superheated conditions. The final result is an increase in cycle efficiency and, therefore, the global efficiency. Khi Solar One uses this two pressure level steam TES configuration effectively.

### 3.3.2 Storage based on molten salts

Molten salt is the most widespread storage material in commercial CSP applications due to its good thermal properties and reasonable cost. Nowadays, molten salts provide a thermal storage solution for the two most mature technologies available in the market (i.e., parabolic trough and solar tower) and they can be used in either direct or indirect storage configuration, depending on the solar field technology of the plant under consideration. In either case, trough and tower technologies, the configuration of the storage system is based on two tanks, at high and low temperature. This concept was successfully demonstrated in different solar thermal demo plants [73]: CESA-1 (Spain) [74, 75], Themis (France) [76, 77], CRTF (USA) [78], Archimede (Italy) [79, 80] and Abengoas 8.1 MWh<sub>th</sub> storage capacity TES-MS (Spain) [81, 82, 83]. The 10 MWe Solar Two demonstration tower plant in USA also demonstrated a 105 MWh<sub>th</sub> storage capacity TES system successfully [69, 84, 85], and it is actually considered the first pre-commercial scale two-tank molten salt storage system.

Solar Two operated from 1996 to 1999 and helped validate nitrate salt technology and reduce the technical and economic risks of molten salt technology [70].

Commonly used molten salts are based on nitrate mixtures with a weight composition of 60%  $\text{NaNO}_3$  and 40%  $\text{KNO}_3$  and an operating temperature range between  $290^\circ\text{C}$  (freezing point is  $240^\circ\text{C}$ ) and  $565^\circ\text{C}$  (limited by thermal degradation). This fluid is usually called Solar Salt and, nowadays, it yields optimum cost and thermal properties for the CSP industry. These sodium and potassium nitrate mixture has been very well known by the solar industry for decades, with wide bibliographic information and proven feasibility at both pilot and commercial scales [86, 87, 69, 73, 74, 75, 76, 78, 79, 80, 81, 82, 83, 84, 85]. However, corrosion phenomena is still an ongoing topic for research, and material compatibility due to impurities in these mixtures is yet to be optimised. Nevertheless, satisfactory performance with the most common materials used in the solar industry can be assured [73, 88, 89, 90, 91, 92, 93].

Due to the strong demand for molten salts by the CSP industry, an active search for suitable molten salts mixtures to be used as heat transfer fluid and storage material has been going on in the last years [6, 94, 95]. In addition to the Solar Salt, the most relevant molten salt candidates to be used in solar thermal power plants are Hitec salt, a ternary mixture of  $\text{NaNO}_2$ ,  $\text{NaNO}_3$ , and  $\text{KNO}_3$ , and Hitec XL<sup>®</sup>, a ternary mixture of  $\text{Ca}(\text{NO}_3)_2$ ,  $\text{NaNO}_3$ , and  $\text{KNO}_3$  [96]. These two ternary mixtures have been considered as potential replacement for the standard Solar Salt due to their low freezing point,  $142^\circ\text{C}$  and  $120^\circ\text{C}$  respectively [10]. However, their maximum operating temperature is also significantly lower than that of the Solar Salt. Hitec is thermally stable at temperatures up to  $454^\circ\text{C}$  and it may be used at temperatures up to  $538^\circ\text{C}$  but for a short period of time only [97]. Hitec XL, a mixture of 48%(wt)  $\text{Ca}(\text{NO}_3)_2$ , 7%(wt)  $\text{NaNO}_3$  and 45%(wt)  $\text{KNO}_3$  may be used at temperature up to  $500^\circ\text{C}$  [10, 98, 99, 100, 101, 102, 103].

In general, molten salts are an interesting storage material due to its high energy storage capacity (per specific volume) and very high thermal inertia (high heat capacity and low thermal conductivity). These thermal properties allow designing storage systems with minimum thermal losses, increasing the global efficiency of the plant. Nevertheless, using molten salts to store thermal energy has inherent risks due to their high freezing point. Electric heat tracing systems and tank heaters are installed to minimise the risk of a freezing event and to avoid critical thermal gradients during start-up. However, these equipment involve high parasitic consumption to maintain the salts in molten state even when the system is completely discharged.

### 3.3.3 Steam Generator

In solar towers using molten salt technology, there are one or more trains of heat exchangers to transfer the energy from the molten salts to the working fluid of the cycle. This working fluid is usually water, which is evaporated and superheated. This process is carried out in two or more heat exchangers. Standard configurations include an economiser to preheat water, a boiler for evaporation, a superheater to increase the temperature of saturated steam and a reheater to increase the temperature of steam that has been partially expanded in the high-pressure section of the turbine. All these heat exchangers are usually of the shell and tube type, with the molten salts flowing on the shell and steam flowing inside the tubes, also for the evaporator. This configuration is nevertheless not standard in the industrial shell and tube boilers, where steam is on the shell side. In molten salt steam generators, molten salts are always on the shell side to simplify the electric heat tracing and to avoid possible salt freezing. This decision is not unanimous in the industry, with different suppliers preferring to have water boiling on the shell side in a standard kettle configuration as typically used in waste heat recovery applications. The tubes are also heat traced but, in this case, with steam coming from an auxiliary boiler. To facilitate free draining and natural circulation, all heat exchanger and piping are installed staggered and with a minimum slope of 10%. The pressure drop across the exchangers is minimised to reduce auxiliary electric power consumption.

## 4 Review of Power Block

### 4.1 Fundamentals of Rankine Cycles for Steam Turbines

Power cycles convert energy in the form of heat  $Q_{in}$  received from a source at high temperature  $T_H$  into shaft work  $W_{shaft}$ . The fraction of energy put into the cycle that is not converted into work is rejected as heat  $Q_{out}$  to a low temperature sink at  $T_L$ . This is shown in Figure 12.

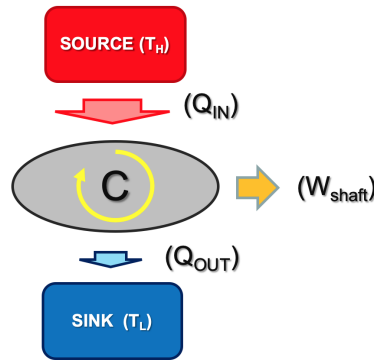


Figure 12: Elementary power cycle.

The restrictions set forth by the First and Second Laws of Thermodynamics imply that the amount of heat rejected to the low-temperature sink be not null ( $Q_{out} > 0$ ), and that the total amount of energy and entropy being exchanged be balanced<sup>12</sup>:

$$Q_{in} = Q_{out} + W_{shaft} \quad (3)$$

$$\frac{Q_{in}}{T_H} + \Delta S = \frac{Q_{out}}{T_L} \quad (4)$$

Where  $\delta S$  stands for the production of entropy within the system (cycle). From Eqs.(3,4), the following mathematical expression to calculate 1<sup>st</sup> Law efficiency can be obtained:

$$\eta_{1st} = \frac{W_{shaft}}{Q_{in}} = \left(1 - \frac{T_L}{T_H}\right) - \frac{T_L \cdot \Delta S}{Q_{in}} \quad (5)$$

Given that, according to the 2<sup>nd</sup> Law,  $\Delta S \geq 0$ , it follows that the highest efficiency is achieved by a reversible engine for which  $\Delta S = 0$ :

$$\eta_{Carnot} = 1 - \frac{T_L}{T_H} \quad (6)$$

In an actual power plant (or engine), heat addition and heat rejection do not take place at constant temperature nor are the energy exchange and conversion processes reversible. Therefore, this efficiency  $\eta_{Carnot}$  sets a higher limit of efficiency which cannot, in practice, be achieved. Nevertheless, the following guidelines for the thermodynamic assessment of power cycles can be drawn:

<sup>1</sup>Not that these conservation equations apply to non-reacting systems where heat and mechanical work only are involved.

<sup>2</sup>In the remainder of this section, it is assumed that heat is added to and rejected by the cycle at constant temperature.

- Heat addition at the highest possible temperature and heat rejection at the minimum temperature possible favour high cycle efficiencies.
- Most of the times, heat addition and rejection do not take place at constant temperature, what increases the irreversibility of these processes. In these cases, the concept of mean thermodynamic temperature of the process might be useful:

$$\bar{T}_{H/L} = \frac{Q_{in/out}}{dS_{in/out}} \quad (7)$$

With this new tool, the foregoing statement can be reworded as follows: **heat addition at the highest possible mean temperature and heat rejection at the minimum mean temperature possible favour high cycle efficiencies.**

- Reducing the irreversibility of the thermo-mechanical energy conversion devices like pumps, compressors and turbines favour high cycle efficiencies.

This simple analysis suffices to assess the interest and limitations of the power cycles commonly used in Concentrated Power Plants and also to evaluate the potential of other cycles like those based on supercritical Carbon Dioxide.

The Carnot cycle is the only cycle able to achieve the efficiency quoted in Eq.(6), as long as both heat transfer between the cycle and the source/sink and thermo-mechanical energy exchange are carried out reversibly. Such cycle is presented in Figure 13 and, even if very efficient, it suffers from very low specific work (i.e., power output per unit mass flow rate of working fluid) inasmuch as most of the work produced by the expander is consumed by the compression process. Additionally, it also happens that the temperature difference between the source and the hot working fluid and between the cold working fluid and the sink is a source of irreversibility, as so are the compressors and turbines. As a result of this, not even a practical Carnot engine would be able to achieve the efficiency quoted above.

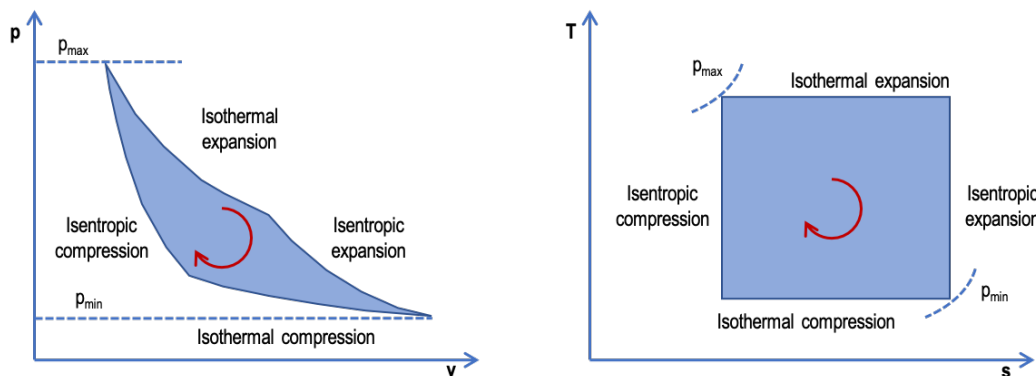


Figure 13: Ideal Carnot cycle.

The Rankine cycle is another embodiment of a power cycle which aims to get as close to the Carnot cycle as possible, thermodynamic-wise. It is characterised by a isothermal/isobaric heat rejection in the condenser, close to ideally isentropic compression of the working fluid in liquid state, isobaric heat addition at variable temperature (except for the phase change part of heat addition) and isentropic expansion. This is shown in Figure ?? for a cycle were compression and expansion are irreversible (non-ideal cycle) and heat addition experiences a non-negligible pressure drop (ca. 20%). The main design parameters of the cycle are:

- Live steam temperature: live steam temperature should be as high as possible in order to enable higher thermal efficiencies, as deduced from Eq.(6). This is limited by either steam turbine materials (this would be the case of a coal power station or a steam turbine in a modern combined cycle power plant) or by

a the temperature of the heat source (this is the case of a Concentrated Solar Power plant where the temperature of the Heat Transfer Fluid is limited by thermo-chemical stability).

- Live steam pressure: high live steam pressure are usually sought as these bring about higher thermal efficiency. Nevertheless, very high turbine steam pressures have a negative effect on cycle efficiency as a consequence of a drastic reduction of specific output (kJ/kg). Therefore, for each live steam temperature, an optimum value of live steam pressure can be found.
- Condenser pressure: reducing the saturation temperature in the condenser has a very strong positive effect on cycle efficiency, according to Eq.(6). Indeed, lower condenser pressures enable much larger turbine expansion ratios which, even though requiring more complex turbine designs, boost specific output substantially.

Condenser pressure is therefore set to the minimum possible value enabled by ambient conditions and by the cooling technology of choice (whether air or wet cooling). In practice, this translates into condenser pressures ranging from 50 to 150 mbar (5 to 15 kPa).

The design space where the values of these parameters can be set is nevertheless bounded by mechanical constraints. In addition to the pressure and temperature limitations, already cited, the most noteworthy limiting factor is humidity. The condensation of steam along the expansion path brings about thermodynamic (supersaturation) and aerodynamic losses which reduce the gross output delivered by the turbine. In practice, increasing live steam pressure and reducing condenser pressure both bring about lower steam quality at turbine exhaust, preventing the cycle from achieving the theoretical, peak thermal efficiency. In order to sort this problem out, it is customary to reheat the working fluid halfway through the expansion process. Partially expanded steam is hence heated up again at constant pressure and then expanded again in the turbine. This shifts the expansion line rightwards in the Mollier diagram what has the effect of leaving the exhaust steam closer to saturated conditions. In practice, steam quality should not be lower than 0.8 if the life of blades in the last stages is to be not compromised [104].

Reheat has thus the objective to increase steam quality in the low pressure section of the turbine and, with this, increase the isentropic efficiency of this component. This has a positive impact on thermal efficiency of the cycle. Additionally, when performed at the correct pressure, reheat brings about a thermodynamic benefit beyond that associated to the better aerodynamic performance. This optimum reheat pressure is between 20 to 25% of the pressure at turbine inlet (live steam) and enables some 4-5% higher thermal efficiency than in non-reheated cycles [105].

The heat addition process is comprised of three different steps. Water delivered by the pump is heated up to the saturation temperature in the economizer, which is an open heat exchanger. Saturated water is evaporated in the evaporator, usually a closed-circuit heat exchanger with either forced or natural circulation. Finally, saturated steam is heated up to the target live steam temperature. Amongst these process, the economizer has a very negative effect on cycle efficiency due to its very low temperature and large enthalpy rise (note that condensate flows into the economizer at around ambient temperature and flows out at the saturation temperature corresponding to live steam pressure, around 340°C). In order to raise the average temperature of (external) heat addition to the cycle, it is customary to preheat the feedwater delivered by the pumps before entering the steam generator. This is done from within the cycle, in a series of feedwater heaters whose heat source is steam bled from the turbine. This steam from the turbine is bled at different locations along the flowpath, in order to accommodate its the corresponding saturation temperature to the target feedwater temperature at the outlet from the preheater. As a result of this, the duty of the economizer (and of the entire steam generator) is reduced and the efficiency of the cycle increases, despite the lower expansion work [105].

Akin to the reheat process, the process of selecting the temperature rise across each feedwater heater, the total number of heaters and the precise location (stage) at which steam is bled from the turbine allows for some optimization. Extracting steam at higher pressure enables a lower mass flow rate for the same heating capacity but it also reduces the enthalpy change of the bled steam flow. Overall, the following general rule of thumb can be put forward, as a simplification of the recommendation provided by Haywood [105]: ”**for maximum**

**efficiency in a non-reheat plant, the feedwater enthalpy rise should, to a first approximation, be the same in all heaters and in the economizer**". This rule applies to non-reheat plants and refers to enthalpy change across each feedwater heater. Nevertheless, it provides a good starting point to be applied to reheat cycles, also applied to temperature rise: **"for maximum efficiency in a reheat plant, the feedwater temperature rise should, to a first approximation, be the same in all heaters and in the economizer"**. This is inaccurate inasmuch as the temperature rise across the feedwater receiving steam from the first extraction port downstream of the reheating process enables a larger temperature rise, and the contrary applies to the last extraction port upstream of the reheater. Nevertheless, it is again stated that this simple rule provides a good approximation from which further cycle refinement can be carried out with simple tools and little computational burden.

A final comment regarding optimization of feedwater heating trains is mandatory when it comes to Concentrated Solar Power plants. Feedwater temperature at the outlet from the last heater before the steam generator is linked to the outlet temperature of the Heat Transfer Fluid serving as heat carrier, be it molten salts or synthetic oil. Therefore, feedwater temperature might be constrained by the minimum temperature of the heat transfer fluid. For molten salts, this is related to freezing of the salts. For synthetic oils, this comes determined by the higher viscosity at low temperatures which can potentially increase pumping power in the solar field significantly. In either case, the final temperature of feedwater in a Concentrated Solar Power plant might be driven by these operational constraints rather than by the thermodynamic optimum.

The layout of a state-of-the-art Concentrated Solar Power plant using tower technology and steam turbines is shown in Figure 14. The following elements are worth noting:

- Live steam temperature is limited by the temperature of molten salts at the outlet from the solar receiver (and hot tank).
- Live steam pressure is at the optimum value balancing specific output and thermal efficiency.
- Reheat is performed at about at one fourth the pressure at the inlet to the high-pressure section of the turbine.
- Reheat temperature is again limited by the temperature of molten salts.
- Steam quality at the outlet from the low-pressure turbine is slightly below 20%, close to the allowable limits of conventional steam turbines.
- A very large number of feedwater heaters are supplied with steam bled from the turbine at different extraction ports. All these heat exchangers work with similar terminal temperature difference.
- The temperature of feedwater at the inlet to the steam generator is such that the molten salt stream returning to the cold tank is above the freezing point (220-240°C). This constraint is of a stronger priority than the optimum temperature rise distribution from a thermodynamic standpoint.

## 4.2 Power Block in a CSP-STE power plant

To extract the thermal energy of the HTF and transform it into mechanical work, most CSP plants use a Rankine cycle. In this cycle, the power block is responsible for generating electricity from the thermal energy carried by the working fluid (water/steam on state of the art CSP plants). The high temperature and high-pressure steam obtained in the steam generator passes through a machine called turbine, where this steam moves a shaft that, in turn, moves a synchronous generator, transforming the thermal energy into mechanical energy and then into electricity that is eventually exported to the grid. A more detailed explanation of the water/steam power block is provided later.

Commercial solar tower plants today make use of a steam Rankine cycle, operated on demineralised water. Water at the outlet from the condenser is pumped towards the steam generator by low and high pressure pumps and through a number of heat exchangers (feedwater heaters) fed by high pressure/temperature steam bled from the turbine. The steam generator receiving this high temperature subcooled water is then responsible

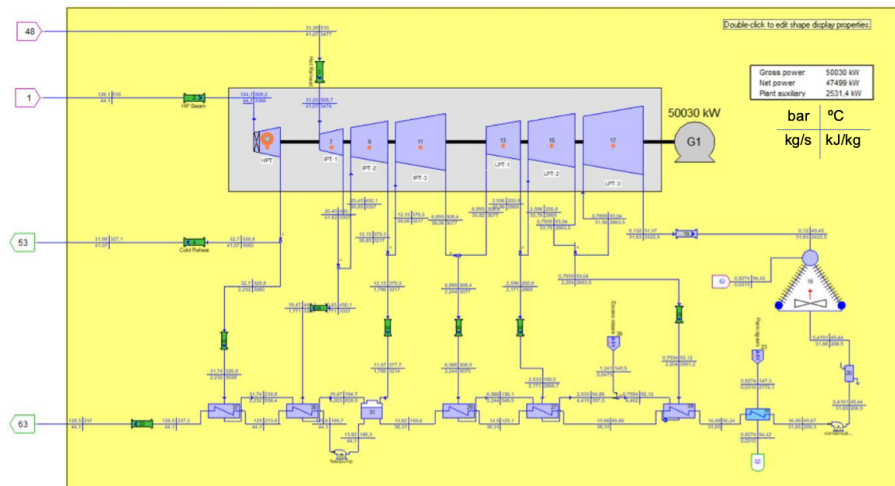


Figure 14: Heat balance of a state-of-the-art Concentrated Solar Power plant using tower technology.

for the production of superheated steam, for which aim it makes use of high temperature molten salts produced by the tower (and stored in the high temperature storage tank). The superheated steam flow coming out from the steam generator is then directed to the turbine where it is expanded to produce shaft power to drive the electric generator. Once expanded to the lowest possible pressure (determined by ambient temperature and condenser technology), the exhaust steam from the turbine is sent to the condenser where it reaches the liquid state again. The associated latent heat is rejected to the environment by means of either water or air cooling.

The main components of the power block are:

- Main cooling system and condensate tank. Most CSP plants today make use of Air Cooled Condensers. In these, exhaust steam from the turbine flows inside inclined, finned pipes on the outside of which ambient air is forced by a number of fans. Older plants made use of water cooled condensers with forced draft cooling towers but this is not used today in an attempt to reduce water consumption of the plant.
- Condensate (low-pressure) pumps are usually two stage pumps that operate with a high vacuum on the suction side.
- Feedwater heating system. Between the condensate tank and the steam generator, a number of heat exchangers are responsible for increasing the temperature of feedwater in order to increase the thermal efficiency of the cycle. These shell and tube heat exchangers take steam from the turbine at high or low pressure and transfer the associated sensible/latent heat to the feedwater flow. Additionally, this turns out beneficial to ensure that the temperature of molten salts in the economiser does not fall below the freezing point. The number of feedwater heaters is in the range from 4 to 6.
- Deaerator. One of the feedwater heaters is nevertheless not of the shell and tube side. Indeed, halfway from the condensate tank to the steam generator, an open heater is used with the same purpose as the heaters mentioned in the foregoing bullet point. Additionally, this large storage tank is used as a reservoir of hot water which can quickly react to a water demand by the steam generator if the plant is ramping-up or operating in transient conditions.

The deaerator is located at the highest elevation of the power block and it is usually sized to enable at least five minutes operation at full load. The water level inside the deaerator is kept at about 70% when the plant operates in stationary conditions.

Finally, the deaerator is also responsible for removing oxygen and other dissolved gases that may be present in the working fluid.

- Feedwater Pumps are usually multi-stage, volute type centrifugal pumps. These pumps, located at the outlet from the deaerator, are responsible for increasing the pressure of feedwater as required by the steam

turbine. The power consumption of these high-pressure pumps is hence not negligible.

- Solar steam generator. The heat transfer fluid in an indirect steam generation plant transfers thermal energy to produce high pressure steam. This steam Generator is comprised of four different heat exchangers: superheater, reheater, evaporator and preheater (or economiser). More information has already been provided in an earlier section.
- Steam turbine. Steam turbines in CSP plants are usually arranged in two sections, high and intermediate-low, with reheat in between them. They are usually assembled on the same shaft along with the electric generator, all rotating at either 3000 or 3600 rpm. The usual gross output of these turbines is 50-100 MWe even though cost optimisation suggests increasing this to 150-200 MWe.

### 4.3 Auxiliary systems of the power block

In order to be able to compare the steam cycle with other alternative cycles like sCO<sub>2</sub>, it is important to note that the power cycle requires auxiliary systems for operation during both start-up and shutdown manoeuvres and also for normal operation (either at full or partial load). The most important auxiliary components are described below:

- Turbine bypass lines (HP and LP): the HP bypass line must be able to manage up to 100% of the steam generator outlet stream, reducing both pressure and temperature down to cold reheat conditions. The LP bypass line performs the same action on the hot reheat steam flowing out from the reheater, whose pressure and temperature are reduced to acceptable conditions to enter the condensate tank. In both cases, high and low pressure, these bypass valves are required to act very rapidly.
- Intermittent/continuous blowdown: removal of dissolved and undissolved solids in water is mandatory in order to control conductivity and other quality parameters of the working fluid. The continuous blowdown (or surface blowdown) is used to remove dirty water (with dissolved solids and impurities in suspension) and replace this by fresh water. The intermittent blowdown has the main purpose of draining dirty water from the bottom of the steam generator (with mud and sediment that accumulates in this area) and replacing this with clean water.
- The lube oil system supplies oil for the turbine-generator assembly elements that are lubricated: bearings, turbine overspeed bolts, turning gear bearings and mechanical drive, oil pumps and seal oil systems. This lube oil circuit must also incorporate oil coolers in order to ensure accurate and reliable management of lube oil temperature.
- An auxiliary boiler is often used to start up the power plant. Initially, the auxiliary boiler generates steam in order to increase piping pressure and temperature (especially piping towards the HP and LP turbines). Steam from the auxiliary boiler is also used to heat the deaerator.
- Gland sealing system. Gland steam is steam used to reduce the amount of steam leaking out of the turbine through the gaps between rotating and stationary turbine parts (mostly casing and shaft but also valve stems and others) and to prevent air from flowing into the water/steam circuit at the low-pressure end of the turbine (which remains below atmospheric pressure). Steam used in the gland seal system is usually condensed in an independent, dedicated condenser rather than in the main condenser. This gland steam condenser operates at a higher pressure than the main condenser and it is cooled by the condensate flowing from the condensate tank to the deaerator.
- Ejector or vacuum pump. These elements enable the low pressure that is needed in the condenser, also ensuring that this turbine exhaust pressure is within the range recommended by the manufacturers of turbine and condenser during start-up or transient operation but also in stationary operation if that is needed.
- Demineralised water production is performed in the treatment plant where raw water is treated to comply with the specific purity requirements defined by the steam cycle. In normal operating conditions, water consumption is mostly due to blowdown in the steam generator, venting from the deaerator and leakage (structural leakage, valves not properly sealed, etc.). The amount of make-up water to compensate for this water consumption in a steam cycle is lower than 2% of the rated mass flow rate but this can change depending on the operation of the cycle (for instance, it will expectedly increase in power plants with

continuous start-ups and shutdowns).

#### 4.4 Design and performance of the steam cycle

As already discussed, the basic steam cycle is optimised with a certain number of extractions in the turbine, and generally with a reheated steam (from cold reheat to hot reheat) in the steam turbine. The turbine expansion process normally ends in the liquid-vapour zone, with the associated appearance of moisture in the last stages of the turbomachinery. The appearance of wet steam causes aerodynamic and even mechanical problems that compromise the performance and mechanical integrity of the turbine.

In order to increase steam quality at turbine exhaust, it is customary to reheat the steam stream halfway through the expansion, between the high pressure and low pressure steam turbine cylinders; this also increases the efficiency and output of the turbine. Additionally, fractions of the expanding steam (extracted from the turbine at certain locations along the expansion line) are used to preheat the feedwater stream flowing from the condensate tank and towards the steam generator, in order to further enhance the efficiency of the power block. Increasing the feedwater temperature at the inlet to the steam generator has the additional benefit of increasing the temperature of the heat transfer fluid (whether molten salts or thermal oil), hence reducing the risk of freezing events and/or minimising pumping power in the solar field.

A typical steam cycle is shown in Figure 15 where the reheat and preheating section are easily identified. The main performance and operating parameters of the cycle, depending on the type of concentration technology, are also shown in Table 2.

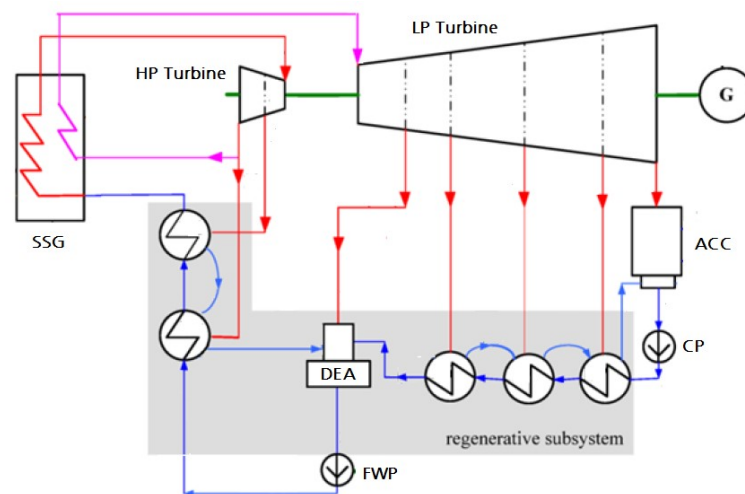


Figure 15: Layout of the power cycle in a state-of-the-art Concentrated Solar Power plant.

#### 4.5 Transient operation mode and control strategies of the steam cycle

In order to maximize the performance and profitability of the power plant, it is essential to optimize the performance when operating in partial load. Therefore, the steam turbine must be designed for:

- daily start-up and shutdown;
- rapid start-up times.

Parameter	Parabolic trough	Central receiver
Net maximum output power ( $MW_{el}$ )	200	150
Net efficiency (%)	37	41
Inlet temperature steam turbine ( $^{\circ}C$ )	383-388	545-555
Inlet HP steam turbine ( $^{\circ}C$ )	120-130	120-150
Extraction number of the steam turbine (-)	6	6-7
Condensation pressure, dry cooling ( $mbar_a$ )	80-120	80-120

Table 2: Operating and performance parameters of a steam power cycle in CSP applications.

The daily start and stop manoeuvres of CSP plants is influenced by mechanical considerations strongly. In addition, steam turbines are subject to high thermal stresses during transient operation, which occurs frequently owing to the variability of solar radiation. In this regard, Thermal Energy Storage, for instance based on molten salts, provides thermal power supply even when sun rays are not available. This increases the number operating hours significantly, either at full or partial load, and even enables continuous operation during the night. As long as the economics make sense, this largely reduces the consumption of energy that is needed to keep the facility warm (hence avoiding freezing in critical sections containing molten salts), to generate steam in the auxiliary boiler and to preheat the cycle before start-up during sunrise in a sunny day.

Regarding the best control strategies of steam cycles, sliding pressure is the optimal turbine control strategy in a Concentrated Solar Power plant. When this mode is used, the following counteracting effects are balanced in the best possible way:

- the thermal efficiency of the cycle is reduced because live steam pressure decreases;
- the thermal efficiency of the heat exchange process in the steam generator is enhanced;
- the blading efficiency of the steam turbine remains approximately constant, in particular the first stages.

As a result of this, the performance decay incurred when operating the power block in partial load based on sliding live steam pressure mode is very small.

#### 4.6 Current development trends of steam cycles in CSP plants

Presently, there are several programs aimed at encouraging technological development to lower investment costs and LCoE of CSP plants. Regarding the power block, the steam cycle does not have much potential for improvement with its current design. Therefore, in order to be more competitive in this section, in addition to the development of alternative power cycles with better performance such as the supercritical Carbon Dioxide cycle ( $sCO_2$  cycle), the evolution of the conventional subcritical cycle could drift towards:

- scaling up the power block based on state-of-the-art steam technology, which would expectedly bring in strong economies of scale;
- in addition, adopting supercritical steam cycles with an expectedly better performance and whose subsequent development would also be able to bring about further cost reductions.

## 5 Techno-Economic Status of Solar Tower Plants

Solar tower technology is a relatively new technology. So far, there are just ten solar tower power plants in operation worldwide [106]. Nevertheless, the experience accumulated to date is promising, and several other projects are under construction (such as Cerro Dominador in Chile, a molten salt tower with 10600 heliostats and a huge storage capacity equivalent to 17.5 operating hours at full capacity). A more detailed list of the solar tower plants in the world, either in operation or in the planning and construction phase, can be found in Table 3. As easily deduced from the list, the number of solar tower plants in operation is substantially lower than the number of working parabolic through power plants, even though the efficiency of the latter is lower than of the solar tower plants. This different level of development is due to some key aspects that solar tower technology must improve to become fully competitive:

- High costs of key components owing to the few Original Equipment Manufacturers that are producing them.
- High financial costs, due to the incipient commercial deployment.
- Low reliability as experienced by some of the plants currently in operation.
- Economies of scale not yet achieved and fully exploited.

The foregoing bullet points are being targeted by both the industry and the R&D community, providing promising results and improvements at a very high pace. The sector is actually under an intense developing period, and the associated electricity prices are decreasing. Noor III Project has reached the best economic performance ever achieved by CSP in terms of USD/MWh, and it is expected that solar tower projects will achieve even lower values in the near future, as represented in Figure 16. Interestingly, Central Receiver Systems (CRS) have the largest potential for cost reduction potential due to the lower maturity (total installed capacity), as opposed to parabolic trough technology, to the lessons learnt in currently operational plants and to the capability to reduce the financial constraints. In this latter regard, increasing the reliability of the plants is a mandatory, crucial step. Speed-up of the ramping up/down capacity and design and operation learning curves are taking longer than expected and this, when coupled to the not so high plant performance, has produced a lack of confidence on the technology as perceived by the potential end-users. In order to revert this situation, the lessons learnt in the plants that are currently in operation have to be applied in the next projects that are already in the pipeline, thus recovering the trust of the potential end-users and contributing to making CSP become a cost-effective and reliable solution. By de-risking the CSP projects, lead lenders will become more confident and the financial costs will decrease substantially. These expectations are also shared by IRENA, as it can be seen in Figure 17. The costs of all renewable technologies are decreasing, but the highest reduction foreseen is for Concentrated Solar Power.

This foreseen reduction needs to be achieved thanks to the combination of different strategies: cost reduction of the key components, new developments, new improvements, improving the supply chain, utilization of local manufacturing, build-up of the demand, new monetizing strategies, etc. The cost of the key components will be reduced by achieving mass production when more projects are constructed, but more R&D actions in the solar field and molten salt components are also necessary in order to adapt both elements to the market needs. Both components have an important share in the total budget of a solar tower power plant, and any improvement or cost reduction of these components largely benefits the total cost of the plant. Also, improving cycle performance, i.e. achieving higher efficiency, is a goal to be achieved in a bright future is sought for solar tower technology. With a higher power block efficiency, the size of the solar field that is needed for a given power output is reduced and, with it, the total cost of the plant. This cycle improvement can be accomplished by upgrading the contemporary steam cycles or by adopting new power cycles such as the sCO<sub>2</sub> cycle discussed later in this document (and adopted by SCARABEUS). Moving to a new cycle is nevertheless not an easy task, and it must hence be analyzed in detail prior to its implementation in a commercial plant; to this end, an important R&D effort is needed. Improving the supply chain and using local manufacturing is a common



Figure 16: Total installed costs of CSP plants by technology and storage capacity [107].

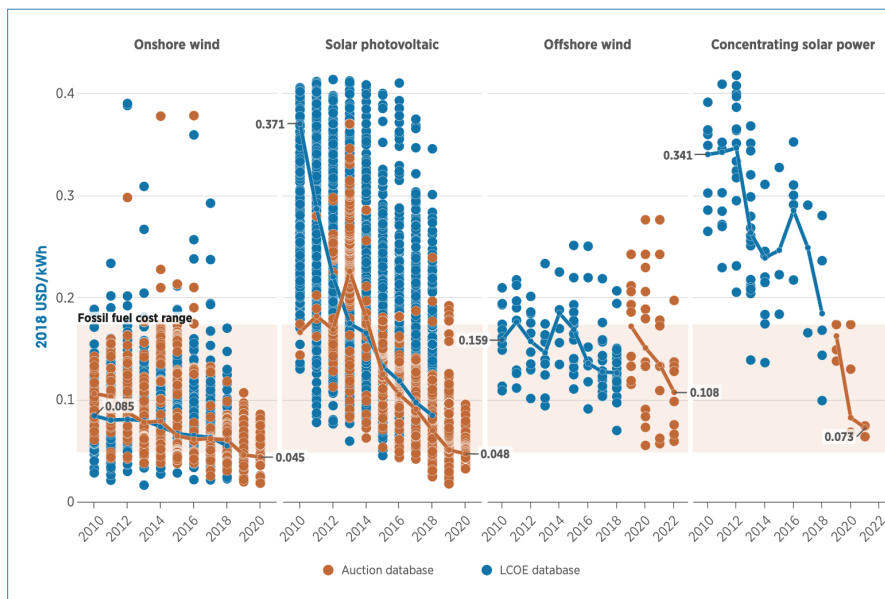


Figure 17: Levelized Cost of Electricity of different projects and globally-weighted average for different renewable technologies [107].

strategy for several industries which is also applicable to CSP, even if with some difficulties due to the highly skilled workforce that is needed by solar tower plants, which implies training the local industries to be able to produce and deliver with the strict standards used by the CSP industry. Besides this, the foreseen increase in

the demand for this technology will also increase the number of providers, therefore reducing the cost thanks to both the exploitation of economies of scale and the development of new manufacturing techniques and procedures, accompanied by standardisation efforts.

Economies of scale will help reduce the costs but it will also pose a series of challenges. As a matter of fact, the logistics for an actual solar tower power plant are quite complicated. Only for the solar field, more than thirty trucks arrive to the site on a daily basis, and some large components have to be transport assembled, with large slow trucks that could affect the normal utilization of roads negatively, hence requiring traffic control and the involvement of transport authorities. For a scaled-up project, these problems will do nothing but increase in severity. Therefore, in order to avoid increasing the logistic-related costs, a detailed monitoring of the solar product supply chain must be applied.

At the moment, one of the most common ways of monetizing a solar tower plant is through a power purchase agreement (PPA), which sets a fixed selling price of the energy produced by the plant. These agreements usually last for 25 years, leading to uncertainty about how the plant will be exploited afterwards. Hence, if the actual lifetime of solar tower plants were considered, an extended period of 35 years could improve the financial model, even if the costs of the components could rise as a result of the new maintenance contracts and guarantee provided by the suppliers.

Finally, the actual value of the CSP concept must be updated in order to account for the flexible dispatching strategies that are provided by the Thermal Energy Storage system. A monetization strategy able to correctly evaluate the flexibility of this technology over other non-dispatchable renewable technologies such as PV or wind should be implemented. This claim is already considered in the last reports of the International Energy Agency [108], where a large increase in PV and wind power capacity is expected, and a cap on renewable is foreseen. To attenuate the effects of this cap, the dispatchable CSP+TES is expected to grow exponentially, providing flexibility to the generation mix of the grid, as shown in Figures 18 and 19.

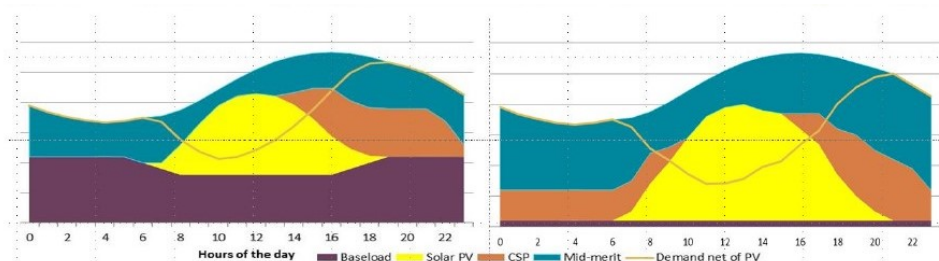


Figure 18: Conceptual daily energy mix with PV and CSP, medium term (left) and long term (right) [1].

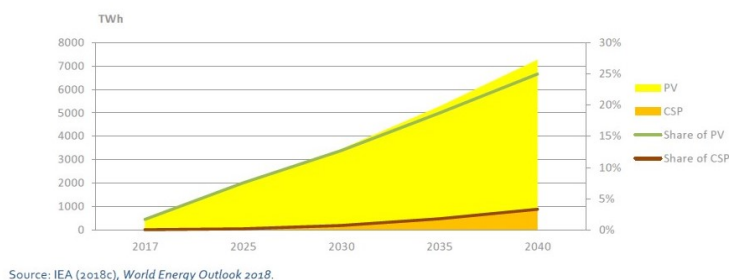


Figure 19: PV and CSP generation in the Sustainable Development scenario. [1]

The increase in demand in addition to the improvements achieved by innovation actions and a new monetizing system able to account for the dispatchability of CSP plants will prove the good health of this technology, needed to proceed to a complete decarbonization of electricity generation without losing the capability to adapt to an increasingly fluctuating demand.

In the mid term, different pathways are under evaluation with the challenge of making CSP cost-competitive. The "Gen 3 CSP roadmap" [109] defines three paths for solar tower technology development to achieve a goal 6 ¢/kWh: the Molten Salts path, the Falling Particle path and the Gas Phase path. The three of them are being explored in depth and a lot of innovation efforts are being dedicated to them, with different difficulties to be overcome as shown in Figure 20. One common particularity to all three paths is the use of a supercritical CO<sub>2</sub> Brayton cycle, described in subsequent sections. The several challenges that this paths pose call for an important effort from the authorities and all the related stakeholders to successfully bring this Gen3 CSP power plants from the R&D phase to a commercial reality.

	Collector Field		
	<ul style="list-style-type: none"> <li>• Cost &lt;\$75/m<sup>2</sup></li> <li>• Concentration ratio &gt;50</li> </ul>	<ul style="list-style-type: none"> <li>• Operable in 35-mph winds</li> </ul>	<ul style="list-style-type: none"> <li>• Optical error &lt;3.0 mrad</li> <li>• 30-year lifetime</li> </ul>
	Molten Salt	Falling Particle	Gas Phase
Receiver	<ul style="list-style-type: none"> <li>• Similarities to prior demonstrations</li> <li>• Allowance for corrosive attack required</li> </ul>	<ul style="list-style-type: none"> <li>• Most challenging to achieve high thermal efficiency</li> </ul>	<ul style="list-style-type: none"> <li>• High-pressure fatigue challenges</li> <li>• Absorptivity control and thermal loss management</li> </ul>
Material & Support	<ul style="list-style-type: none"> <li>• Potentially chloride or carbonate salt blends; ideal material not determined</li> <li>• Corrosion concerns dominate</li> </ul>	<ul style="list-style-type: none"> <li>• Suitable materials readily exist</li> </ul>	<ul style="list-style-type: none"> <li>• Minimize pressure drop</li> <li>• Corrosion risk retirement</li> </ul>
Thermal Storage	<ul style="list-style-type: none"> <li>• Direct or indirect storage may be superior</li> </ul>	<ul style="list-style-type: none"> <li>• Particles likely double as efficient sensible thermal storage</li> </ul>	<ul style="list-style-type: none"> <li>• Indirect storage required</li> <li>• Cost includes fluid to storage thermal exchange</li> </ul>
HTF to sCO <sub>2</sub> Heat Exchanger	<ul style="list-style-type: none"> <li>• Challenging to simultaneously handle corrosive attack and high-pressure working fluid</li> </ul>	<ul style="list-style-type: none"> <li>• Possibly greatest challenge</li> <li>• Cost and efficiency concerns dominate</li> </ul>	<ul style="list-style-type: none"> <li>• Not applicable</li> </ul>
Supercritical CO <sub>2</sub> Brayton Cycle			
	<ul style="list-style-type: none"> <li>• Net thermal-to-electric efficiency &gt; 50%</li> </ul>	<ul style="list-style-type: none"> <li>• Power-cycle system cost &lt; \$900/kW<sub>e</sub></li> </ul>	<ul style="list-style-type: none"> <li>• Dry-cooled heat sink at 40° C ambient</li> <li>• Turbine inlet temperature ≥ 700°C</li> </ul>

Figure 20: Gen3 roadmap for solar tower technology [109].

Project name	Location	Capacity [MW]	HTF	Status	Developer	TES type [h]	TES
DEWA CSP Tower Project	UAE	100	Molten Salt	Under construction	ACWA Power	2-tank direct	15
Planta Solar 10	Spain	11	Water/steam	Operational	Abengoa Solar	Steam accumulator	1
Planta Solar 20	Spain	20	Water/steam	Operational	Abengoa Solar	Steam accumulator	1
Crescent Dunes	United States	110	Molten Salt	Operational	SolarReserve, LLC	2-tank direct	10
Ivanpah Solar	United States	392	Water/steam	Operational	BrightSource Energy	None	-
Cerro Dominador	Chile	110	Molten Salt	Under construction	Abengoa Solar	2-tank direct	17.5
Noor III	Morocco	150	Molten Salt	Operational	ACWA Power	2-tank direct	7
Huanghe Qinghai Delingha	China	135	Water/steam	Non-operational	BrightSource Energy	2-tank indirect	3.7
Luneng Haixi	China	50	Molten Salt	Operational	SEPCO3	2-tank direct	12
SunCan Dunhuang	China	100	Molten Salt	Operational	Shouhang	2-tank direct	11
Gemasolar	Spain	20	Molten Salt	Operational	Torresol Energy	2-tank direct	15
Khi Solar One	South Africa	50	Water/steam	Operational	Abengoa Solar	Steam accumulator	2
Ashalim	Israel	121	Water/steam	Operational	Megalim Solar Power	Steam accumulator	3.7

Table 3: Current operational and under constructions solar tower power plants.

## 6 Hybridization

The share of renewable energy technologies in the global energy mix has increased in the last two decades. There are several reasons for this, for instance the need for alternative energy sources to secure energy supply or to fight rising prices of conventional energies in certain regions, the need to mitigate climate change and the need for a global approach to sustainable development which can eliminate local (and not only global) CO<sub>2</sub> emissions. For these reasons, these technological developments focused on clean energy must be accelerated.

Regarding solar energy, it is widely acknowledged that it is the most abundant energy source on earth and it can be exploited cost-effectively. Photovoltaic technology is cheap, modular and it can be used virtually anywhere. However, one of its main shortcomings is that it is a highly intermittent form of power generation. This brings about issues regarding grid stability. Electric energy storage can be added to improve dispatchability but it is currently too costly to be used at the large scale. Concentrated Solar Power also converts solar energy into electricity and it is also an intermittent form of generation, but it has the added value of dispatchability when combined with thermal energy storage. TES systems are a cost-competitive solution to seamlessly balance energy demand and supply in the grid. In this sense, hybridization of photovoltaic and CSP technologies yields a complementary power generation technology which exhibits the best features of each constituent. In term of flexibility, a certain proportion of CSP with a high thermal storage capacity allows maximum penetration of PV at a more than acceptable cost and with lower curtailment. Therefore, the new hybrid plant combining low-cost renewable energies technologies such as PV or wind, with batteries for fast response, and CSP with TES for long-term dispatchability would be a new hybrid product with a strong potential for cost reduction in solar power generation.

Such hybridization is key in order for these technologies to gain a competitive advantage against traditional power generation based on fossil fuels. A so-called smart solar plant would satisfy a given generation profile during both day and night: the energy generated during the day would come from a highly cost-competitive photovoltaic field whilst, in the evening -when a second peak demand with high prices of electricity must be expected-, the solar thermal plant with storage capacity would go into operation. These are flexible and dispatchable plants that can adapt to the energy demand and where resources are optimized to yield lowest operation and maintenance costs, Figure 21.

This hybrid concept is already under-construction in the Atacama Desert, Chile. The Cerro Dominador power plant, property of EIG Global Energy Partners and developed and constructed by Abengoa and Acciona, will have the capacity to operate at full load (110 MW) continuously (24 hours a day), thanks to a hybrid mix of technologies (CSP / PV / TES /BESS). This unprecedented operating capability is shown in Figure 22.

Different strategies are available for a hybrid CSP plant to exploit power generation economically. One of these is base-load production, presented in Figure 22. Another option would be to concentrate power generation in peak demand periods (where revenues are higher). In this case, the PV system would produce a significant amount of (excess) power that could be stored in the TES system. To accomplish this, an electric heater would be integrated in the plant with low additional technical and financial efforts. The electric heater would transform the excess electricity into thermal energy, which would then be stored in the Thermal Energy Storage CSP if storage capacity were still available. This could also be implemented with electricity originated in a wind farm, as shown in Figure 23.

The first electric heaters for a CSP plant are going to be installed in the recently awarded Noor Midelt I project in Morocco, at an affordable cost. The successful demonstration of this solution is very important since these components can easily be integrated not only in new plants but also in existing plants. This is thanks to the very strong modularity of the heaters, which enable easy retrofitting in existing facilities.

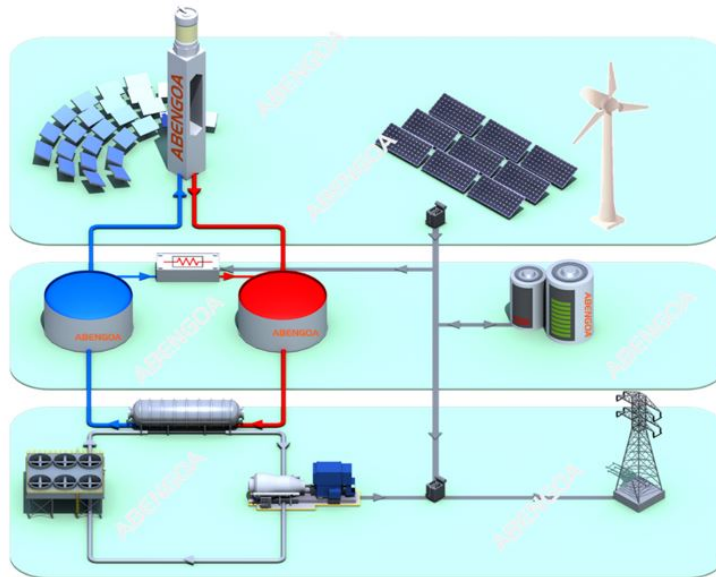


Figure 21: Hybrid CSP-PV-BESS-TES configuration by Abengoa ©

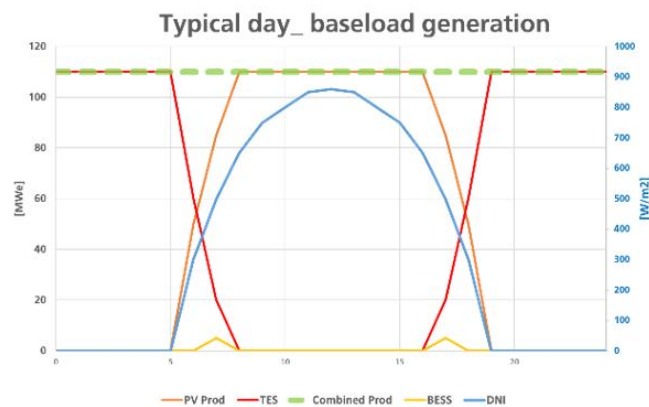


Figure 22: Base-load generation profile of Cerro Dominador, Chile

Aside from the utilization in CSP plants, the integration of molten salt storage, electric heaters and steam generators (operated on molten salts) can provide new life to fossil-fueled or nuclear power plants which would otherwise be dismantled, transforming these plants into strategic energy reserves for the grid. In this configuration, during low demand or low energy price periods, the electric heater would store the excess electricity in the form of thermal energy. Then, when demand of electricity were higher or during growing demand periods, this energy would be used to produce steam that would eventually run the steam cycle of the cited power plants. There are several other possibilities for this technology, such as the integration with conventional coal plants, where steam generation based on molten salts would have the potential to either accelerate start-up by providing thermal energy during to the slower coal boiler, or to use this energy for the production of process heat, hence contributing solutions adapted to the needs of strategic sectors such as the mining, chemical and petrochemical industries.

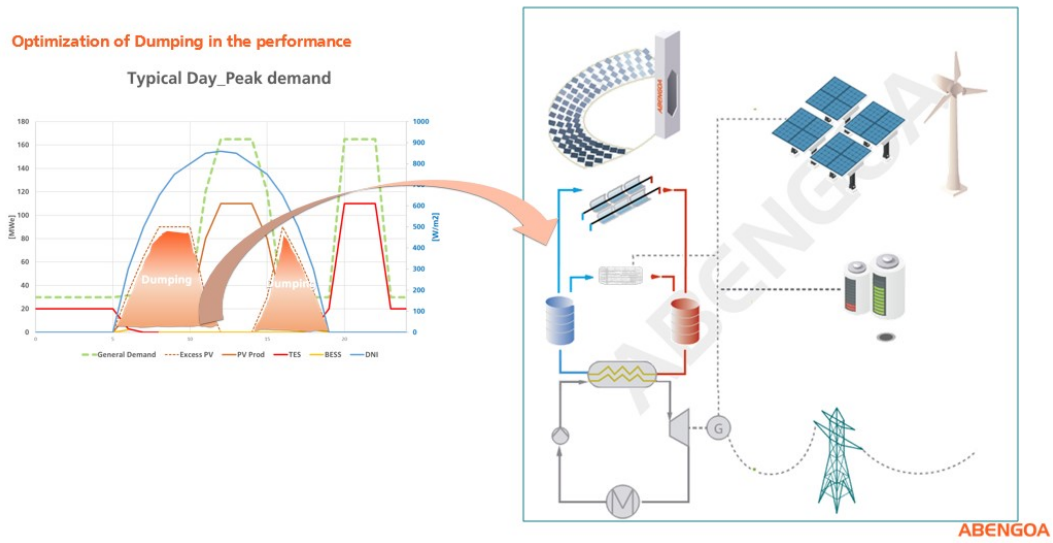


Figure 23: Utility-scale solar+storage competing with new peaker plants (PV/W+CSP+TES+BESS+Heater) by Abengoa ©

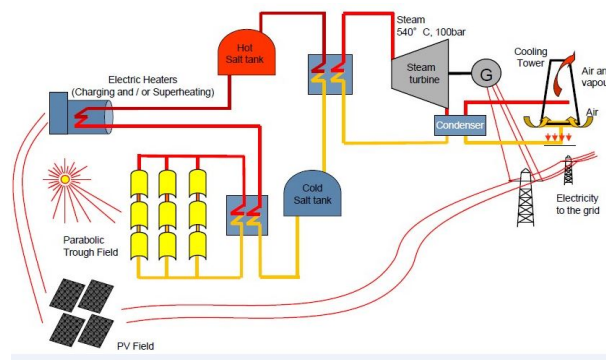


Figure 24: Working principle of the Midelt Noor I plant by TSK Flagsol ©

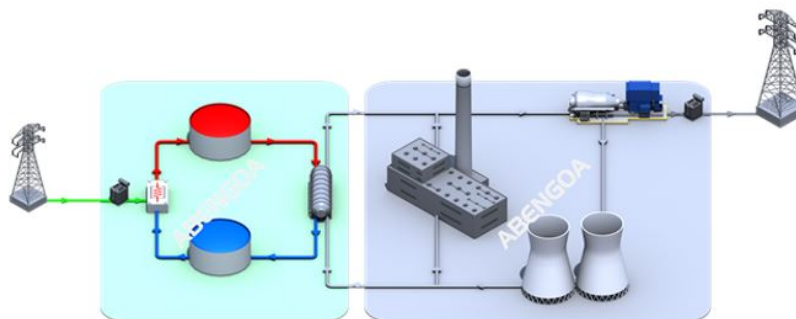


Figure 25: Decarbonization solution offered by Abengoa ©

## 7 Power Block based on supercritical CO<sub>2</sub> cycles

### 7.1 Origins of the supercritical CO<sub>2</sub> cycles

Most of the thermodynamic cycles using Carbon Dioxide at supercritical or transcritical pressure and temperature that have been studied by the scientific community in the last years and, more specifically, those which have been implemented in the few experimental loops available derive from the initial proposals of Angelino and Feher [110, 111]. For this reason, and in order to better understand the evolution of sCO<sub>2</sub> technology, it is worth starting from a comprehensive review of their work.

Angelino proposed several configurations of condensation (transcritical) cycles for intermediate temperature applications [110], able to achieve similar or even higher efficiency than Rankine cycles using steam turbines but with the simplicity of Brayton cycles (gas turbines). The original simple, transcritical condensation cycle proposed by Angelino experienced a number of modifications in order to reduce the destruction of exergy in the recuperators, the most effective of which proved to be splitting the low temperature, low pressure flow in parallel streams following different thermodynamic pathways. This modification eventually produced the Recompression cycle which has been recognised as one of the most interesting embodiments of the supercritical CO<sub>2</sub> cycle [110]. Another interesting modification of the cycle proposed by Angelino targets the expansion process with the objective to provide flexible turbine back-pressure (pressure ratio) regardless of condensation pressure at low temperature (near compressor inlet). This was implemented in the Partial condensation with precompression cycle and, more recently, the Partial Cooling cycle. A very detailed review of the historical evolution of supercritical CO<sub>2</sub> cycles was recently published by Crespi et al. [112].

Along with the research carried out by Angelino in Europe, Edward Feher studied alternative power cycles which could potentially improve the performance of state-of-the-art Rankine and Brayton cycles in United States [111]. Feher found that, lying in between them, supercritical cycles could overcome some of the limitations experienced by Rankine and Brayton cycles:

- Rankine:
  - Peak operating temperature.
  - Wet expansion, therefore internal losses.
  - Very large volumetric expansion ratio and shaft work, bringing about a large number of turbine stages with complex geometries in the gas path.
- Brayton:
  - Large compression work (fluid behaves close to ideal gas).
  - Strong sensitivity to pressure losses and compressor efficiency.
  - Large size of heat transfer equipment due to large specific volume.

The conclusions drawn from Feher's work were similar to those obtained by Angelino in [110], for both the supercritical and transcritical sCO<sub>2</sub> cycles. Higher efficiency than in conventional Brayton and Rankine cycles with moderate turbine inlet temperatures (from 600 to 1000°C) seemed possible, in spite of the oversimplification of their basic thermodynamic analysis. Some later studies, in fact, declared that a correction factor lower than unity should be applied to the efficiency estimated by these authors, in addition to accounting for auxiliary power consumption (neglected in the cited seminal works) [113].

## 7.2 Fundamentals of the supercritical CO<sub>2</sub> cycle and comparison against gas and steam cycles

The working principle of a gas turbine is based on the Brayton cycle, patented in 1874 by George Brayton upon the conceptual development of John Barber in 1791. The ideal (simple) Brayton Cycle, shown in Figure 26, is comprised of two isentropic processes, compression (12) and expansion (34), and two isobaric processes, heat addition (23) and rejection (41). A standard gas turbine draws atmospheric air in (1) and increases its pressure in the compressor (2). This air is then heated up through combustion of natural gas (3) and, finally, combustion gases are expanded down to atmospheric pressure again (4). The heat rejection process is not performed in any component of the engine but merely by exhausting gases to the environment and dragging fresh air in again.

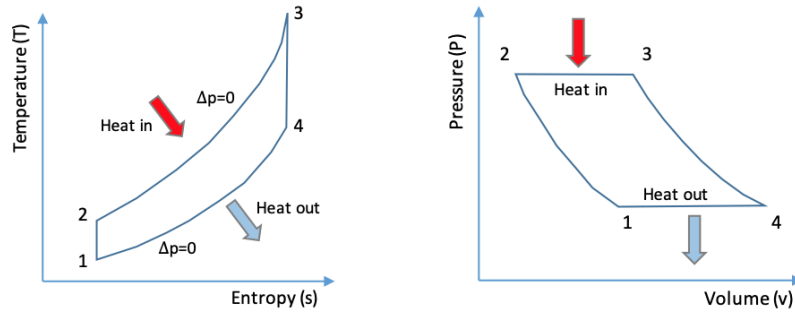


Figure 26: Brayton cycle. Temperature-entropy and pressure-volume diagrams.

The thermal efficiency of an ideal Brayton cycle depends on pressure ratio as follows:

$$\eta_{Br,i} = 1 - \frac{1}{PR^{\frac{k-1}{k}}} = 1 - \frac{1}{\delta} \quad (8)$$

where  $k$  is the isentropic exponent.  $\delta$  is usually termed *pseudo pressure ratio* for simplicity. Nevertheless, an actual engine is not made up of isentropic compression and expansion but, rather, non-reversible pressure change. If this is considered, whilst still considering that heat addition and rejection are carried out at constant pressure, and neglecting the impact of composition and temperature changes on fluid properties, the thermal efficiency of the engine is expressed as follows:

$$\eta_{Br} = \frac{\frac{\theta}{\delta} \cdot \eta_c \cdot \eta_t - 1}{\frac{\theta-1}{\delta-1} \cdot \eta_c - 1} \quad (9)$$

where  $\eta_c$  and  $\eta_t$  are the isentropic efficiencies of compressor and turbine and  $\theta = T_{03}/T_{01}$  is the ratio from highest to lowest cycle temperature (temperature ratio).

Figure 27 shows the influence of the pressure and temperature ratios on thermal efficiency and specific work. Thermal efficiency increases with pressure ratio but, beyond a certain optimum pressure ratio, cycle performance deteriorates. This is due to the increasing share of turbine work that is taken by the compressor, as shown in Figure right. Once the pressure ratio for peak efficiency is achieved, the only means of increasing cycle efficiency further is by increasing temperature ratio (i.e., turbine inlet temperature), which is equivalent to increasing expansion work whilst keeping compression work constant.

Compression work of a fluid can be defined as follows:

$$W_c = \int_{01}^{02} v \cdot dp = \int_{01}^{02} Z \cdot v_i \cdot dp = \int_{01}^{02} \frac{v \cdot R_g \cdot T}{p} \cdot v_i \cdot dp \quad (10)$$

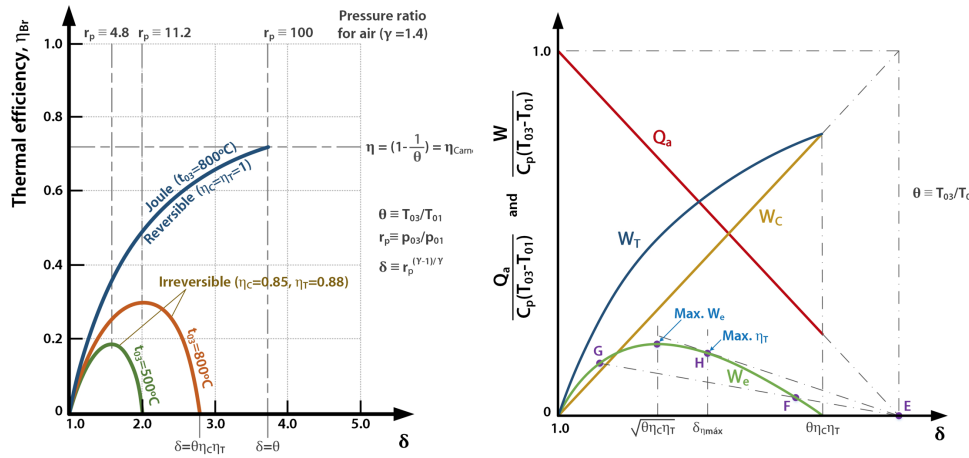


Figure 27: Brayton cycle performance. Influence of design parameters.

where the second equality makes use of the compressibility factor  $Z$ : ratio from the specific volume of a fluid at given pressure and temperature to specific volume of the same fluid at the given pressure and temperature if it behaved like an ideal gas. This equation suggests a new way to rise thermal efficiency by reducing compression work, in those applications where it is not possible or economically not interesting to increase turbine inlet temperature. Reducing the compressibility factor at the beginning of the compression process enables higher efficiency and also other beneficial features:

- The fraction of turbine work that is used to drive the compressor is lower, meaning a higher resistance to pressure losses in the cycle.
- For given flow rate, the compressor is more compact thanks to the lower specific volume of the working fluid.

This concept can be taken further if condensation is adopted, as it is done in a Rankine cycle. Nevertheless, such cycle would present the following shortcomings as currently identified by the industry and the scientific community:

- The working fluid (demineralized water) is expensive.
- The maximum inlet temperature of a modern steam turbine is not higher than 600°C, maybe 650°C in some experimental units. This values are very far from the typical turbine inlet temperatures of contemporary gas turbines.
- A large section of the cycle operates under vacuum conditions, making it necessary to expel non-condensable gases from the installation.
- The specific volume of the working fluid in the low-pressure section of the cycle is very large, bringing about very large and bulky equipment which increase the capital cost of the plant.
- The need for feedwater heating increases the capital cost and footprint of the plant.

It is therefore seen that reducing compression work as in a Rankine cycle leads to other technical and economic shortcomings, thus creating counteracting effects which can be best balanced by supercritical CO<sub>2</sub> cycles.

The introduction of the concepts presented in this section leads to a number of supercritical CO<sub>2</sub> cycles whose performance is competitive against conventional Rankine and Brayton cycles under certain operating parameters. This is shown in Figure 28 [110, 114], which yields the following conclusions:

- For turbine inlet temperatures lower than 1000°C, supercritical CO<sub>2</sub> cycles are more efficient than Brayton cycles operating on ideal gas.

- For turbine inlet temperatures higher than 650°C, these cycles are also more efficient Rankine cycles operating on water/Steam.
- Supercritical CO<sub>2</sub> cycles have the potential to reach 60% thermal efficiency for turbine inlet temperatures lower than 1000°C.

The analyses of Angelino and Feher built the foundation of the technology but were soon interrupted. It was not until the beginning of the twenty first century when the interest in the technology was reborn. Amongst the new cycle proposals though, only a few of them are worth noting, in particular the Allam cycle [115]. This is a transcritical power cycle working between 37 and 300 bar and with condensation at supercritical pressure. The developers of the technology announce 59% thermal efficiency at 1150°C and the availability of pipeline-ready carbon dioxide for storage; however, the need to produce oxygen for the oxycombustion process still poses some questions regarding the business case of such power plant.

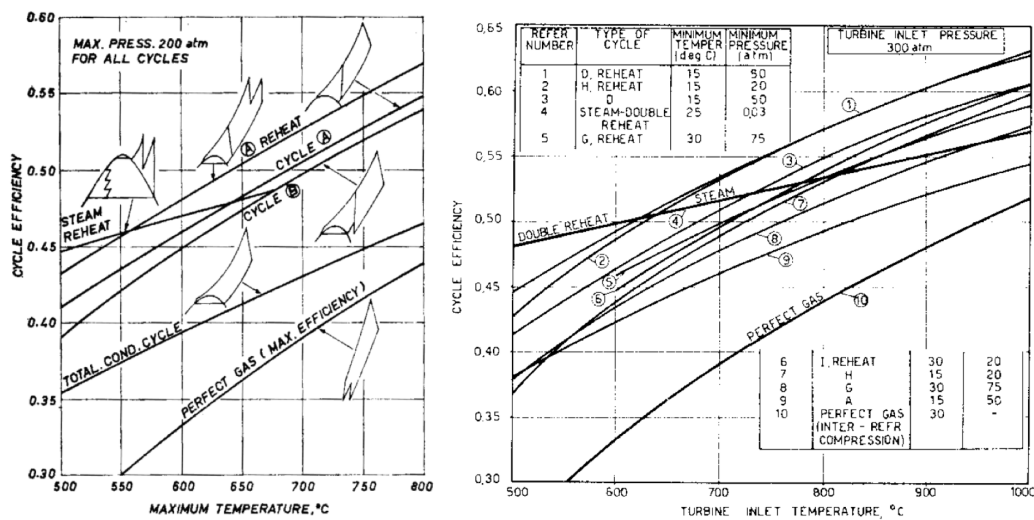


Figure 28: Comparison of supercritical CO<sub>2</sub>, air Brayton and water/steam Rankine cycle. Condensing and non-condensing cycles are considered [110, 114].

The exhaustive review of Crespi et al. provides an excellent overview of the current state-of-the-art of supercritical CO<sub>2</sub> power cycles for power generation from different primary energy sources, including solar energy [112]. A summary of the expected performance is presented in Figure 29 where the large variability of declared performances and an upper limit of cycle efficiency for a given turbine inlet temperature can be deduced.

### 7.3 Candidate sCO<sub>2</sub> cycles for CSP-STE applications

This section is based on the available scientific literature in the topic of supercritical CO<sub>2</sub> cycles for power generation, either specifically for Concentrated Solar Power applications or for a general purpose. The most representative cycles proposed in literature are reviewed and their suitability for CSP-STE plants is discussed.

- **Simple Recuperated and Transcritical:**

This cycle aims to counterbalance the the high compression work and large heat transfer area of conventional Brayton cycles, brought about by the low specific volume of the working fluid. The lower specific work needed to compress CO<sub>2</sub> near the critical region, and the larger temperature difference between compressor delivery and turbine exhaust that enables a much larger heat recovery potential, bring about a higher thermal efficiency of the cycle. On the negative side, the variability of the thermodynamic properties of the working fluid near the critical point limit the effectiveness that low temperature recuperators

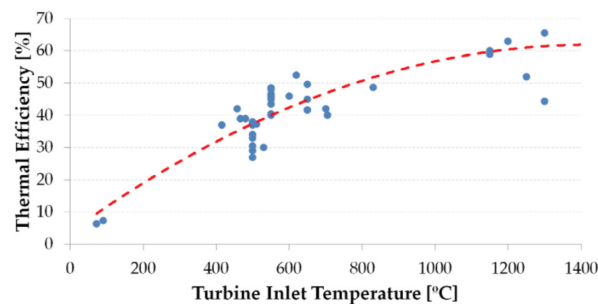


Figure 29: Influence of turbine inlet temperature on thermal efficiency, based on a literature survey. Different cycle layouts and applications are considered.

can achieve, therefore limiting the theoretical thermodynamic potential of the cycle.

The Transcritical CO<sub>2</sub> follows the same concept as the Simple Recuperated cycle but based on a pseudo-Rankine cycle [116, 117, 118, 119]. This is a suitable configuration for low-temperature waste heat recovery applications and, therefore, it can also be used in combined cycle power plants.

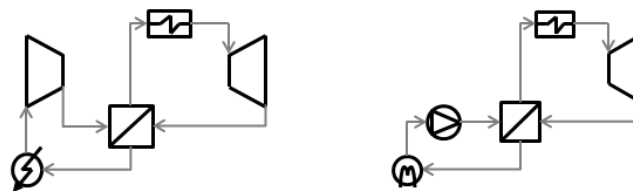


Figure 30: Simple Recuperated Cycle (Right) and Transcritical Cycle (Left) layouts.

- **Allam cycle:**

This is an oxy-combustion cycle that burns natural gas (or syngas) with pure oxygen. It achieves high thermal efficiencies and provides pipeline-ready CO<sub>2</sub> without the need of an additional absorption process, but this is at the cost of having a large Air Separation Unit producing oxygen for the combustion process. The Allam cycle is highly recuperative cycle and exhibits a tight thermal integration between the power cycle and the Air Separation Unit which enhances the overall performance of the plant. The fact that combustion gases are comprised of carbon dioxide and water steam only (except for traces of other gases) enables CO<sub>2</sub> capture through cooling/condensation only.

- **Brayton sCO<sub>2</sub> GT:**

The Brayton sCO<sub>2</sub> GT cycle is a common reference to the Intercooling II cycle based on the Simple Recuperated layout with intercooled compression. Originally proposed for nuclear applications, it is now considered for Concentrated Solar Power.

- **Matiant:**

This cycle was developed by Mathieu and Iantovski. Akin to the Allam cycle, it is based on oxycombustion and incorporates three expanders and one reheater. The Matiant cycle enables capturing pipeline-ready CO<sub>2</sub> by mere condensation.

- **Forced Cooler Cycle:**

The Forced Cooler cycle is also based on the Simple Recuperated layout with the incorporation of an intercooler and a reheater. The name is justified by the additional cooler, known as Forced Cooler, which

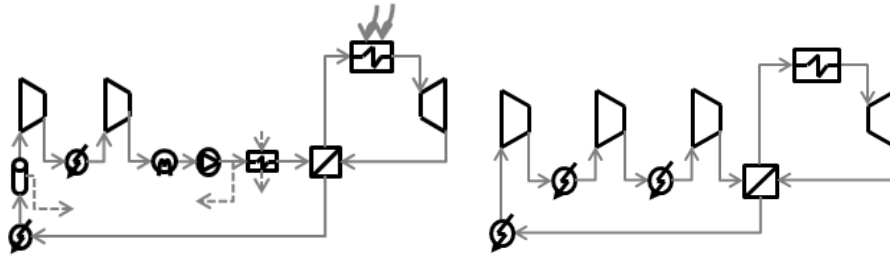


Figure 31: Allam Cycle (Right) and Brayton sCO<sub>2</sub> GT Cycle (Left) layouts.

is found between the standard cooler and the first compressor. The Forced Cooler is cooled by a two-stage vapor-compression refrigeration cycle with a flash chamber, using R134-a as working fluid.

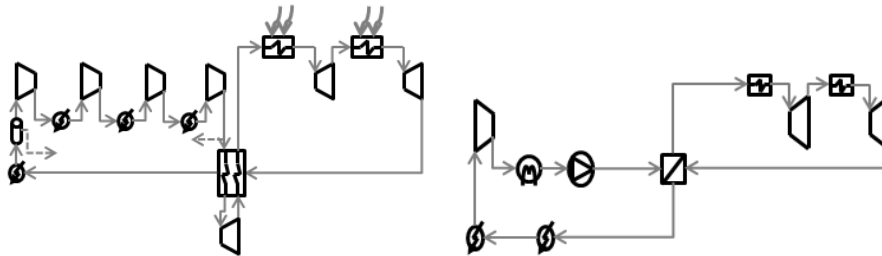


Figure 32: Matiant Cycle (Right) and Forced Cooler Cycle (Left) layouts.

- **S-EJ:**

This cycle is also based on the Simple Recuperated layout where an ejector is added just before the heater. The outlet stream of the heater is then divided in two: the first fraction is expanded and then flows into the recuperator. The remaining fraction is expanded in the second turbine and then sent to the ejector for mechanical compression. The addition of this ejector can potentially lead to a higher thermal efficiency, according to the authors [120].

- **RC-EJ:**

The RC-EJ cycle is similar to the S-EJ configuration but, in this case, based on a Recompression cycle assisted by an ejector. This configuration is characterized by the same features as the S-EJ (ejector) and Recompression (split-flow) cycles.

- **MC-EJ:**

The MC-EJ cycle is the third configuration proposed by Vasquez [120]. It is also based on the Recompression cycle assisted by an ejector, as in the RC-EJ cycle, but with the addition of intercooling in the main compression line. It exhibits the same characteristics as the RC-EJ cycle plus a reduction of compression work thanks to intercooling.

- **Inter-recuperated & Recompression:**

The Inter-recuperated is similar to the Simple Recuperated cycle, except for the recuperating process which is comprised of two recuperators.

Based on this cycle, Angelino proposed the Recompression cycle, with a clear connection to Feher's work. The low-pressure flow at the outlet from the low-temperature recuperator is split in two. One fraction is cooled down further in a cooler and then compressed in the main compressor at the outlet from which the flow is sent to the high-pressure side of the low-temperature recuperator. The second fraction is

compressed in the re-compressor and then joins the former stream at the outlet from the low-temperature recuperator, on the high-pressure side. The resulting stream is then sent to the high-pressure side of the high-temperature recuperator.

This configuration is aimed at reducing the mass flow rate of CO<sub>2</sub> on the high-pressure side of the low-temperature recuperator thus overcoming the internal pinch point problem brought about by the variability of CO<sub>2</sub> properties in the vicinity of the critical point. This yields higher LT recuperator effectiveness and therefore higher cycle efficiency. The Supercritical Recompression layout is the most extensively researched cycle in literature along with the Supercritical Simple Recuperated.

- **Partial condensation & Precompression:**

The Precompression cycle based on the partial condensation cycle with precompression proposed by Angelino. It aims to release the constraints posed on the low and high cycle pressures: when compressor inlet pressure is increased to supercritical values, either the expansion ratio is reduced (lower specific work) or turbine inlet pressure increases to prohibitive values (more complex and expensive mechanical design).

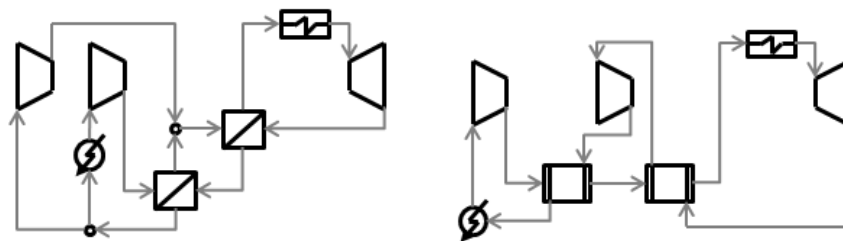


Figure 33: Recompression Cycle (Right) and Precompression Cycle (Left) layouts.

- **Recompression+IC+RH & Partial Cooling+Reheating:**

This layout is aimed at improving the performance of the Recompression and Partial Cooling cycles by merely adding multi-stage intercooled compression and reheated expansion processes. The benefits provided by these configurations are the same as previously discussed for their standard configurations without reheat.

- **Double Reheated Recompression:**

This configuration adds a second reheater to the configuration proposed by Moisseytsev. Additionally, Mecheri and LeMoullec proposed to separate a fraction of the main flow downstream of the main compressor, before the low-temperature recuperator. After this separation, the split fraction would be heated up in another heater and re-injected before the high-temperature recuperator. The aim of this flow split is to overcome the usual pinch-point problems and associated irreversibility in the internal heat recovery process.

- **Cascade Supercritical CO<sub>2</sub>:**

The Cascade configuration is actually a Recompression cycle where a flow-split valve is added downstream of the low-temperature recuperator. Both fractions follow the layout of a Simple Recuperated cycle and rejoin upstream of the low-temperature recuperator. This cycle was included in the sCO<sub>2</sub> cycle development programme at Pratt Whitney Rocketdyne for solar thermal applications. Thanks to this configuration, it is possible to recover heat from the solar plant using two heaters, thus better fitting the large temperature change that is typical of this technology.

- **Schroder-Turner:** The Schroder-Turner cycle is a highly recuperative cycle, based on the Partial Cooling layout but with an improved heat recovery system incorporating three compressors and a single turbine. There is a way to simplify the complex configuration, by removing the low-temperature recuperator.

- Quasi-Combined:** The Quasi-combined system is an oxycombustion cycle proposed by Zhang and Lior. As in the Partial Cooling cycle, the flow is split into two streams downstream of the first compressor. The first stream is condensed in an LNG evaporator, and then pumped and heated in the low and intermediate temperature recuperators. This stream is then expanded in a high-pressure turbine and heated to a higher temperature in a high-temperature recuperator before rejoining the second stream (as in the Matiant cycle). This second stream is compressed after the flow-split valve, heated up in the intermediate temperature recuperator and finally mixed with the first stream. The resulting stream is heated to the peak cycle temperature in oxycombustor with methane and pure oxygen (from an Air Separation Unit) and the combustion gases are expanded in the low-pressure turbine. The name Quasi-combined derives from the fact that the sCO<sub>2</sub> and H<sub>2</sub>O stream coming from the low-pressure turbine and flowing towards the water separator and CO<sub>2</sub> compression lines serve as heat source ("topping cycle") for the pure sCO<sub>2</sub> flow that acts as the corresponding Rankine-like "bottoming cycle".

### 7.4 Expected thermal performance of CSP-STE power plants based on sCO<sub>2</sub> cycles

For the configurations considered in the previous section, the dependence of specific work and thermal efficiency on pressure ratio and turbine inlet temperature is now analyzed. The aim is to separate the thermodynamic potential of each cycle from the pressure and temperature limits posed by mechanical integrity and technical availability. Temperatures lower than 550°C are not considered, given that Angelino itself claimed that sCO<sub>2</sub> cycles are able to achieve efficiencies higher than (steam) Rankine cycles only if turbine inlet temperature is significantly higher than 550°C [114].

#### 7.4.1 Results

The performances of the cycles presented in the preceding section are provided below for four different turbine inlet temperatures -550, 750, 950 and 1150°C- and variable turbine inlet pressures, Figure 34. The lower boundary is set to 550°C, as suggested by Angelino, whilst the maximum temperature is set to a reasonable value based on the current heat exchanger temperature capabilities. Cycle pressures are varied from almost no compression to the pressure ratios implying unfeasible inlet temperatures to the heat exchangers. These pressure limits do change from cycle to cycle, as they are strongly dependent on the configuration of the recuperators.

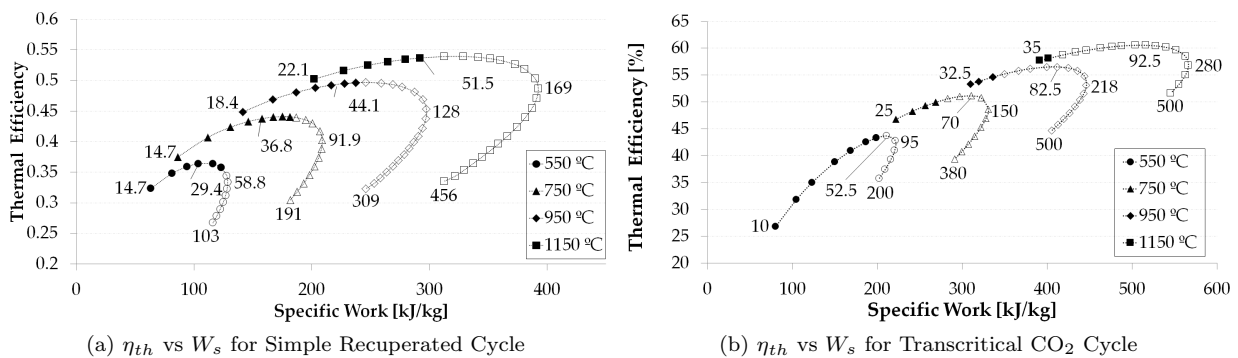


Figure 34: Performance of Simple Recuperated and Transcritical CO<sub>2</sub> cycles [121].

Black markers in Figure 34 correspond to cycles where peak pressure is not higher than 40 MPa whereas white markers indicate that the peak cycle pressure is above this value. This transition value is higher than the

values usually employed in literature, 25-30 MPa [122, 115] but still representative of next generation power plants. As a matter of fact, supercritical steam power stations demonstrated that operation at 35MPa was possible as early as 1960 [123], and this pressure level is expected in next generation ultra-supercritical steam power plants [124].

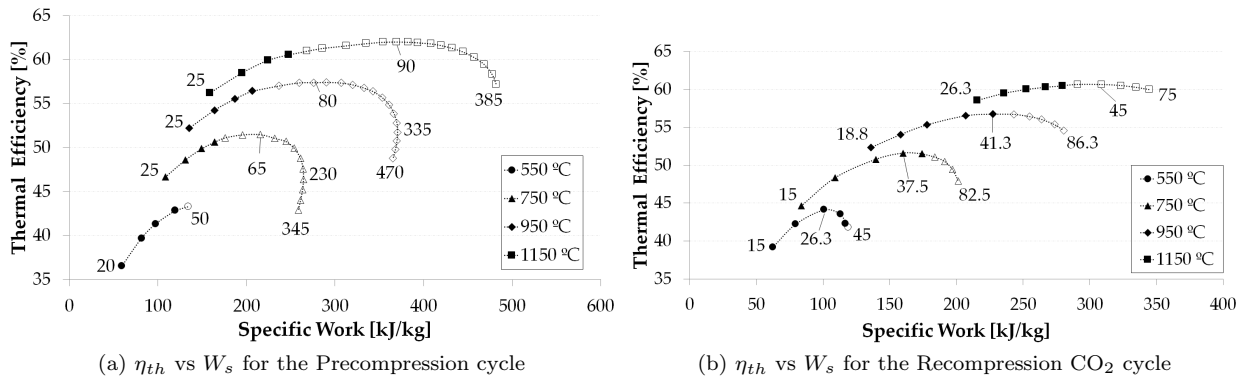


Figure 35: Performance of the Precompression and Recompression CO<sub>2</sub> cycles [121].

The pressure labels reported in Figure 34 correspond to the first and last calculations (i.e., cycles with minimum and maximum peak pressure) and to the live steam pressure for which peak thermal efficiency and peak specific work are achieved. In some cases though, the last value is not reported if associated to unfeasible, very high pressure ratios).

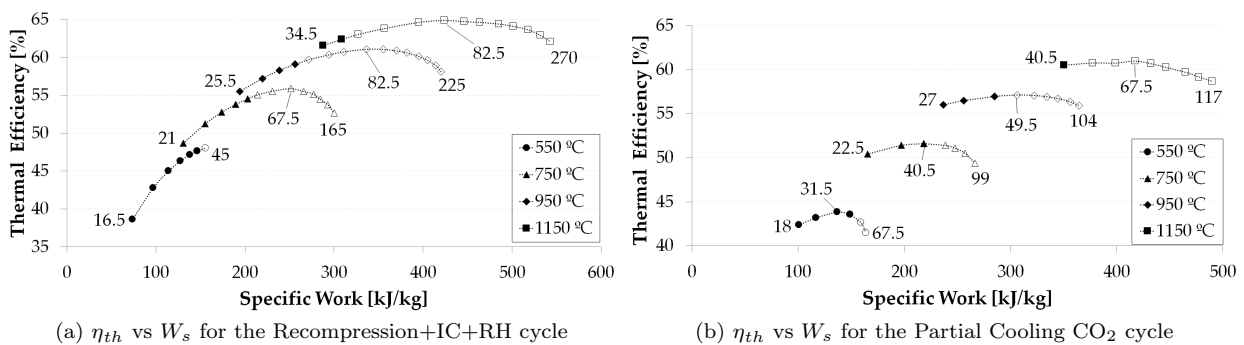


Figure 36: Performance of the Recompression+IC+RH and Partial Cooling cycles [121].

Even though the shape of the  $\eta_{th}$  vs.  $W_s$  plots changes significantly from one configuration to another, there are visible similarities between cycles with similar thermodynamic (or topological) characteristics. For instance, the Recompression+IC+RH and Double Reheated Recompression layouts are based on the Recompression cycle and they show similar patterns in Figures 35(a), 36(a) and 38(a).

Some common features of the plots are:

- At low turbine inlet temperature, the plots have a more circular shape. When this temperature increases, they turn elliptical and flatter.
- Most cycles achieve peak thermal efficiency and specific work at pressures higher than 40MPa when turbine inlet temperature is higher than 550°C. If this temperature is lower, it is unsure whether or not

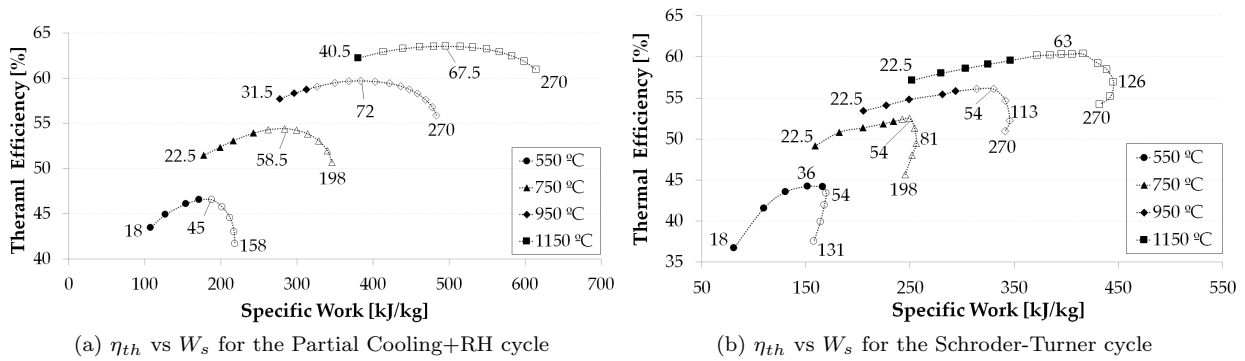


Figure 37: Performance of the Partial Cooling+RH and Schroder-Turner cycles [121].

peak efficiency is achieved within the feasible pressure range. This is shown in Figures 34(a), 35(a), 35(b), 36(b), 37(b), 38(a), 39(b).

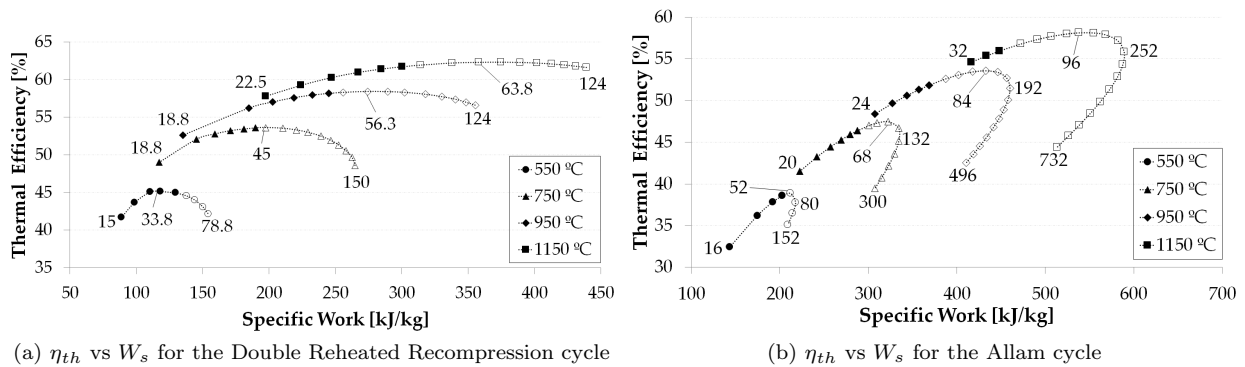


Figure 38: Performance of the Double Reheated Recompression and Allam cycles [121].

### 7.4.2 Compared Analysis

According to the information in the preceding sections, for some cycles it should be possible to exploit an untapped thermodynamic potential for further efficiency increase (should higher pressures be attainable) whereas other cycles seem to have already achieved the best performance possible for a given turbine inlet temperature; this would nevertheless imply working at extremely high pressures (for instance, the Transcritical CO<sub>2</sub> cycle could exceed 50% efficiency at 750°C turbine inlet temperature if pressures higher than 75 MPa were attainable). Despite this observation though, the most efficient cycles (or so regarded), like the Recompression layout, seem to have already achieved the best performance attainable for the the current turbine inlet temperatures.

Overlaying the foregoing plots yields interesting information about the relative performance of the cycles considered at each turbine inlet temperature; this is shown in Figures 40 and 41. At 550 °C, the highest specific work corresponds to the Allam cycle if a cap on turbine inlet pressure is set whilst the Transcritical CO<sub>2</sub> has higher  $W_s$  if there are no pressure limits. Regarding efficiency, the Partial Cooling + RH and Recompression+IC+RH layouts have highest efficiencies (46.5 and 47.6% respectively) at turbine inlet pressures below 40 MPa whereas efficiency rises to a higher value (48%) for the Recompression+IC+RH cycle if this limit is released. Globally, the Partial Cooling+RH and Transcritical CO<sub>2</sub> cycles provide a good compromise between

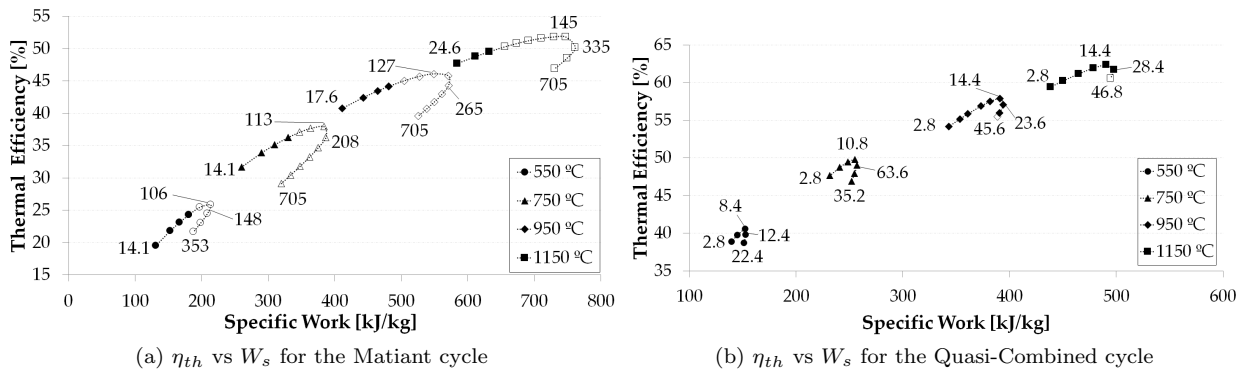


Figure 39: Performance of the Matiant and Quasi-Combined cycles [121].

thermal efficiency and specific work.

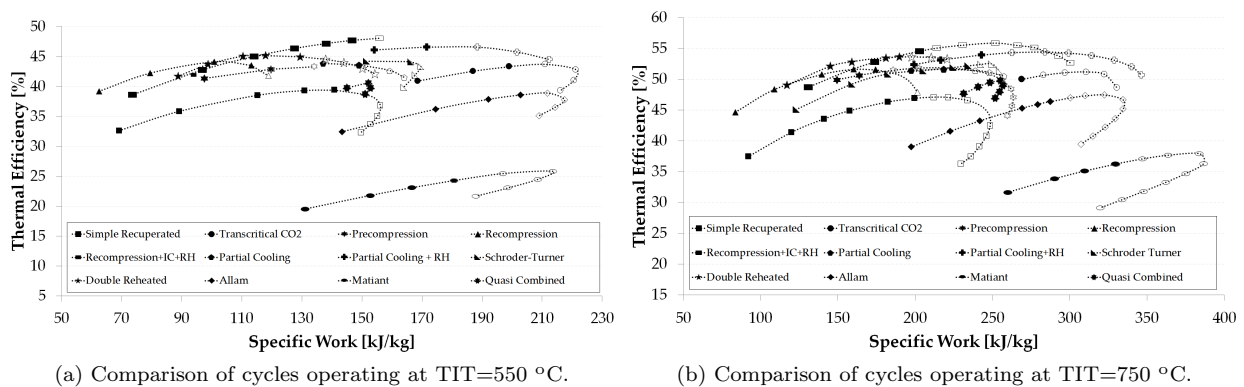


Figure 40: Comparison of cycles operating at TIT=550 °C and TIT=750 °C [121].

Turbine inlet temperature has a very strong influence on thermal efficiency and specific work and on the shape of the  $\eta_{th}$  vs.  $W_s$  plots. For instance, at 550 or 750 °C, Figure 40 shows that those cycles based on oxycombustion layouts (Matiant and Allam) have very high specific work but moderate thermal efficiency. On the contrary, the Recompression+IC+RH cycle attains highest efficiency, 54.5 or 55.8% depending on turbine inlet pressure limits, and the Double Reheated Recompression and Partial Cooling + RH layouts exhibit good performance also.

At the other end of the turbine inlet temperature range, 950 and 1150 °C, a significant efficiency and specific work rise is experienced, Figure 41. Indeed, thermal efficiencies higher than 60% seem possible if turbine inlet pressure is limited to 40 MPa, and 65% can be exceeded at higher pressure. The drift of the plots towards the top right region of the  $\eta_{th}$  vs.  $W_s$  is also interesting and changes the relative performance of the cycles considered. As a consequence of this, the Precompression, Recompression+IC+RH, Partial Cooling+RH, Transcritical CO<sub>2</sub>, Allam and Quasi-Combined layouts become most interesting, in particular the latter which yields the most leveraged performance with 63% thermal efficiency and  $\sim 475$  kJ/kg.

As a further consideration to this comparison, Crespi et al. [125] investigate two of the cycles in this section, highlighting that a) temperature rise across the solar receiver is a crucial figure of merit impacting the economics of the system (and must therefore be taken into consideration), and b) for a given turbine inlet

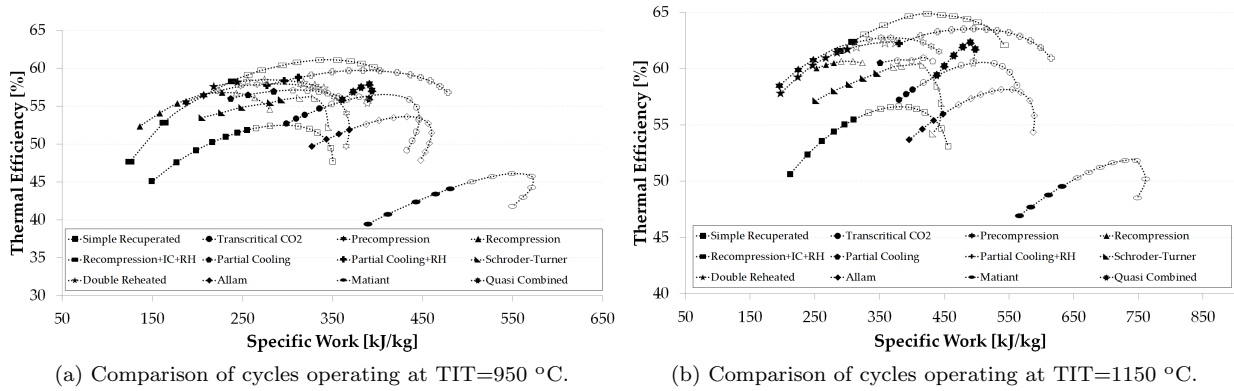


Figure 41: Comparison of cycles operating at TIT=950 °C and TIT=1150 °C [121].

temperature, higher pressure ratios increase the temperature rise across the receiver strongly, but the effect on thermal efficiency is uncertain as this can either increase or decrease, depending on the cycle considered.

## 7.5 Expected economic performance of CSP-STE power plants based on sCO<sub>2</sub> cycles

### 7.5.1 Capital costs

The thermal performance of the cycles presented in the foregoing section is now complemented by an economic assessment of the capital and energy costs of an associated Concentrated Solar Power plant making use of these supercritical CO<sub>2</sub> power cycles. Detailed information about this techno-economic assessment can be found in [126].

The foreseen capital cost of a 50 MWe CSP-STE power plant with 10 h Thermal Energy Storage capacity and the specifications in Table 4 is shown in Figure 42(a), along with the cost of the power block only in Figure 42(b). In general, the overnight capital cost decreases for increasing turbine inlet pressure until a minimum cost is achieved, and this then increases if turbine inlet pressure is increased further. The Power Block exhibits the opposite trend, Figure 42(b); costs are higher at very lower very high pressures, and they decrease for intermediate turbine inlet pressures. It is observed that most configurations achieve the minimum OCC at around 30 MPa, even if the exact value depends on the complexity of the layout (cycles with a large number of heat exchangers are more sensitive to operating pressures due to the higher cost of this equipment)<sup>3</sup>.

Output [MW <sub>el</sub> ]	$P_{max,sCO_2}$ [MPa]	TIT [°C]	$T_{s,min}$ [°C]	$T_{s,max}$ [°C]	TES <sub>capacity</sub> [h]	SM [-]
50	30	750	480	770	10	2.4

Table 4: Specifications of reference CSP-STE plant based on sCO<sub>2</sub> power cycles

It must be acknowledged that the foregoing costs of supercritical CO<sub>2</sub> power plants incorporates an inevitable degree of uncertainty, as it is the case in any economic assessment of precommercial technology [128]. Therefore, in order to ensure that the results presented are credible, Crespi et al. also provide an assessment of

<sup>3</sup>It is worth noting that the reported costs are sensitive to the operating pressure, according to the original reference [126]

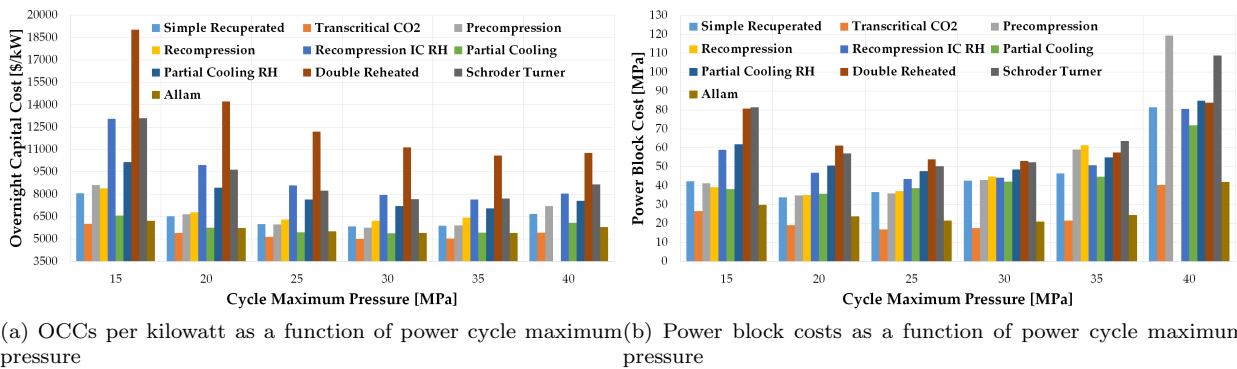


Figure 42: OCCs and Power Block Costs vs maximum power cycle pressure [127]

the impact of uncertainty in [126], based on the expected probability functions of different cost items integrated through the Montecarlo methodology. To this end, the authors rely on a similar analyses to select the appropriate probability distributions and ranges of each individual equipment cost, setting the number of samples to 10,000 to calculate the OCC of the plant.

This approach to calculating the probability density function of the Overnight Capital Cost per kilowatt yields the information shown in Figure 43. This plot can be divided in three distinct regions. On the right hand side, the Double Reheated cycle has the highest OCC-per-kW, getting up to 13000 \$/kW for a 90% confidence interval. In the mid section, the Recompression+IC+RH, Schroder-Turner and Partial Cooling+RH cycles have OCC-per-kW ranging between 8500 and 9500 \$/kW for a 90% confidence interval. Finally, the remaining layouts on the left hand side show the lowest installed costs with between 5500 and 7000 \$/kW for the same confidence interval. Further to the absolute values of installation costs, the plot also confirms that cycles with more complex layouts (for instance the Double Reheated cycle) experience a stronger impact of uncertainty as a consequence of the potential changes of the cost of each component. This is symptomatic of a larger data dispersion in the Montecarlo simulation, due to the higher relative importance of the thermal energy storage system and the tower/receiver.

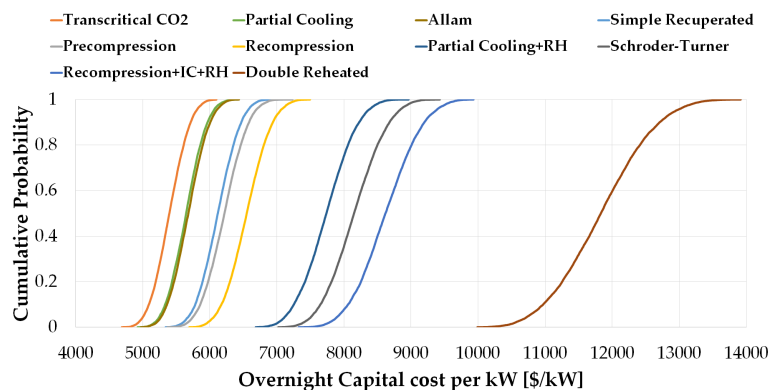


Figure 43: Cumulative probability distribution of Overnight Capital Costs per kilowatt [126].

### 7.5.2 Capital cost breakdown

The capital cost breakdown of the layouts compared, for the 85% confidence interval are presented in Figure 44. The Recompression+IC+RH and Schroder-Turner layouts (e and h in Figure 44) have very large installations costs, owing to the contributions of the thermal energy storage system and tower/receiver, and this is also the case for the Recompression, Partial Cooling+RH and Double Reheated cycles (d, g and i respectively). As shown in Table 5, this is due to the very low  $\Delta T_{solar}$  across the solar receiver, bringing about a dramatic increase in the inventory of salts that is needed to transfer thermal energy from the solar field to the power cycle. For instance, the Double Reheated layout presents a  $\Delta T_{solar}$  of 80°C, a value three times lower than the maximum  $\Delta T_{solar}$  achieved by some of the other configurations (290°C).

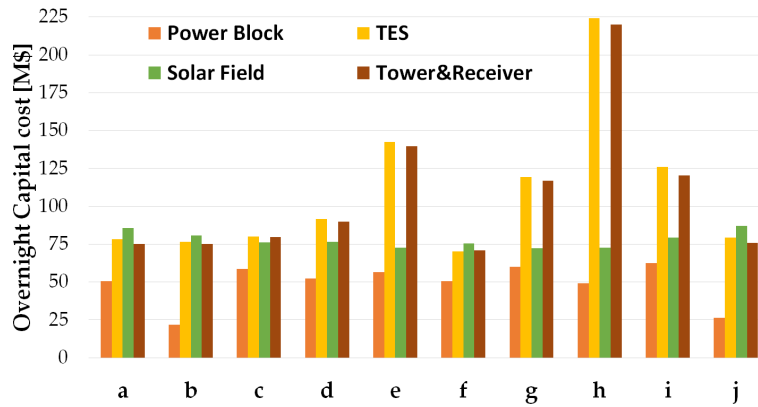


Figure 44: Breakdown of Capital Costs. (a) Simple Recuperated, (b) Transcritical CO<sub>2</sub>, (c) Precompression, (d) Recompression, (e) Recompression+RH+IC, (f) Partial Cooling, (g) Partial Cooling+RH, (h) Schroder-Turner, (i) Double Reheated, (j) Allam, and (j) Quasi-Combined [126].

Cycle	$T_{in,compr}$ [°C]	$P_{in,compr}$ [MPa]	$\eta_{th}$ [%]	$W_s$ [kJ/kg]	$\Delta T_{solar}$ [°C]
a	32	7.5	45.8	171	290
b	15	5	48.3	242	290
c	32	7.5	50.6	164	254
d	32	7.5	50.5	142	220
e	32	7.5	52.8	174	130
f	32	5	51.1	192	290
g	32	5	53.0	210	157
h	32	5	52.8	159	80
i	32	7.5	49.0	200	160
j	32	3	45.0	252	290

Table 5: Thermal performance of the cycles considered.

More complex layouts enable higher efficiency which, in turn, reduces the cost of the solar field (e,g,h,i). Unfortunately, this is at the cost of a higher cost of the power block and other subsystems of the plant (for instance, the thermal energy storage system), which, in some cases, more than offsets the previous saving. Conversely, simpler cycles imply lower costs of the power block and, also, larger and more expensive solar fields (b,j). This is all seen in Figure 45 where a breakdown of the power block cost is provided, showing the impact of the number of turbomachines and of the very expensive heater whose cost is tightly linked to  $|\Delta T_{solar}|$ .

The latter feature can be inferred from the parallel trends of TES and heaters costs, yellow bars in Figures 44 and 45 respectively

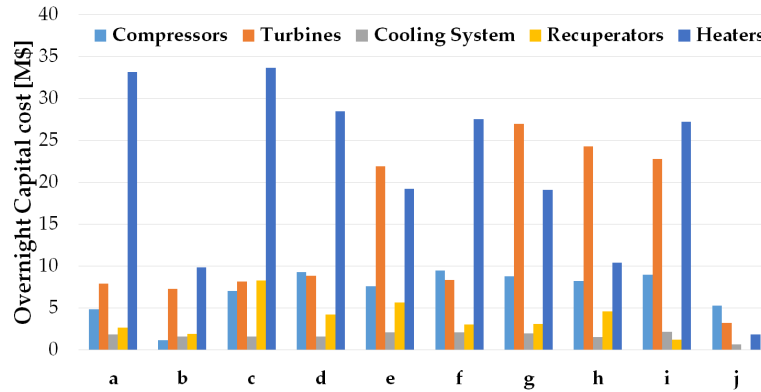


Figure 45: Breakdown of Capital Costs of the power block. (a) Simple Recuperated, (b) Transcritical CO<sub>2</sub>, (c) Precompression, (d) Recompression, (e) Recompression+RH+IC, (f) Partial Cooling, (g) Partial Cooling+RH, (h) Schroder-Turner, (i) Double Reheated, (j) Allam, and (j) Quasi-Combined [126].

The thermodynamic and economic information presented so far is summarized in Figure 46, showing a comparison of the ten cycles considered in terms of First and Second Law efficiencies and of OCC. This chart is interesting to assess the thermal and economic performance of each cycle; for instance, the Transcritical CO<sub>2</sub> (b), Allam (j) and Partial Cooling (f) cycles have equally low costs but, amongst them, only the Partial Cooling system yields acceptable thermal performance. In Figure 46, thermal efficiency has a direct impact on the size of the solar field and, accordingly, the tower and receiver whilst the Carnot Factor is a measure of the overall irreversibility of the cycle, hence the temperature gap (between the hot and cold reservoirs) needed to achieve a given thermal efficiency.

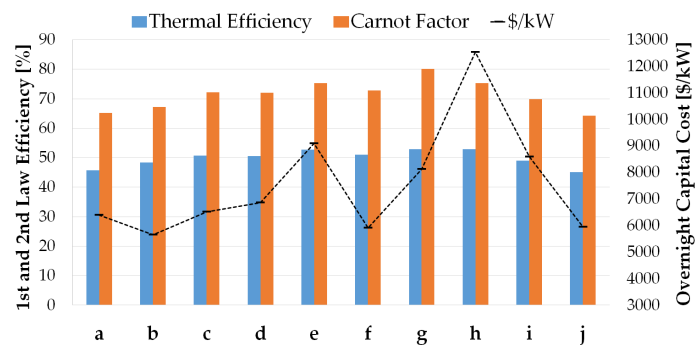


Figure 46: Thermo-economic comparison of supercritical CO<sub>2</sub> cycles

As a conclusion of the foregoing thermodynamic and economic analysis, the Transcritical CO<sub>2</sub> cycle is thought to enable installation costs lower than 6000 \$/kW with almost complete certainty. Moreover, if the 85% confidence interval is considered, the capital cost of this cycle decreases to about 5500 \$/kW, which is very competitive against typical values of coal power plants -3800 \$/kW [129]- or state-of-the-art CSP plants using tower technology - 5800 \$/kW [130]-. Interestingly, this is in spite of not achieving very high thermal efficiency ( $\eta_{th} < 48.5\%$ ) or Carnot Factor. The Partial Cooling and the Allam layouts have moderate costs also, in the order of 6000 \$/kW respectively. For the Partial Cooling cycle, this is also accompanied by a very good

thermodynamic performance, with thermal efficiencies higher than 50%. Finally, very complex layouts are of no interest despite the high  $\eta_h$ .

### 7.5.3 Levelized Cost of Electricity

Further to the economic assessment of capital costs presented in the previous section, the associated Levelized Cost of Electricity of the layouts of interest is presented now. This is done for the Allam and Partial Cooling cycles, inasmuch as the Transcritical CO<sub>2</sub> cycle is very difficult to implement in practice. This is because it requires very low ambient temperatures which are not usually found in typical locations of Concentrated Solar Power plants.

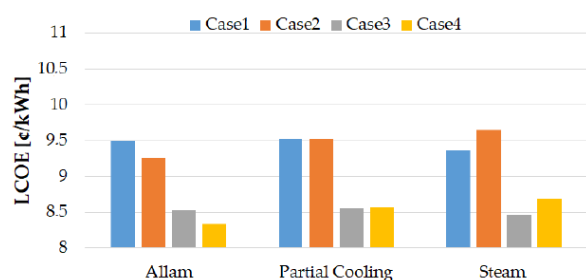
A good assessment of LCoE in CSP-sCO<sub>2</sub> power plants is provided in [131] where the general methodology to estimate partial load conditions of the Allam and Partial Cooling power is discussed, along with the off-design operating strategies. In this regard, three different control strategies are compared to estimate the performance in partial load: Inventory, By-pass and Temperature:

- **Inventory:** the circulating mass flow rate in the system is reduced when the power demand decreases. Carbon Dioxide is bled from the system, usually in the high pressure section, which brings about a lower power output and, also, a general descent of pressures throughout the system. When power demand increases, the Carbon Dioxide stored at high pressure in a vessel is reinjected back, usually in the low pressure section to minimize pumping power.
- **By-pass:** this is similar to the previous one, but in this case the mass flow rate is only reduced across the high pressure and high temperature section of the power block. The turbine operates with a lower mass flow rate, hence producing less power, whilst the circulating flow rate across the compressor remains essentially the same. This control scheme is less efficient than *inventory* but, on the other hand, it enables fast response of the system to power output changes.
- **Temperature:** the circulating mass flow rate remains the same so, when the heat input to the cycle decreases, turbine inlet temperature is reduced. This is the simpler control scheme but it also brings about a negative impact on thermal efficiency of the cycle.

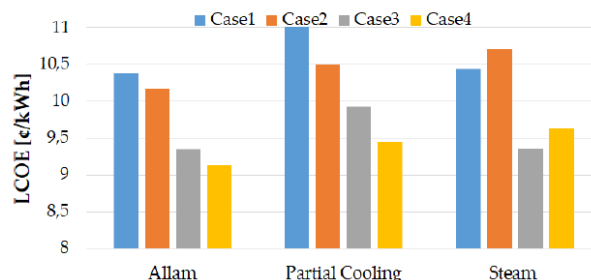
A combination between the two first strategies is found to obtain the best results, leading to good off-design cycle thermal performances without detrimental effects on compressor operation.

With the resulting optimum operating strategy, the analysis presented by Crespi suggests that Levelized Costs of Electricity in the range 8.5-9.5 ¢/kWh for a good location and 9.5-11.0 ¢/kWh in a location that is not as favourable should be expected from a CSP-sCO<sub>2</sub> power plant. Such values are slightly lower than those achievable by a state-of-the-art CSP plant using a standard steam cycle, in particular for the Allam cycle which seems to be able to enable a 10% reduction with respect to the latter technology. This is shown in Figure 47.

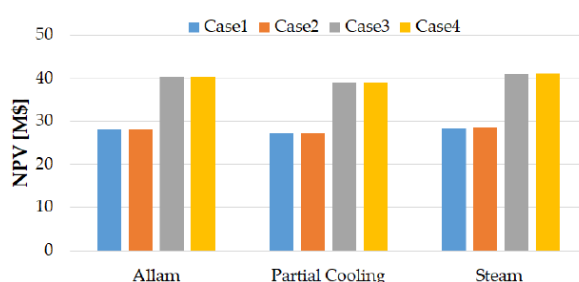
It is worth remarking that these LCoE ranges are obtained by the author for different load dispatch modes and boundary financial conditions. The dispatch control model defines the operating schedule of the thermal energy storage system and power block. For the default System Advisor Model dispatch control (System Advisor Model SAM is a free techno-economic software model developed by the National Renewable energy Laboratory which facilitates decision-making for people in the renewable energy industry), the turbine works at full load whenever possible except in summer, when a 5% overload is enabled during the central hours of the day characterized by the highest solar irradiation. For the SunShot Vision case, the load is reduced during winter in order to enable longer operating hours while maintaining the rated conditions during spring and summer. The financial parameters in the LCoE calculation tool are also set to the values reported by these two sources, as summarized in Table 6. The possible combinations of dispatch control and financial models yield four cases, shown in Table 10 for which Crespi obtains the range of Levelized Costs of Electricity presented in Figure 47.



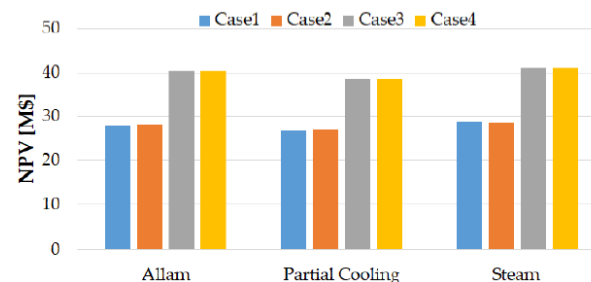
(a) Levelized Cost of Energy obtained with SAM for a CSP located in Las Vegas.



(b) Levelized Cost of Energy obtained with SAM for a CSP located in Tonopah.



(c) Net Present Value obtained with SAM for a CSP located in Las Vegas.



(d) Net Present Value obtained with SAM for a CSP located in Tonopah.

Figure 47: LCOE and NPV obtained with SAM considering three different cycles and four financial/control combinations. The locations of choice are Las Vegas and Tonopah, both in United States of America.

	SAM Default	SunShot Vision Study
IRR target [%]	11	15
IRR target Year	20	30
Analysis period [years]	25	35
Inflation rate [%]	2.5	3
Nominal Discount rate [%]	8.14	8.66
Loan Percent of total capital cost [%]	50	60
Loan Duration [years]	18	15
Loan Annual interest rate [%]	7	7.1

Table 6: Financial parameters employed in the SAM's default and SunShot Vision cases. More information available in [131].

As a complement to the results presented earlier in this section, and for the sake of clarity, a summary for the results is presented in Figure 48, confirming that Concentrated Solar Power plants using standard supercritical Carbon Dioxide power cycles have a very narrow margin to improve the economic performance of contemporary CSP plants based on steam turbines. This comes to confirm the need to developed the SCARABEUS technology to significantly reduce the cost of dispatchable solar electricity.

	Financial Model	Dispatch Control
Case 1	SAM Default	SAM Default
Case 2	SAM Default	SunShot Vision Study
Case 3	SunShot Vision Study	SAM Default
Case 4	SunShot Vision Study	SunShot Vision Study

Table 7: Different combinations of Dispatch Control and Financial models

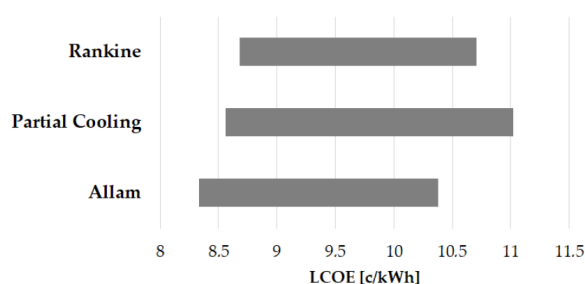


Figure 48: Ranges of Levelized Cost of Electricity for a number of technologies and boundary techno-economic conditions.

## 7.6 Projects under development worldwide

### 7.6.1 North America

Supercritical CO<sub>2</sub> power cycles are not commercially available yet. The largest plant based on this technology has been developed by Net Power but this is yet a large-scale demonstration plant. This plant, located in La Porte (TX), USA, is rated at 50 MWth (equivalent to some 25 MWe output) and has a total cost of about 150 MUSD. The power is produced from natural gas which is burned with oxygen only, hence producing water steam and carbon dioxide in the combustion gases. The tight integration between the Air Separation Unit (needed to produce oxygen) and the power cycle enables thermal efficiencies in the order of 60%.

A conceptual scheme of the Allam cycle is presented in Figure 49, along with the associated enthalpy (h) versus pressure (p) diagram in Figure 50. The latter confirms the main flaw of the cycle when it comes to Concentrated Solar Power applications: the need to reduce the working temperature at the inlet to the compression process to around 15°C. This pretty much prevents this cycle from being applied to hot environments as it is mostly the case in solar thermal power plants. This was already highlighted in an earlier section.

Net Power's demonstration plant, which does not incorporate the Air Separation unit with the aim to cut costs down (piped oxygen is used), underwent first firing in oxycombustion mode on May 2018 and, according to recent articles featured in specialised publications like Gas Turbine world, it is reportedly completing the preliminary test programme [132]. Upon successful completion of this test programme, the plans of the company are to upscale the concept to 300 MWe which is deemed to most cost-effective size for natural gas fired power plants incorporating carbon capture.

Another flaship project in United States is currently being developed by The Gas Technology Institute, General Electric and Southwest Research Institute, along with the National Renewable Energy Technology Laboratory of the Department of Energy. This STEP (Supercritical Transformational Electric Power) pilot plant has a budget of about 120 MUSD and it aims to deliver a first-of-a-kind 10 MWe supercritical CO<sub>2</sub> power plant. According to the Department of Energy (<https://www.energy.gov/sco2-power-cycles/pilot-plant-supercritical->

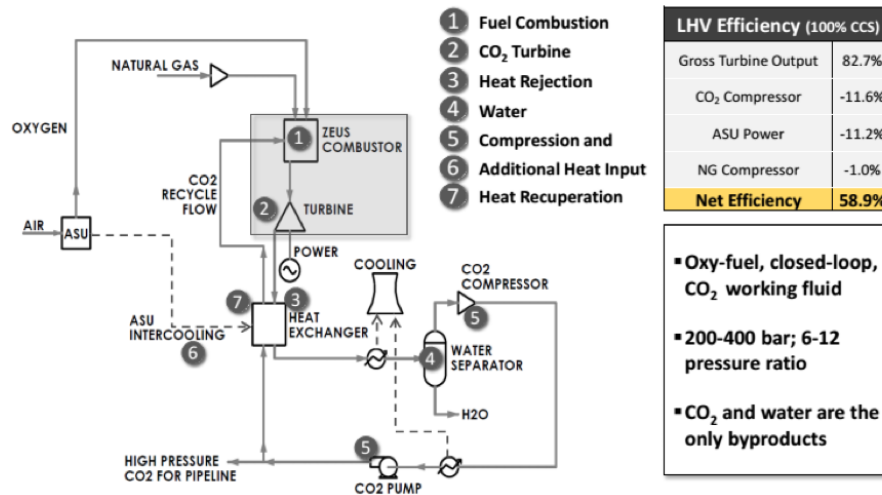


Figure 49: Layout and main specifications of the Allam cycle [133].

co<sub>2</sub>-power-cycles), ”this pilot project will provide valuable data on potential challenges for continuous operation on a larger scale. Key features of the project include the following:

- Indirectly heated cycle applicable to advanced combustion boilers.
- Thermal efficiency  $\geq 50\%$  possible.
- High fluid density and low pressure ratio enable compact turbomachinery.
- Ideally suited to constant temperature heat sources.
- Adaptable for dry cooling”.

The pilot plant is conceived to be able to adapt to operating on a Simple Recuperated layout and on a Recompression layout for flexibility and it is expected to be in operation by the end of 2022, according to the schedule made public by The Gas Institute, Figure 51. The main research items are shown in Figure 52.

In addition to these demonstration projects at representative scale, the North American research facilities listed in Table 8 are also worth noting. Even if they cannot be considered as precommercial (they are not actually intended to be so), they have contributed to developing the technology to the current state-of-the-art.

Location	Size	Cycle Layout	Institution
West-Mifflin (PA)	100 kW <sub>e</sub>	Simple Recuperated	Bechtel Marine Propulsion Co.
Akkron (OH)	7.3 MW <sub>e</sub>	Simple Recuperated	Echogen
Albuquerque (NM)	125 kW <sub>e</sub>	Brayton cycle (without turbine)	SANDIA National Laboratories (New Mexico)
Albuquerque (NM)	1 MW <sub>t</sub>	Brayton cycle (without turbine)	SANDIA National Laboratories (New Mexico)
Arvada (CO)	20 kW <sub>e</sub>	Recompression	SANDIA-DOE-Barber Nichols (USA)
San Antonio (TX)	1 MW <sub>e</sub>	Simple Recuperated	SWRI & GE
Ottawa, Canada	50-250 kW <sub>e</sub>	Recompression	Carleton University (in the design phase)
San Antonio (TX)	10 MW <sub>t</sub>	Simple Recuperated & Recompression	STEP programme
La Porte (TX)	50 MW <sub>t</sub>	Allam	Net Power

Table 8: Supercritical CO<sub>2</sub> facilities currently available in United States.

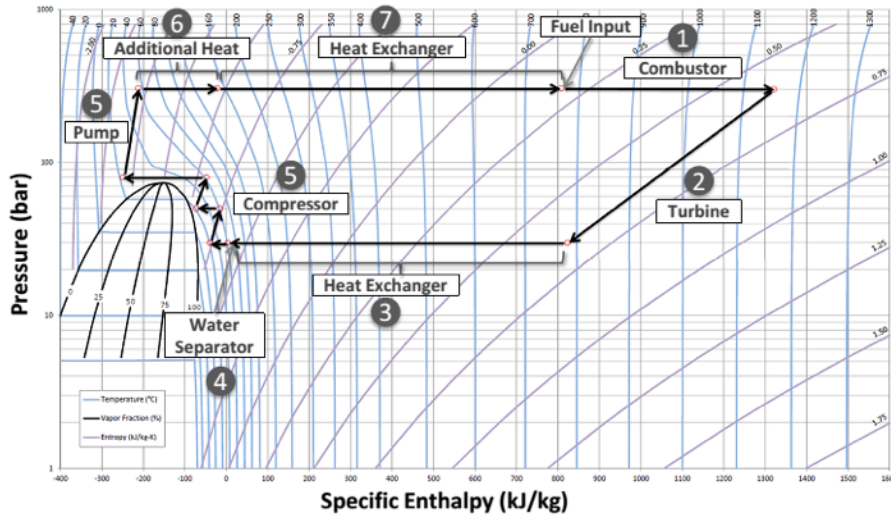


Figure 50: Pressure vs. enthalpy diagram of the Allam cycle [133].

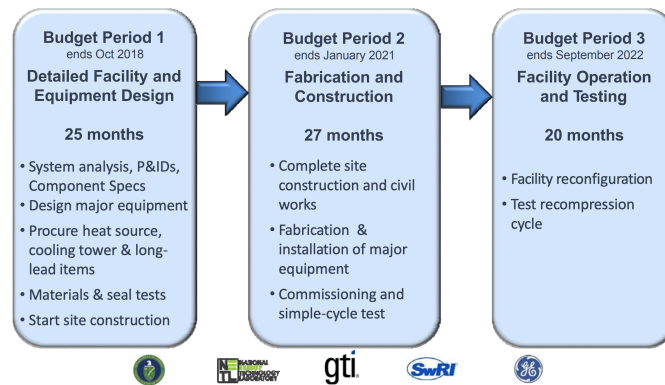


Figure 51: Development plan of the STEP facility [134].

7.6.2 Europe

The experimental development of supercritical Carbon Dioxide technologies in Europe lags behind the activities carried out in North America and even Asia. Despite some research projects funded by the member states and the European Commission, the few testing facilities are of a much smaller size than the American counterparts.

The available facilities in Europe are listed in Table 9. None of them is in the megawatt scale nor is it able to implement a complete Recompression cycle. Amongst them though, the loop currently available at the Technical University of Vienna (TUW) will be expanded within SCARABEUS to enhance its flexibility and testing capabilities, both in terms of capacity, maximum temperature and working fluid.

7.6.3 Rest of the world

Asia is, together with North America and Europe, the third largest contributor to sCO<sub>2</sub> technology development in the world. The Tokyo Institute of Technology constructed one of the first experimental loops to demonstrate the Recompression cycle in the early 2000s, Figure 53 but this was at a very small scale (target output was

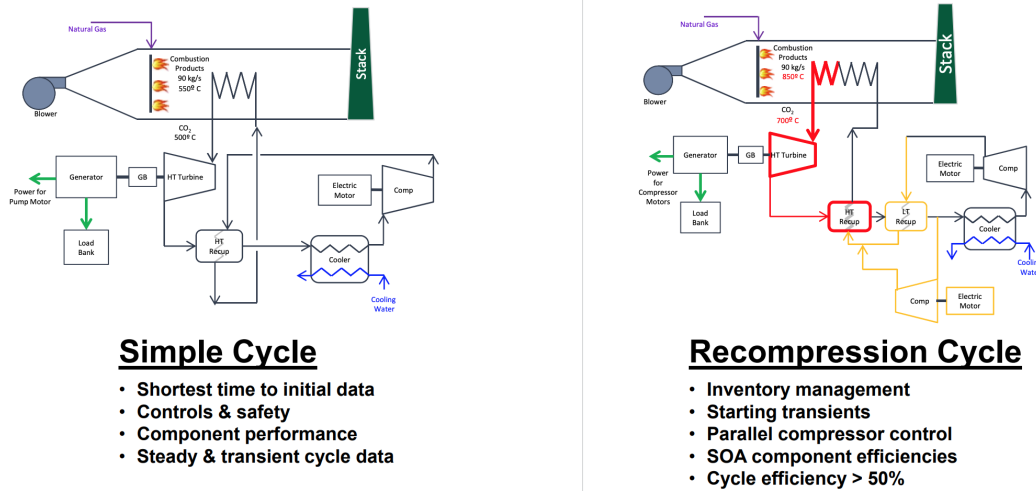


Figure 52: Foreseen configurations in the STEP facility [134].

Site of Construction	Size	Power Cycle	Institution
Husinec-Rez, Czech Republic	0.35 kg/s	Recompression (without turbine)	Research Center Rez (Czech Republic)
Stuttgart, Germany	not declared	Brayton cycle (only heat exchangers)	sCO <sub>2</sub> Hero Project partners
Wien, Austria	0.35 kg/s	Simple Recuperated	TU Wien

Table 9: Supercritical CO<sub>2</sub> facilities currently available in Europe.

below 10 kW<sub>e</sub>) and the activity was interrupted soon after [135, 136].

The development of sCO<sub>2</sub> technologies has been more active in South Korea in recent years. Aimed at nuclear application initially and with a focus on coal later, several National Research Institutes like The Korea Advance Institute of Science and Technology KAIST, Korea Atomic Energy Research Institute KAERI and the Korea Institute of Energy Research KIER have been actively developing experimental small-scale loops to test different cycle layouts and demonstrate cycle performance [137, 138]. More recently, the Gas Technology Institute (USA), the Korean Electric Power Research Institute KEPRI, and the Korean Electric Power Company KEPCO, national utility, have signed a Memorandum of Understanding to develop supercritical CO<sub>2</sub> power cycle technologies that could impact power generation efforts. This MoU enables the active involvement of KEPCO in the aforecited STEP plant.

Other facilities available worldwide are

Site of Construction	Size	Power Cycle	Institution
Daejeon, South Korea	10 kW <sub>e</sub>	Brayton Cycle	KIER (South Korea)
Daejeon, South Korea	80 kW <sub>e</sub>	Dual Simple Recuperated Cycle	KIER (South Korea)
Daejeon, South Korea	1 kW <sub>e</sub>	Recuperated Cycle	KIER (South Korea)
Daejeon, South Korea	kW-scale	Recuperated Cycle	KAIST (South Korea)
Tokyo, Japan	10 kW <sub>e</sub>	Simple Recuperated	Tokyo Institute of Technology (Japan)

Table 10: Supercritical CO<sub>2</sub> facilities currently available in Asia.

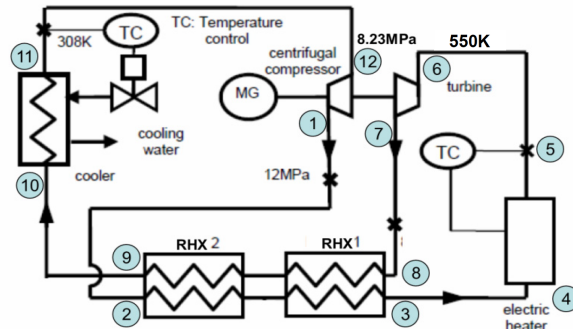


Figure 53: Layout of the experimental loop at Tokyo Institute of Technology [136].

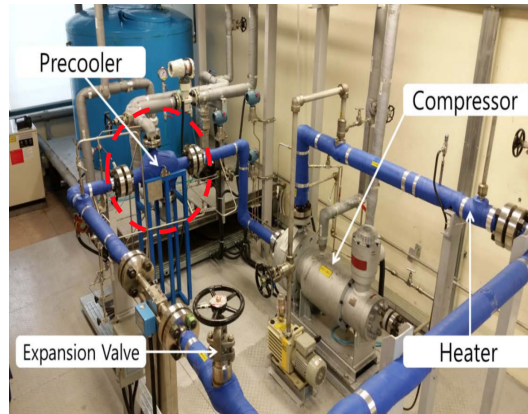


Figure 54: Layout of the experimental loop at Korea Advance Institute of Science and Technology [137].

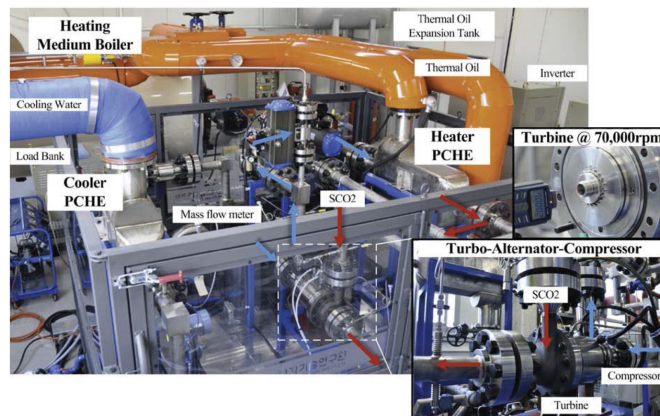


Figure 55: Layout of the experimental loop at Korea Institute of Energy Research [138].

In addition to the experimental activities cited in this section, there are other initiatives planned or under development in other regions of the world like Australia or India. They all contribute to the development of the technology, even if they are not listed in this section due to their somewhat smaller impact internationally.

## 8 Conclusions

This report assessing the current state of the art provides an overview of the technology used in Concentrated Solar Power plants based on central receiver technology (tower). The main subsystems of a power plant incorporating Thermal Energy Storage are discussed as so are the foreseen development trends.

The potential of conventional supercritical Carbon Dioxide power cycles to supersede steam turbines has also been explored in the report. An assessment of the layouts with larger potential for Concentrated Solar Power applications along with discussions about their thermodynamic and economic potential allows for a reasoned comparison between this technology and the steam technology used by default in commercial power plants.

Overall, based on data and forecasts issued by the International Renewable Energy Agency IRENA, it is concluded that the current cost of electricity produced by Concentrated Solar Power plants is in the order of 8-15 ¢/kWh, though these values are very site-specific and they can increase in certain sites with specific boundary conditions. This cost is not expected to drop substantially in the short term as this would only be enabled by a similar increase of thermal efficiency, and only a slight reduction seems possible if economies of scale are implemented.

On the other hand, supercritical CO<sub>2</sub> technologies do have the potential to enable lower costs, mostly thanks to the higher efficiency of the power block (bringing about a reduction of the solar field size) and the smaller footprint, therefore cost, of this part of the plant. According to the analyses available in literature, levelized costs of electricity of conventional supercritical CO<sub>2</sub> based CSP are expected to be in the order of 9.5-10 ¢/kWh in favourable conditions. Nevertheless, these figures are very conservative and incorporate a large safety margin to account for uncertainty which means that the actual LCoE is likely to be substantially lower than these values. Indeed, the potential of sCO<sub>2</sub>-CSP to enable lower costs of electricity than conventional CSP is widely acknowledged; unfortunately, the usual boundary conditions found in typical CSP sites prevent the implementation of the most efficient supercritical CO<sub>2</sub> layouts, what brings about an inevitable rise of the electricity costs achievable by this innovative power block technology. Therefore, for warm environments, the levelized cost of electricity of CSP-sCO<sub>2</sub> plants is expected to be not significantly lower than that of conventional CSP.

In the light of these results, it becomes clear that in order to exploit the full potential of supercritical CO<sub>2</sub> technology, it is mandatory to enable the implementation of the most efficient sCO<sub>2</sub> cycle layouts, which is the main driver of SCARABEUS. This key enabling project is thus supported on the need to implement condensing cycles whose performance, as discussed in this report, clearly exceeds that of conventional steam power plants. By doing so, the cost reduction brought about by sCO<sub>2</sub> power blocks will be larger than the possible uncertainty inherent to the calculations of thermal performance and costs of this new generation of power plants, therefore ensuring the economic and technical advantage of CSP-sCO<sub>2</sub> over conventional CSP.

## 9 References

- [1] IEA (International Energy Agency). World Energy Outlook Special Report 2018: Energy and Climate change - executive summary.
- [2] WRI (World Resource Institute). climate analysis indicators tool (CAIT) 2.0: WRI's climate data explorer, 2014, accessed September 2019.
- [3] FAO (Food and Agriculture Organization). FAOSTAT: Emissions - land use, 2014, accessed November 2018.  
URL [http://faostat3.fao.org/faostat-gateway/go/to/download/G2/\\*/E](http://faostat3.fao.org/faostat-gateway/go/to/download/G2/*/E)
- [4] IPCC (Intergovernmental Panel on Climate Change). mitigation of climate change: Trends in stocks and flows of GHGs and their drivers, 2014, accessed November 2018.  
URL [https://www.ipcc.ch/pdf/unfccc/sbsta40/SED/1\\_blanco\\_sed3.pdf](https://www.ipcc.ch/pdf/unfccc/sbsta40/SED/1_blanco_sed3.pdf)
- [5] L. F. Cabeza, E. Galindo, C. Prieto, C. Barreneche, A. I. Fernández, Key performance indicators in thermal energy storage: Survey and assessment, *Renewable Energy* 83 (2015) 820 – 827. doi:<https://doi.org/10.1016/j.renene.2015.05.019>.
- [6] A. Gil, M. Medrano, I. Martorell, A. Lázaro, P. Dolado, B. Zalba, L. F. Cabeza, State of the art on high temperature thermal energy storage for power generation. part 1—concepts, materials and modellization, *Renewable and Sustainable Energy Reviews* 14 (1) (2010) 31 – 55. doi:<https://doi.org/10.1016/j.rser.2009.07.035>.
- [7] S. J. Wagner, E. S. Rubin, Economic implications of thermal energy storage for concentrated solar thermal power, *Renewable Energy* 61 (2014) 81 – 95, world Renewable Energy Congress – Sweden, 8–13 May, 2011, Linköping, Sweden. doi:<https://doi.org/10.1016/j.renene.2012.08.013>.
- [8] J. Hernández-Moro, J. Martínez-Duart, CSP electricity cost evolution and grid parities based on the IEA roadmaps, *Energy Policy* 41 (2012) 184 – 192, modeling Transport (Energy) Demand and Policies. doi:<https://doi.org/10.1016/j.enpol.2011.10.032>.
- [9] E. González-Roubaud, D. Pérez-Osorio, C. Prieto, Review of commercial thermal energy storage in concentrated solar power plants: Steam vs. molten salts, *Renewable and sustainable energy reviews* 80 (2017) 133–148.
- [10] U. Herrmann, D. W. Kearney, Survey of thermal energy storage for parabolic trough power plants, *Journal of solar energy engineering* 124 (2) (2002) 145–152.
- [11] O. Behar, A. Khellaf, K. Mohammedi, S. Ait-Kaci, A review of integrated solar combined cycle system (ISCCS) with a parabolic trough technology, *Renewable and Sustainable Energy Reviews* 39 (2014) 223–250.
- [12] Solar Paces website CSP technology description, visited September 2019.  
URL <https://www.solarpaces.org/how-csp-works/>
- [13] Linear concentrator system basics for concentrating solar power, visited September 2019.  
URL [https://www.energy.gov/eere/solar/articles/linear-concentrator-system-basics-concentrating-solar-power?\\_sm.au\\_=i5VJs1P6vNVRTjT7](https://www.energy.gov/eere/solar/articles/linear-concentrator-system-basics-concentrating-solar-power?_sm.au_=i5VJs1P6vNVRTjT7)
- [14] C. J. Noone, M. Torrilhon, A. Mitsos, Heliostat field optimization: A new computationally efficient model and biomimetic layout, *Solar Energy* 86 (2) (2012) 792 – 803. doi:<https://doi.org/10.1016/j.solener.2011.12.007>.

- [15] A. Poullikkas, G. Kourtis, I. Hadjipaschalis, Parametric analysis for the installation of solar dish technologies in mediterranean regions, *Renewable and Sustainable Energy Reviews* 14 (9) (2010) 2772 – 2783. doi:<https://doi.org/10.1016/j.rser.2010.07.021>.
- [16] F. Téllez, M. Burisch, C. Villasante, M. Sánchez, C. Sansom, P. Kirby, C. Caliot, A. Ferriere, C. A. Bonanos, C. Papanicolas, A. Montenon, R. Monterreal, J. Fernández, State of the Art in Heliostats and Definition of Specifications (Survey for a low cost heliostat development) (Jul. 2017). doi:10.5281/zenodo.834887.  
URL <https://doi.org/10.5281/zenodo.834887>
- [17] F. Arbes, G. Weinrebe, M. Wöhrbach, Heliostat field cost reduction by ‘slope drive’ optimization, *AIP Conference Proceedings* 1734 (1) (2016) 160002. doi:10.1063/1.4949243.
- [18] Visited September 2019. [link].  
URL <http://www.poweroilandgas.sener/project/he54-heliostat>
- [19] W. B. Stine, M. Geyer, *Power From The Sun* by William B. Stine and Michael Geyer, 2001.
- [20] F. J. Collado, J. Guallar, A review of optimized design layouts for solar power tower plants with campo code, *Renewable and Sustainable Energy Reviews* 20 (2013) 142 – 154. doi:<https://doi.org/10.1016/j.rser.2012.11.076>.
- [21] J. Wang, L. Duan, Y. Yang, An improvement crossover operation method in genetic algorithm and spatial optimization of heliostat field, *Energy* 155 (2018) 15 – 28. doi:<https://doi.org/10.1016/j.energy.2018.05.004>.
- [22] S. Kiwan, A. L. Khammash, Investigations into the spiral distribution of the heliostat field in solar central tower system, *Solar Energy* 164 (2018) 25 – 37. doi:<https://doi.org/10.1016/j.solener.2018.02.042>.
- [23] M. Zhang, L. Yang, C. Xu, X. Du, An efficient code to optimize the heliostat field and comparisons between the biomimetic spiral and staggered layout, *Renewable Energy* 87 (2016) 720 – 730. doi:<https://doi.org/10.1016/j.renene.2015.11.015>.
- [24] M. Zhang, X. Du, L. Yang, C. Xu, Y. Yang, Comparing study of biomimetic spiral and radial staggered layouts of the heliostat field, *Energy Procedia* 69 (2015) 242 – 249, international Conference on Concentrating Solar Power and Chemical Energy Systems, SolarPACES 2014. doi:<https://doi.org/10.1016/j.egypro.2015.03.028>.
- [25] Y. Yao, Y. Hu, S. Gao, Heliostat field layout methodology in central receiver systems based on efficiency-related distribution, *Solar Energy* 117 (2015) 114 – 124. doi:<https://doi.org/10.1016/j.solener.2015.04.029>.
- [26] S. Kim, I. Lee, B. J. Lee, Development of performance analysis model for central receiver system and its application to pattern-free heliostat layout optimization, *Solar Energy* 153 (2017) 499 – 507. doi:<https://doi.org/10.1016/j.solener.2017.05.093>.
- [27] E. Scouros, A. Cosmetatos, Placement of heliostats on an uneven landscape, *Energy Procedia* 49 (2014) 220 – 228, proceedings of the SolarPACES 2013 International Conference. doi:<https://doi.org/10.1016/j.egypro.2014.03.024>.
- [28] N. Cruz, S. Salhi, J. Redondo, J. Álvarez, M. Berenguel, P. Ortigosa, Hector, a new methodology for continuous and pattern-free heliostat field optimization, *Applied Energy* 225 (2018) 1123 – 1131. doi:<https://doi.org/10.1016/j.apenergy.2018.05.072>.
- [29] E. Carrizosa, C. Domínguez-Bravo, E. Fernández-Cara, M. Quero, An optimization approach to the design of multi-size heliostat fields, 2014.

- [30] R. Perez-Enciso, A. Gallo, D. Riveros-Rosas, E. Fuentealba-Vidal, C. Perez-Rábago, A simple method to achieve a uniform flux distribution in a multi-faceted point focus concentrator, *Renewable Energy* 93 (C) (2016) 115–124. doi:10.1016/j.renene.2016.02.
- [31] N. Cruz, J. Álvarez, J. Redondo, M. Berenguel, P. Ortigosa, A two-layered solution for automatic heliostat aiming, *Engineering Applications of Artificial Intelligence* 72 (2018) 253 – 266. doi:https://doi.org/10.1016/j.engappai.2018.04.014.
- [32] A. Sánchez-González, M. R. Rodríguez-Sánchez, D. Santana, Aiming strategy model based on allowable flux densities for molten salt central receivers, *Solar Energy* 157 (2017) 1130 – 1144. doi:https://doi.org/10.1016/j.solener.2015.12.055.
- [33] A. Salomé, F. Chhel, G. Flamant, A. Ferrière, F. Thiery, Control of the flux distribution on a solar tower receiver using an optimized aiming point strategy: Application to themis solar tower, *Solar Energy* 94 (2013) 352 – 366. doi:https://doi.org/10.1016/j.solener.2013.02.025.
- [34] H. Benoit, L. Spreafico, D. Gauthier, G. Flamant, Review of heat transfer fluids in tube-receivers used in concentrating solar thermal systems: Properties and heat transfer coefficients, *Renewable and Sustainable Energy Reviews* 55 (2016) 298 – 315. doi:https://doi.org/10.1016/j.rser.2015.10.059.
- [35] P. K. Falcone, A handbook for solar central receiver design, Tech. rep., Sandia National Labs., Livermore, CA (USA) (1986).
- [36] W. Apley, Systems analysis of solar thermal power systems. report on task 1: determination and characterization of solar thermal conversion options, Tech. rep., Battelle Pacific Northwest Labs., Richland, WA (USA) (1978).
- [37] M. Haeger, A. Valverde, W. Meinecke, S. Cordes, Phoebus technology program solar air receiver (TSA) operational experience and test evaluation of the 2.5 mw (th) volumetric air receiver test facility at the plataforma solar de almeria, 1994.
- [38] J. Spelling, Hybrid solar gas-turbine power plants: a thermoeconomic analysis, Ph.D. thesis, KTH Royal Institute of Technology (2013).
- [39] M. Quero, R. Korzynietz, M. Ebert, A. Jiménez, A. Del Río, J. Brioso, Solugas–operation experience of the first solar hybrid gas turbine system at mw scale, *Energy Procedia* 49 (Supplement C) (2014) 1820–1830.
- [40] R. Korzynietz, J. Brioso, A. Del Río, M. Quero, M. Gallas, R. Uhlig, M. Ebert, R. Buck, D. Teraji, Solugas–comprehensive analysis of the solar hybrid brayton plant, *Solar Energy* 135 (2016) 578–589.
- [41] G. Flamant, D. Gauthier, H. Benoit, J.-L. Sans, B. Boissière, R. Ansart, M. Hemati, A new heat transfer fluid for concentrating solar systems: Particle flow in tubes, *Energy Procedia* 49 (2014) 617–626.
- [42] P. Falcone, J. Noring, J. Hruby, Assessment of a solid particle receiver for a high temperature solar central receiver system, Tech. rep., Sandia National Labs., Livermore, CA (USA) (1985).
- [43] L. Radosovich, A. Skinrood, The power production operation of solar one, the 10 mwe solar thermal central receiver pilot plant, *Journal of solar energy engineering* 111 (2) (1989) 144–151.
- [44] B. Kelly, M. Singh, Summary of the final design for the 10 mwe solar two central receiver project, Tech. rep., American Society of Mechanical Engineers, New York, NY (United States) (1995).
- [45] M. Sánchez, Advanced molten salt receiver RAS (in spanish), Tech. rep., Ciemat (1998).
- [46] R. Fernández, Receiver technology: Short course on concentrating solar systems (in spanish), Tech. rep., Ciemat (2009).

- [47] D. Bellard, A. Ferriere, F. Pra, R. Couturier, Experimental characterization of a high-temperature pressurized air solar absorber for the pegase project, in: Proceedings of the 18th SolarPACES Conference, Marrakech, Morocco, 2012.
- [48] E. S. Freeman, The kinetics of the thermal decomposition of sodium nitrate and of the reaction between sodium nitrite and oxygen, *The Journal of Physical Chemistry* 60 (11) (1956) 1487–1493.
- [49] K. Stahl, J. Griffin, B. Matson, R. Pettit, Optical characterization of solid particle solar central receiver materials, Tech. rep., Pacific Northwest Lab., Richland, WA (USA) (1986).
- [50] N. P. Siegel, C. K. Ho, S. S. Khalsa, G. J. Kolb, Development and evaluation of a prototype solid particle receiver: on-sun testing and model validation, *Journal of solar energy engineering* 132 (2) (2010) 021008.
- [51] H. Chen, Y. Chen, H.-T. Hsieh, N. Siegel, Computational fluid dynamics modeling of gas-particle flow within a solid-particle solar receiver, *Journal of solar energy engineering* 129 (2) (2007) 160–170.
- [52] K. Kim, N. Siegel, G. Kolb, V. Rangaswamy, S. F. Moujaes, A study of solid particle flow characterization in solar particle receiver, *Solar Energy* 83 (10) (2009) 1784–1793.
- [53] T. Tan, Y. Chen, Z. Chen, N. Siegel, G. J. Kolb, Wind effect on the performance of solid particle solar receivers with and without the protection of an aerowindow, *Solar Energy* 83 (10) (2009) 1815–1827.
- [54] T. Tan, Y. Chen, Review of study on solid particle solar receivers, *Renewable and Sustainable Energy Reviews* 14 (1) (2010) 265–276.
- [55] K. M. Armijo, C. Ho, R. Anderson, J. Christian, S. Babiniec, J. Ortega, Magnetic field flow phenomena in a falling particle receiver, in: AIP Conference Proceedings, Vol. 1734, AIP Publishing, 2016, p. 030004.
- [56] L. Amsbeck, R. Buck, T. Prosin, Particle tower technology applied to metallurgic plants and peak-time boosting of steam power plants, in: AIP Conference Proceedings, Vol. 1734, AIP Publishing, 2016, p. 070001.
- [57] J. Christian, C. Ho, Design requirements, challenges, and solutions for high-temperature falling particle receivers, in: AIP Conference Proceedings, Vol. 1734, AIP Publishing, 2016, p. 030008.
- [58] C. K. Ho, J. M. Christian, J. Yellowhair, N. Siegel, S. Jeter, M. Golob, S. I. Abdel-Khalik, C. Nguyen, H. Al-Ansary, On-sun testing of an advanced falling particle receiver system, in: AIP Conference Proceedings, Vol. 1734, AIP Publishing, 2016, p. 030022.
- [59] H. Ibrahim, A. Ilinca, Techno-economic analysis of different energy storage technologies, in: *Energy Storage-Technologies and Applications*, IntechOpen, 2013.
- [60] IRENA (International Renewable Energy Agency). renewable energy technologies: Cost analysis series, power Sector Issue 2/5 Concentrating Solar Power (2012).
- [61] H. Zhao, Q. Wu, S. Hu, H. Xu, C. N. Rasmussen, Review of energy storage system for wind power integration support, *Applied energy* 137 (2015) 545–553.
- [62] D. Akinyele, R. Rayudu, Review of energy storage technologies for sustainable power networks, *Sustainable Energy Technologies and Assessments* 8 (2014) 74–91.
- [63] X. Luo, J. Wang, M. Dooner, J. Clarke, Overview of current development in electrical energy storage technologies and the application potential in power system operation, *Applied energy* 137 (2015) 511–536.
- [64] K. Divya, J. Østergaard, Battery energy storage technology for power systems—an overview, *Electric power systems research* 79 (4) (2009) 511–520.

- [65] P. K. Choubey, M.-s. Kim, R. R. Srivastava, J.-c. Lee, J.-Y. Lee, Advance review on the exploitation of the prominent energy-storage element: Lithium. part i: From mineral and brine resources, *Minerals Engineering* 89 (2016) 119–137.
- [66] S. Kuravi, J. Trahan, D. Y. Goswami, M. M. Rahman, E. K. Stefanakos, Thermal energy storage technologies and systems for concentrating solar power plants, *Progress in Energy and Combustion Science* 39 (4) (2013) 285–319.
- [67] U.S. department of energy. 2014 sunshot initiative portfolio book: concentrating solar power. washington, dc: Office of energy efficiency & renewable energy, U.S. department of energy; 2014.
- [68] R. Sioshansi, P. Denholm, The value of concentrating solar power and thermal energy storage, *IEEE Transactions on Sustainable Energy* 1 (3) (2010) 173–183.
- [69] H. E. Reilly, G. J. Kolb, An evaluation of molten-salt power towers including results of the solar two project; topical, Tech. rep., Sandia National Labs. (2001).
- [70] U. Herrmann, M. Geyer, D. Kearney, Overview on thermal storage systems; workshop on thermal storage for trough power systems (2006).
- [71] W. Goldstern, Steam storage installations: Construction, design and operation of industrial heat accumulators, Oxford: Pergamon Press, 1970.
- [72] W.-D. Steinmann, M. Eck, Buffer storage for direct steam generation, *Solar Energy* 80 (10) (2006) 1277–1282.
- [73] M. Geyer, Solar Power Plants. Chapter 6: Thermal storage for solar power plants, Springer-Verlag Berlin Heidelberg, 1991. doi:[https://doi.org/10.1007/978-3-642-61245-9\\_6](https://doi.org/10.1007/978-3-642-61245-9_6).
- [74] J. Avellaner, C. Ortiz, F. Martinez, F. Sanchez, Cesa-1 project status report, in: *Thermo-Mechanical Solar Power Plants*, Springer, 1985, pp. 73–82.
- [75] J. Andujar, F. Rosa, M. Geyer, Cesa-1 thermal storage system evaluation, *Solar Energy* 46 (5) (1991) 305–312.
- [76] J. Beziau, B. Bonduelle, B. Rivoire, Prospective evaluation of molten salt solar plants based on themis results, in: *Advances In Solar Energy Technology*, Elsevier, 1988, pp. 1666–1670.
- [77] G. J. Kolb, An evaluation of possible next-generation high-temperature molten-salt power towers, Sandia National Laboratories, Albuquerque, NM, Report No. SAND2011-9320 122 (2011) 149.
- [78] S. Guillot, A. Faik, A. Rakhmatullin, J. Lambert, E. Veron, P. Echegut, C. Bessada, N. Calvet, X. Py, Corrosion effects between molten salts and thermal storage material for concentrated solar power plants, *Applied Energy* 94 (2012) 174–181.
- [79] M. Liu, W. Saman, F. Bruno, Review on storage materials and thermal performance enhancement techniques for high temperature phase change thermal storage systems, *Renewable and Sustainable Energy Reviews* 16 (4) (2012) 2118–2132.
- [80] A. Maccari, D. Bissi, G. Casubolo, F. Guerrini, L. Lucatello, G. Luna, A. Rivaben, E. Savoldi, S. Tamano, M. Zuanella, Archimede solar energy molten salt parabolic trough demo plant: a step ahead towards the new frontiers of csp, *Energy Procedia* 69 (2015) 1643–1651.
- [81] C. Prieto, R. Osuna, A. I. Fernández, L. F. Cabeza, Thermal storage in a mw scale. molten salt solar thermal pilot facility: Plant description and commissioning experiences, *Renewable energy* 99 (2016) 852–866.

- [82] G. Peiró, J. Gasia, L. Miró, C. Prieto, L. F. Cabeza, Experimental analysis of charging and discharging processes, with parallel and counter flow arrangements, in a molten salts high temperature pilot plant scale setup, *Applied energy* 178 (2016) 394–403.
- [83] C. Prieto, L. Miró, G. Peiró, E. Oró, A. Gil, L. F. Cabeza, Temperature distribution and heat losses in molten salts tanks for csp plants, *Solar Energy* 135 (2016) 518–526.
- [84] M. Medrano, A. Gil, I. Martorell, X. Potau, L. F. Cabeza, State of the art on high-temperature thermal energy storage for power generation. part 2—case studies, *Renewable and Sustainable Energy Reviews* 14 (1) (2010) 56–72.
- [85] J. E. Pacheco, R. W. Bradshaw, D. B. Dawson, W. De la Rosa, R. Gilbert, S. H. Goods, M. J. Hale, P. Jacobs, S. A. Jones, G. J. Kolb, et al., Final test and evaluation results from the solar two project, Report No. SAND2002-0120, Sandia National Laboratories, Albuquerque, NM 45.
- [86] J. E. Pacheco, R. Gilbert, Overview of recent results of the solar two test and evaluations program, Tech. rep., Sandia National Labs., Albuquerque, NM (US) (1999).
- [87] M. Liu, N. S. Tay, S. Bell, M. Belusko, R. Jacob, G. Will, W. Saman, F. Bruno, Review on concentrating solar power plants and new developments in high temperature thermal energy storage technologies, *Renewable and Sustainable Energy Reviews* 53 (2016) 1411–1432.
- [88] F. J. Ruiz-Cabañas, C. Prieto, R. Osuna, V. Madina, A. I. Fernández, L. F. Cabeza, Corrosion testing device for in-situ corrosion characterization in operational molten salts storage tanks: A516 gr70 carbon steel performance under molten salts exposure, *Solar Energy Materials and Solar Cells* 157 (2016) 383–392.
- [89] K. Federsel, J. Wortmann, M. Ladenberger, High-temperature and corrosion behavior of nitrate nitrite molten salt mixtures regarding their application in concentrating solar power plants, *Energy Procedia* 69 (2015) 618–625.
- [90] J. E. Pacheco, H. E. Reilly, G. J. Kolb, C. E. Tyner, Summary of the solar two test and evaluation program, Tech. rep., Sandia National Labs., Albuquerque, NM (US); Sandia National Labs . . . (2000).
- [91] R. W. Bradshaw, W. M. Clift, Effect of chloride content of molten nitrate salt on corrosion of a516 carbon steel, Sandia report.
- [92] K. Vignarooban, X. Xu, A. Arvay, K. Hsu, A. M. Kannan, Heat transfer fluids for concentrating solar power systems—a review, *Applied Energy* 146 (2015) 383–396.
- [93] G. García-Martín, M. Lasanta, V. Encinas-Sánchez, M. De Miguel, F. Pérez, Evaluation of corrosion resistance of a516 steel in a molten nitrate salt mixture using a pilot plant facility for application in csp plants, *Solar Energy Materials and Solar Cells* 161 (2017) 226–231.
- [94] D. M. Blake, L. Moens, M. J. Hale, H. Price, D. Kearney, U. Herrmann, New heat transfer and storage fluids for parabolic trough solar thermal electric plants, in: *Proceedings of the 11th SolarPACES International Symposium On concentrating Solar Power and Chemical Energy Technologies*. Zurich, Switzerland, 2002.
- [95] M. M. Kenisarin, High-temperature phase change materials for thermal energy storage, *Renewable and Sustainable energy reviews* 14 (3) (2010) 955–970.
- [96] Coastal Chemical Co, HITEC heat transfer salt. information provided by coastal chemical.
- [97] Badger Energy Corp, Design, handling, operation and maintenance procedures for hitec molten salt, SAND 81-8179 (1981).
- [98] U. Herrmann, B. Kelly, H. Price, Two-tank molten salt storage for parabolic trough solar power plants, *Energy* 29 (5-6) (2004) 883–893.

- [99] G. J. Kolb, R. B. Diver, Conceptual design of an advanced trough utilizing a molten salt working fluid., Tech. rep., Sandia National Lab.(SNL-NM), Albuquerque, NM (United States) (2008).
- [100] J. W. Raade, D. Padowitz, Development of molten salt heat transfer fluid with low melting point and high thermal stability, *Journal of Solar Energy Engineering* 133 (3) (2011) 031013.
- [101] G. J. Janz, Physical properties data compilations relevant to energy storage. parts i, ii and iv, Tech. rep., NATIONAL STANDARD REFERENCE DATA SYSTEM, nSRDS-NBS 61 (1981).
- [102] R. W. Bradshaw, N. P. Siegel, Development of molten nitrate salt mixtures for concentrating solar power systems, SolarPACES, Berlin.
- [103] C.-J. Li, P. Li, K. Wang, E. E. Molina, Survey of properties of key single and mixture halide salts for potential application as high temperature heat transfer fluids for concentrated solar thermal power systems, *AIMS Energy* 2 (2) (2014) 133–157.
- [104] A. Leyzerovich, *Steam Turbines for Modern Fossil-Fuel Power Plants*, The Fairmont Press, 2007.
- [105] R. Haywood, *Analysis of Engineering Cycles*, Pergamon Press, 1998.
- [106] NREL database, 29/11/2019, <https://solarpaces.nrel.gov>.
- [107] IRENA, *Renewable Power Generations Costs in 2018*.
- [108] U. EIA, *Annual energy outlook 2015: with projections to 2040*.
- [109] M. Mehos, C. Turchi, J. Vidal, M. Wagner, Z. Ma, C. Ho, W. Kolb, C. Andraka, A. Kruiženga, Concentrating solar power Gen3 demonstration roadmap, Tech. rep., National Renewable Energy Lab.(NREL), Golden, CO (United States) (2017).
- [110] G. Angelino, Carbon Dioxide Condensation Cycles for Power Production, *Journal of Engineering for Power* 90 (3) (1968) 287–295.
- [111] E. Feher, The Supercritical Thermodynamic Power Cycle, *Energy Conversion and Management* 8 (1968) 85–90.
- [112] F. Crespi, G. Gavagnin, D. Sánchez, G. S. Martínez, Supercritical carbon dioxide cycles for power generation: A review, *Applied Energy* 195 (2017) 152–183.
- [113] V. Dostal, M. Driscoll, P. Hejzlar, A supercritical carbon dioxide cycle for next generation nuclear reactors, Ph.D. thesis, Massachusetts Institute of Technology (2004).
- [114] G. Angelino, Real Gas Effects in Carbon Dioxide Cycles., in: *ASME 1969 Gas Turbine Conference and Products Show*, Cleveland,OH, 1969.
- [115] R. Allam, J. Fetvedt, B. Forrest, D. Freed, The Oxy-Fuel, Supercritical CO<sub>2</sub> Allam Cycle: New Cycle Developments to Produce Even Lower-Cost Electricity From Fossil Fuels Without Atmospheric Emissions, in: *ASME Turbo Expo 2014: Turbine Technical Conference and Exposition*, American Society of Mechanical Engineers, Dusseldorf, 2014.
- [116] G. Klemenic, S. Flegkas, A. Werner, M. Haider, H. Leibinger, Comparison of conventional and CO<sub>2</sub> power generation cycles for waste heat recovery, in: *The 5<sup>th</sup> Supercritical CO<sub>2</sub> Power Cycles Symposium*, San Antonio, TX, 2016, pp. 1–15.
- [117] Y. Chen, P. Lundqvist, A. Johansson, P. Platell, A comparative study of the carbon dioxide transcritical power cycle compared with an organic Rankine cycle with R123 as working fluid in waste heat recovery, *Applied Thermal Engineering* 26 (17) (2006) 2142–2147.

- [118] E. Cayer, N. Galanis, M. Desilets, H. Nesreddine, P. Roy, Analysis of a carbon dioxide transcritical power cycle using a low temperature source, *Applied Energy* 86 (7) (2009) 1055–1063.
- [119] Y. Song, J. Wang, Y. Dai, E. Zhou, Thermodynamic analysis of a transcritical CO<sub>2</sub> power cycle driven by solar energy with liquified natural gas as its heat sink, *Applied energy* 92 (2012) 194–203.
- [120] R. V. Padilla, Y. C. S. Too, R. Benito, R. McNaughton, W. Stein, Thermodynamic feasibility of alternative supercritical CO<sub>2</sub> Brayton cycles integrated with an ejector, *Applied Energy* 169 (2016) 49–62.
- [121] F. Crespi, G. Gavagnin, D. Sánchez, G. S. Martínez, Analysis of the Thermodynamic Potential of Supercritical Carbon Dioxide Cycles: A Systematic Approach, *Journal of Engineering for Gas Turbines and Power* 140 (2017) 051701.
- [122] Y. Ahn, J. I. Lee, Study of various Brayton cycle designs for small modular sodium-cooled fast reactor, *Nuclear Engineering and Design* 276 (2014) 128–141.
- [123] G. Silvestri, Eddystone Station, 325 MW Generating Unit, A Brief History (2003).
- [124] A. Armor, Ultrasupercritical Steam Turbines: Design and Materials Issues for the Next Generation (2002).
- [125] F. Crespi, D. Sánchez, J. M. Rodríguez, G. Gavagnin, A thermo-economic methodology to select sco<sub>2</sub> power cycles for csp applications, *Renewable Energy*.
- [126] F. Crespi, D. Sánchez, T. Sánchez, G. S. Martínez, Capital Cost Assessment of Concentrated Solar Power Plants Based on Supercritical Carbon Dioxide Power Cycles, *Journal of Engineering for Gas Turbines and Power* 141 (2019) 071011.
- [127] F. Crespi, D. Sánchez, T. Sánchez, G. S. Martínez, Integral techno-economic analysis of supercritical carbon dioxide cycles for concentrated solar power, in: *ASME Turbo Expo 2018: Turbomachinery Technical Conference and Exposition*, American Society of Mechanical Engineers Digital Collection, 2018.
- [128] A. Daabo, S. Mahmoud, R. Al-Dadah, The optical efficiency of three different geometries of a small scale cavity receiver for concentrated solar applications, *Applied Energy* 179 (2016) 1081–1096.
- [129] Various, Cost and Performance Data for Power Generation Technologies, Tech. rep., Black & Veatch for the National Renewable Energy Laboratory, Cambridge, MA (2012).
- [130] Various, The Power to Change: Solar and Wind Cost Reduction Potential to 2025, Tech. rep., IRENA, Abu Dhabi, United Arab Emirates (2016).
- [131] F. Crespi, Thermo-Economic Assessment of Supercritical co<sub>2</sub> Power Cycles for Concentrated Solar Power Plants, Ph.D. thesis, University of Seville (2020).
- [132] D. Flin, First Fire for La Porte Carbon Demo, *Gas Turbine World*.
- [133] R. Allam, Carbon Capture & Utilisation from Power Generation, in: *Proceedings of NEPIC International Bioresources Conferences*, North East of England Process Industry Cluster, Newcastle, UK, 2014.
- [134] V. Bush, GTI STEP forward on sCO<sub>2</sub> Power, in: *The 6<sup>th</sup> Supercritical CO<sub>2</sub> Power Cycles Symposium*, Pittsburgh, PA, 2018, pp. 1–24.
- [135] M. Utamura, H. Hasuike, T. Yamamoto, Demonstration Test Plan of Closed Cycle Gas Turbine with Super-Critical CO<sub>2</sub> as Working Fluid, in: *5<sup>th</sup> Conference on Sustainable Development of Energy Water and Environment Systems*, Dubrovnik, 2009, pp. 459–465.
- [136] M. Utamura, H. Hasuike, K. Ogawa, T. Yamamoto, T. Fukushima, T. Watanabe, T. Himeno, Demonstration of Supercritical CO<sub>2</sub> Closed Regenerative Cycle in a Bench Scale Experiment, in: *ASME Turbo Expo 2012: Turbine Technical Conference and Exposition*, American Society of Mechanical Engineers, Copenhagen, 2012.

- [137] J. Ik Lee, Activities at the Korea Institute of Science and Technology, in: The 5<sup>th</sup> Supercritical CO<sub>2</sub> Power Cycles Symposium, San Antonio, TX, 2016.
- [138] J. Cho, H. Shin, H.-S. Ra, G. Lee, C. Roh, B. Lee, Y.-j. Baik, Development of the Supercritical Carbon Dioxide Power Cycle Experimental Loop in KIER, in: ASME (Ed.), Proceeding of ASME Turbo Expo 2016: Turbomachinery Technical Conference and Exposition, Seoul, 2016.